FACULTY OF SCIENCE
Department of Geosciences and Geography

M.Sc. Thesis

The Siivikkovaara Ni-Cu-Zn-Pb(-Au) deposit, Kuhmo-Suomussalmi greenstone belt, eastern Finland: Implications for Archean ocean-floor mineralization processes.

Christos Ioannou

June 2020

Supervisors:
Dr. Tuomo Törmänen (GTK) and Prof. Tapani Rämö (HU),
Prof. Christoph Beier (HU) and Dr. Tapio Halkoaho (GTK)

Tiedekunta/Osasto Fakultet/Sektion – Faculty
Faculty of Science

Laitos/Institution– Department
Department of Geosciences and Geography

Tekijä/Författare – Author
Christos Ioannou

Työn nimi / Arbetets titel – Title
The Siivikkovaara Ni-Cu-Zn-Pb(-Au) deposit, Kuhmo-Suomussalmi greenstone belt, eastern Finland: Implications for Archean ocean-floor mineralization processes

Oppiaine /Läroämne – Subject
Geology (petrology and economic geology)

Työn laji/Arbetets art – Level	Aika/Datum – Month and year	Sivumäärä/ Sidoantal – Number of pages
M.Sc. thesis	06/2020	78

Tiivistelmä/Referat – Abstract

The Siivikko-Kellojärvi area forms the southern part of the Kuhmo greenstone belt. The rocks in the area are mainly tholeiitic and komatiitic lavas. In some occasions primary textures can still be observed in the rocks, including spinifex and pillow lavas in mafic and ultramafic volcanic rocks, evident of marine environment. The purpose of this M.Sc. thesis is to investigate the possible hydrothermal alteration processes involved in the formation of the Siivikkovaara Ni-Cu-Zn-Pb mineralized sulfide body. The goal of the M.Sc. thesis is to examine the Siivikkovaara Ni-Cu-Zn-Pb mineralized body using mineralogy, whole-rock geochemistry, mineral chemistry and sulfur isotope geochemistry ($\delta^{34}S$ values).

Komatiites in the present study have a Cr content of 0.28-0.62 wt.% and show a positive correlation between MgO and Cr, following a cotectic olivine-chromite cumulate trend. Analyses of the studied samples show an average Pd + Pt value of 300 ppb. Given the results, the mineralization represents an enriched body in Pd + Pt, relative to the majority of deposits in Finland. Samples presented in the current study are mildly depleted in $(La/Sm)_N$ and generally LREE, relative to chondrite values. The analysed minerals show an average $\delta^{34}S$ value of 0.45‰.

The source of sulfur is magmatic and cannot be related with any other geological setting. Enrichment in some elements may be attributed to later post-magmatic modification of the mineralization and remobilization of the elements. Komatiitic rocks of the studied samples were derived from Cr-saturated magmas. Cr depletion in tremolite rock may be related with alteration processes or post-magmatic modification. REE data suggest a rather primitive and uncontaminated magma for the studied samples. The studied komatiites are principally of Aluminum-Undepleted komatiite-type.

Owing to the poor exposure and extensive post-magmatic modification, any solid conclusions on the origin of the mineralized body are rather difficult. Therefore, more work can be done in the studied samples to further examine the assumption of a possible black-smoker setting.

Avainsanat – Nyckelord – Keywords
Komatiites, Sulfides, Sulfur, Isotopes, Hydrothermal, Alteration, Laser Ablation, Multicollector ICP-MS,

Säilytyspaikka – Förvaringställe – Where deposited
Helsinki University Library

Muita tietoja – Övriga uppgifter – Additional information
This thesis was done in collaboration with the Geological Survey of Finland (GTK) and the University of Helsinki

Contents

1. Introduction

1.1. Statement of the problem

Komatiite-hosted sulfide deposits host some the most important commodities in the modern industry, like Ni-Cu and Co, with an ever-increasing demand. On a global scale, komatiite hosted nickel sulfide deposits represent ~20% (Hronsky and Schodde 2006) of the worlds Ni deposits but these deposits have not been studied to the fullest. The goal of this study is to examine hydrothermal alteration processes involved in the formation of the Siivikkovaara Ni-Cu-Zn-Pb mineralized sulfide body, hosted by komatiites and komatiitic basalts in the Kuhmo-Suomussalmi greenstone belt, eastern Finland. The main question is whether the formation of this Precambrian sulfide body can be linked to processes related to modern black smokers.

Apart from the main question stated above, the source of sulfur in komatiite hosted sulfide ores and how these specific S sources influence the formation of komatiite hosted sulfide deposits (Mercier- Langevin et al. 2012) needs to be examined in more detail. Utilizing the sulfur isotopic data from the mineralized body, insights on the source of sulfur will be given in the current study. Deeper understanding of ore forming processes for komatiite-hosted sulfide ores will help us define new metallogenic provinces to identify new deposits to secure the supply of commodities hosted in these deposits in the future.

2. Komatiites

2.1. Komatiite petrology and classifications

Komatiites are formed by decompression melting of the mantle and requires such elevated temperature that komatiites are almost exclusively restricted to the Archean Eon. Komatiites represent primitive mantle melts and require high degrees of partial melting of mantle peridotite. They can be emplaced as extrusions, dikes, sills, and subvolcanic intrusions (Nesbitt and Sun 1976, Sun and Nesbitt 1978, Hertzberg 1992). Geochemically, komatiites are enriched in Mg, Ni, and Cr and relatively depleted in Si, Al and Ti. In the official International Union of Geological Sciences (IUGS) recommendation, komatiite is defined as a high-Mg volcanic rock with 52 wt.% > SiO_2 > 30 wt.%, MgO > 18 wt.%, (NaO_2 + K_2O) < 2 wt.% and TiO_2 < 1 wt.% (Le Bas 2000, Le Maitre et al. 2002). High-MgO volcanic rocks can also be classified by

their MgO and TiO_2 contents into komatiites (MgO > 18 wt.% and TiO_2 < 1 wt.%) and komatiitic basalts (MgO < 18 wt.% and TiO_2 < 1 wt.%) (Arndt et al. 2008). A further classification of komatiites by Nesbitt et al. (1979) classifies them based of their Al contents into either Al-Depleted Komatiites (ADKs) or Al-Undepleted Komatiites (AUKs). A third, rarer group, Al-Enriched Komatiites (AEK), has also been defined by Jahn et al. (1982). ADKs are specified as subchondritic with Al/Ti ratios of 10, superchondritic with $(Gd/Yb)_N$ ratios ~1.3–1.6 and are products of partial melting in the presence of residual garnet (Nesbitt et al. 1979, Nesbitt et al. 1982), which partitions Al and heavy rare earth elements (HREE) with respect to Ti and the middle REE (MREE). AUKs show chondritic Al/Ti ratios ~20, unfractionated $(Gd/Yb)_N$, and are considered to have formed by larger degrees of partial melting at lower, non-garnet stability field pressures (Arndt et al. 2008).

2.2. Komatiite-hosted sulfide deposits

Komatiite-hosted sulfide deposits are an important source of base (Ni, Cu, Co) and precious platin group element (PGE) metals. Komatiite hosted nickel sulfide deposits represent ~20% of the world nickel reserves (Hronsky and Schodde 2006). The formation of many komatiite-hosted sulfide deposits is synchronous with elevated mantle plume activity and crustal growth (ca. 2.95, 2.7, 1.9 Ga) and the age of formation of komatiite hosted deposits is similar to the age formation of banded iron formations (BIF), sulfidic deep-sea sediments, and volcanogenic massive sulfide (VMS) deposits (Bekker et al. 2009). The key mechanisms that control the formation of komatiite-hosted sulfide deposits are:

- high abundances of Ni-Cu-PGE in komatiitic melts
- sulfur undersaturation of komatiitic melts
- the ability of komatiitic melts to erode and assimilate country rocks, and thus incorporate external sulfur
- post-magmatic modification of magmatic ores, which may enhance enrichment of base and precious metals (e.g., Barnes 2006, Lesher and Barnes 2008, Konnunaho 2016).

Because of the high-degree partial melting, komatiitic melts partition large amounts of olivine and naturally incorporate large amounts of elements from their mantle sources, such as Ni, Cu, Co, Cr, PGEs and S. Because of the high degree of melting and high temperature, S is more susceptible to dissolution in komatiitic melts. Sulfur is incompatible during mantle melting and

so its abundance decreases in the partial melt when the degree of melting increases. Primitive komatiite melts are thus undersaturated in major sulfur-bearing phases (e.g., Robb 2005, Lesher and Barnes 2008). To reach sulfide saturation in a komatiitic system, external sulfur sources and/or considerable amounts of magma fractionation are needed so the sulfide melt is physically separated from the silicate magma. Apart from massive primary sulfide bodies, disseminated ores can form during later stages of magma fractionation (Lesher and Barnes 2008). In such formations, chalcophile element partitioning, controls the sulfur concentration at sulfide saturation (SCSS). If all the above requirements are met, to form an economic deposit specific zones-traps are required (Lesher et al. 2001, Lesher and Barnes 2008).

2.3. Post-magmatic modification of komatiite hosted sulfide deposits

Because of their age (e.g., Archean and Proterozoic), komatiite-hosted deposits have in many cases undergone post-magmatic modification. Disseminated ores are more vulnerable to post-magmatic alteration than massive ores and massive ores are more susceptible to tectonic remobilization due to their ductile nature (after Stone and Archibald 2004, Barnes 2006, Barnes et al. 2016). Post-magmatic and metamorphic alteration can modify the primary sulfides and result in a second stage of metal enrichment. Barnes et al. (2009) and Konnunaho et al. (2013) argued that a strong talc-carbonate CO_2 metasomatism and serpentinization can oxidize the primary Fe sulfide, release S and Ni, and replace the original assemblage by secondary magnetite-pyrite. This process is usually referred to as desulfurization. The released S then enhances Ni release from olivine and may form secondary Ni-sulfide assemblages (e.g., millerite), which under ideal conditions may precipitate and lead to a further enrichment of the ore endowment. Barnes (2006), showed that in many cases the secondary stage of enrichment forms the bulk of an economic deposit.

3. Geological setting

3.1 General geological setting of the Fennoscandian Shield

The Fennoscandian Shield is divided into three main lithological provinces (Fig. 1.A): (1) the 3500–2500 Ma Archean basement, (2) its Paleoproterozoic (2500–1900 Ma) sedimentary-volcanic cover, and (3) the Svecofennian orogenic belt, 1930–1800 Ma in age. The Archean basement has usually been divided into two main crustal segments, the Karelian and Kola cratons, which are separated by the Belomorian mobile belt and the Lapland granulite belt. A characteristic feature of the tectonic structure of the Karelia Province is the presence of narrow and elongated, N–S-trending greenstone belts surrounded by gneissic and migmatitic tonalite trondhjemite gneiss (TTG) formations. In the part of the Karelian province that extends into eastern Finland (Fig. 1.B), the Archaean greenstone belts are in accordance with the other N-S structures found in the Karelian Province and are up to 10 km wide and trend about 200 km are also enclosed by typical tonalite trondhjemite gneisses (TTG). The Karelia Province can be further divided into three main subprovinces (Fig. 2). The three groups are: Western Karelia subprovince, Central Karelia subprovince, and Vodlozero subprovince (Slabunov et al. 2006, Hölttä et al. 2012, 2014, Fig. 1.A). The Karelian province has undergone multiple deformation and metamorphic events at 2.84–2.81 Ga, 2.72–2.60 Ga and 1.9 Ga (Kontinen et al. 1992, Stone and Archibald 2004, Käpyaho et al. 2007, Hölttä et al. 2000, Mänttäri and Hölttä 2002, Mikkola et al. 2011, Lauri et al. 2011).

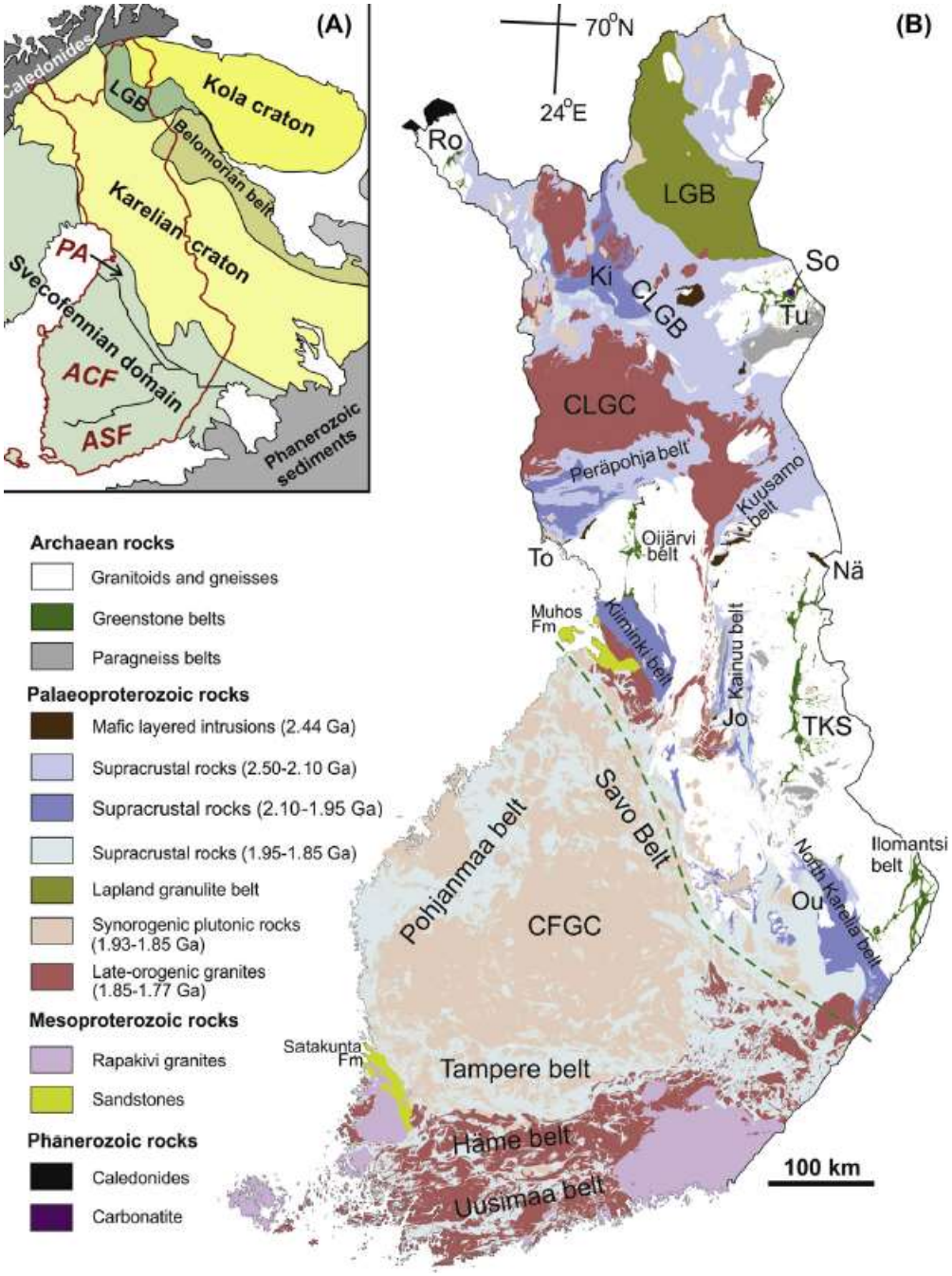

Figure 1. (A) Main bedrock units of the eastern part of the Fennoscandian Shield. (B) Geological map of Finland. A abbreviations: PA = Primitive arc complex of central Finland, ACF = Accretionary arc complex of central and western Finland, ASF =Accretionary arc complex of southern Finland. B abbreviations: CFGC = Central Finland Granitoid Complex, CLGC = Central Lapland Granitoid Complex, Jo = Jormua ophiolite, Ki = Kittilä greenstone complex, Nä = Näränkävaara, Ou = Outokumpu ophiolite, Ro = Rommaeno complex, So = Sokli carbonatite, TKS = Tipasjärvi-Kuhmo-Suomussalmi belt, To = Tornio, Tu = Tulppio.

Sources: (A) Modified after Vaasjoki et al. (2005) and Lahtinen et al. (2005). (B) Based on Bedrock of Finland – DigiKP. Digital map database [Electronic resource]. Espoo: Geological Survey of Finland [9 May 2020], Version 2.2., available at: https://gtkdata.gtk.fi/Kalliopera/index.html. The green dashed line shows the southwestern boundary of the Karelian craton, based on Nd isotopic compositions of intrusive rocks (modified after Huhma et al. 2011).

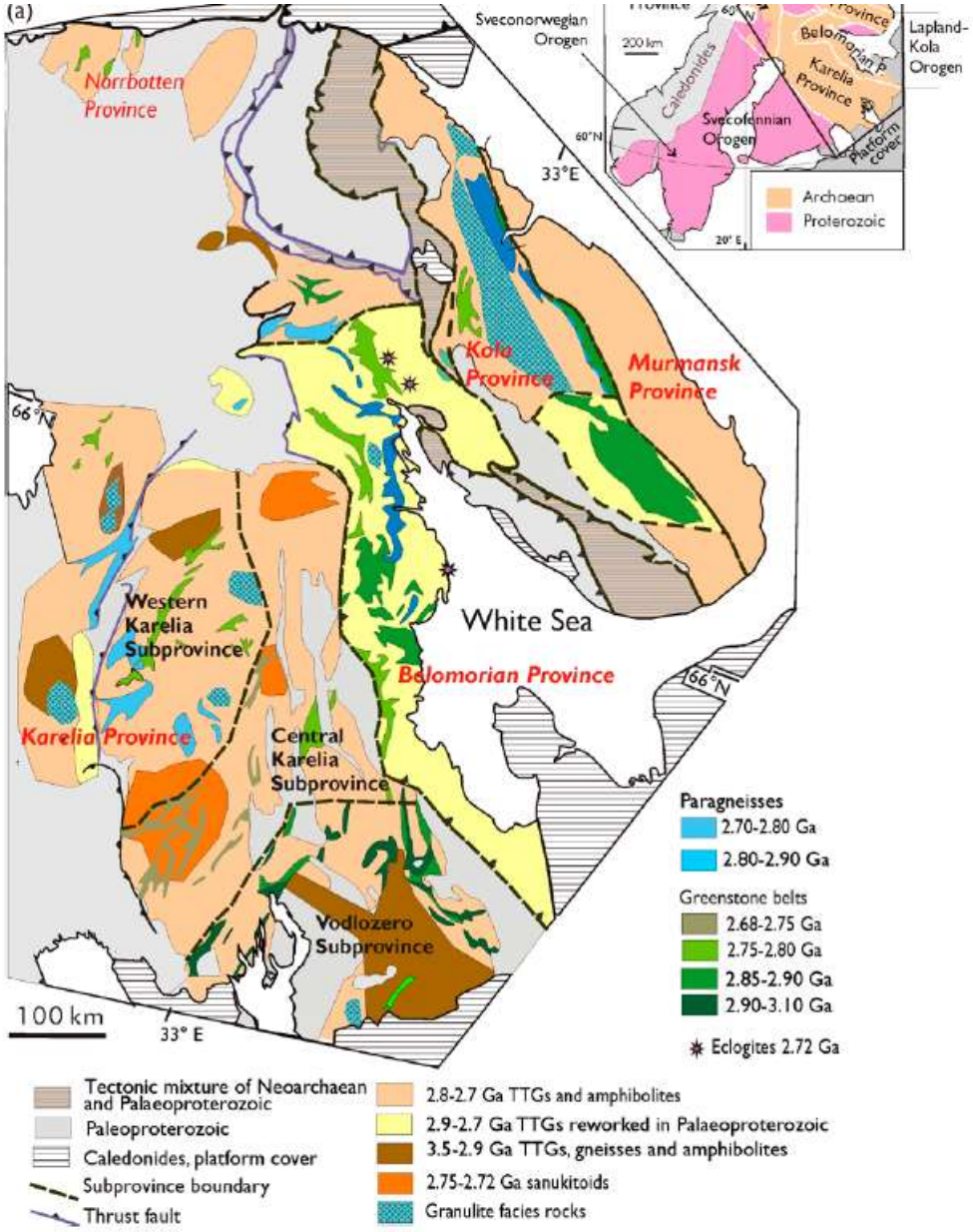

Figure 2. Generalised geological map of the Archaean of Fennoscandia, modified after Slabunov et al. (2006) and Hölttä et al. (2008).

Dating has been carried out using zircon U–Pb isotope data. The ages of the volcanic rocks in the Karelia Province greenstone belts (GSB) range from ca. 3.05 Ga to 2.75 Ga (e.g., Hyppönen 1983, Luukkonen 1988, Vaasjoki et al. 1999, Svetov and Svetova 2011, Huhma et al. 2012). The age of the volcanic rocks in the Western Karelia subprovince vary from 2.94 Ga to 2.73 Ga, with the youngest ones in the Kostomuksha, Kuhmo and Tipasjärvi greenstone belts, the oldest in the Suomussalmi greenstone belt (Hyppönen 1983,Vaasjoki et al. 1999, Huhma et al. 2012, Puchtel et al. 1999, Samsonov et al. 2005, Kozhevnikov et al. 2006).

3.2 Geology of Kuhmo greenstone belt

For the Kuhmo GSB (Fig. 3), a significant amount of geological information has been assembled from drilling programs executed by the Geological Survey of Finland and Outokumpu Co. The three separate greenstone belts are geographically in the same area and they have been treated together (Piirainen 1988, Papunen et al. 2009), although some of the volcanic rocks of the Suomussalmi greenstone are older (ca. 2.94 Ga) in age than those of the Kuhmo and Tipasjärvi belts (Huhma et al. 2012).

Three genetic models have been proposed for the study area by Piirainen (1988), Papunen et al. (2009) and Maier et al. (2013):

- Piirainen (1988) suggested that the stratigraphy of the Kuhmo greenstone belt can be divided into two groups based on the volcanic rocks. Tholeiitic-komatiitic rocks with minor calc-alkalic intermediate volcanic rocks, and bimodal volcanic rocks. As for the geotectonic environment, he suggested a failed rift, followed by subduction that generated the post-greenstone TTG magmatism which surrounds the GSB in the present day as discussed.
- Papunen et al. (2009) suggested that the Suomussalmi-Kuhmo-Tipasjärvi greenstone complex was formed in a plume-driven rifting of the continental crust with the first volcanic rocks being the calc-alkalic felsic-mafic volcanic rocks, followed by tholeiitic lavas. This was followed by a volcanic episode with eruptions of MgO-rich komatiitic volcanic rocks ending with a final eruptive phase of calc-alkalic volcanic rocks and deposition of a sedimentary cover that overlays the entire sequence.
- Maier et al. (2013) argued that an oceanic plateau setting is probable based on the Zr/Nb and Nb/Th ratios of the komatiitic rocks in the Siivikko-Kellojärvi area and the Tipasjärvi greenstone belt. For the komatiitic rocks in the Suomussalmi greenstone belt, they suggested interaction with older continental crust.

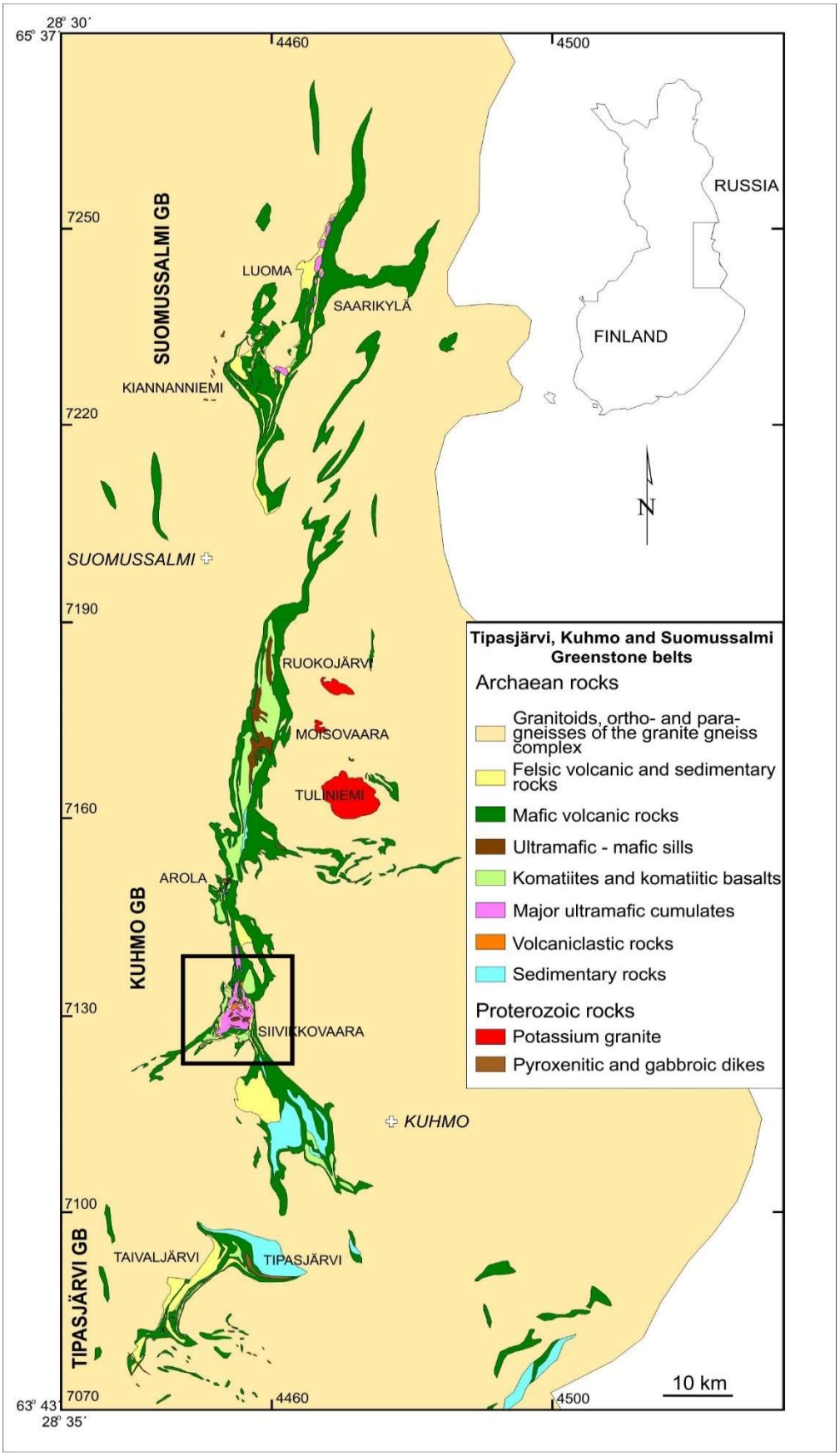

Figure 3. Tipasjärvi-Kuhmo-Suomussalmi greenstone complex in eastern Finland. Area of Siivikkovaara-Kellojärvi (Fig. 4) indicated with black rectangle. Modified after Korsman et al. (1997).

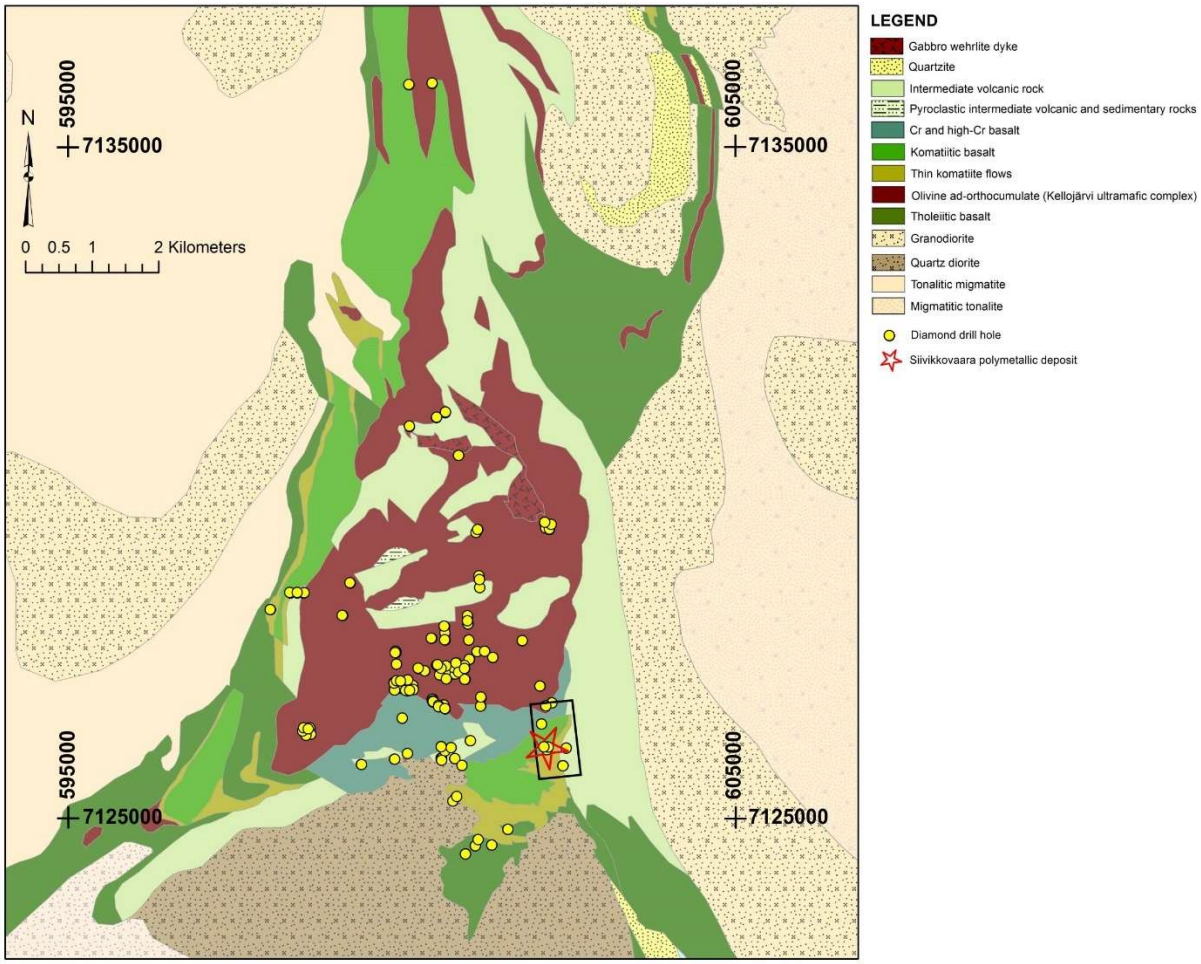

Figure 4. Geological map of the Siivikkovaara-Kellojärvi area. The map is the rectangle area of Fig. 3. Mineralization is indicated by the star inside the rectangle. Yellow circles indicate diamond drill holes. Modified after Halkoaho et al. (2018).

The Siivikko-Kellojärvi area (Fig. 4) forms the southern part of the Kuhmo greenstone belt. The rocks in the area are mainly tholeiitic and komatiitic lavas. In some occasions primary textures can still be observed in the rocks, including spinifex and pillow lavas (Fig. 6) in mafic and ultramafic volcanic rocks, evident for formation in the marine environment (Hanski 1980). Detailed field work, drilling programmes and geophysical surveys have been conducted in this area (Halkoaho and Niskanen 2009, 2012). A noteworthy geochemical characteristic of the volcanic rocks in the area is a basaltic formation with a notably high Cr content of 1300–4500 ppm (Halkoaho et al. 2000). This Cr-rich basalt is interlayered with komatiitic flows. This structure is an indicator that the komatiitic and high-Cr basaltic volcanism where synchronous. Overlying this unit is another basaltic formation, equally thick and with a Cr content of 450–1300 ppm.

3.3 Stratigraphy of the study area

The stratigraphy of the study area (Fig. 5, Halkoaho et al. 2000) is, from the bottom to the top:

- Ruokojärvi formation, gneissic-granodiorite basement and associated supracrustal rocks. Felsic volcanic rocks, volcanic conglomerates, tuffs and tuffites are located at the eastern margin of the northern extension of the Kuhmo greenstone belt. The TIMS U-Pb age of four zircon fractions from recrystallized homogeneous felsic tuff is 3007±7 Ma (Luukkonen et al. 2002).
- Mäkisensuo formation, bimodal calc-alkaline felsic to mafic volcanic rocks with sedimentary interlayers. This formation is intensely deformed and displays a low-grade Zn-Pb mineralization about 1 km west of the study area.
- Pahakangas formation, composed of tholeiitic (pillow) basalts with thin sedimentary interlayers such as BIFs and black schists. Description of the formation has been carried out by Papunen (1960) and Hanski (1980). The Pahakangas-Siivikkovaara formation is helpful for the interpretation of the stratigraphy of the GSB because it resembles a cross section through it. This forms a good basis for the stratigraphic interpretation as the rocks in the area have not experienced high-strain deformation and the lava flow layering is subvertical, trending roughly E-W, with the direction of the younger strata towards the north. Alternating layers of massive and pillow basalts can be observed in the area. The upper contacts of the pillow textured basalts are in places covered with a thin layer of chert or banded iron formation (BIF), the lower contacts against the massive parts of the flows are sharp and the pillows are brecciated by the lower injected massive lava. These

observations show that the massive lower parts of the flows extruded later and inflated the pillow-textured lava flow tops. The pillow layers range up to 10–20 m in thickness, whereas the massive parts may reach thicknesses of 70 m.

- The Komatiitic Vaara formation, the lower part of the Kellojärvi cumulate complex. A komatiitic unit, composed of thin komatiitic flows with lenses of olivine meso- and ortho-cumulates along prominent lava pathways. A thin tremolite rock forms the lower layer of the unit, which overlies the BIF formation of the Pahakangas group. The olivine ortho-meso-cumulate represents the B-layer of the first fractionated komatiite flow. Above the olivine ortho-meso-cumulate is a thin layer of aligned hopper olivines, followed by a 4 m layer of olivine spinifex and a 2 m layer of random spinifex.
- Mäkinen formation, the upper part of the Kellojärvi cumulate complex composed of komatiitic high-Mg basalts. The rock formations at the Siivikkovaara area are intensely faulted and composed of tens of small tectonic blocks. The structure of the komatiitic basalts, with stringy beef pyroxene spinifex A-layers at the upper part of the komatiitic sequence, indicates contemporaneous eruptions of komatiitic basalt and komatiite lava flows. The top of the Mäkinen group is composed of non-fractionated flows of komatiitic basalt with well-preserved pillow structures with variolitic textures (Fig. 6.A).
- High-Cr basalts with Cr concentrations ranging from 1300 to 4500 ppm. They are found interlayered with thin komatiitic flows and in places they show pillow structures (Fig. 6.B). The other basaltic group has lower but still anomalously high Cr. With concentrations ranging from 450 to 1300 ppm have been called Cr basalts and overlie the high-Cr basalts. The lower part of the group is composed by 250 m of the high-Cr basalt by Halkoaho et al. (2000). Xenolithic inclusions of komatiitic basalt have been observed within the high-Cr basalt formation.
- The mafic Cr basalts are stratigraphically above the high-Cr basalt group. The separation of the two basaltic groups is based on their Cr content. The Cr basalt has lower Cr (500–1300 ppm) than the high Cr-basalt. Between the two groups is a 6 m layer of tremolite-biotite/chlorite rock with 12.5 wt.% MgO and 3800 ppm Cr, and a weak sulfide dissemination. The sequence of basaltic lava flows is 250 m thick.
- Above the volcanic units there is an unconformable felsic to mafic volcaniclastic and sedimentary formation.
- The stratigraphy of the area is finalised by metasediments (phyllites, quartzites, metagreywackes and conglomerates). The volcanic rocks were formed during subaerial volcanism.

The presented stratigraphic sequence cannot be found in all areas of the Kuhmo GSB. Komatiites and of Cr-rich basalts are common in the Tipasjärvi, Siivikkovaara and Arola sequences.

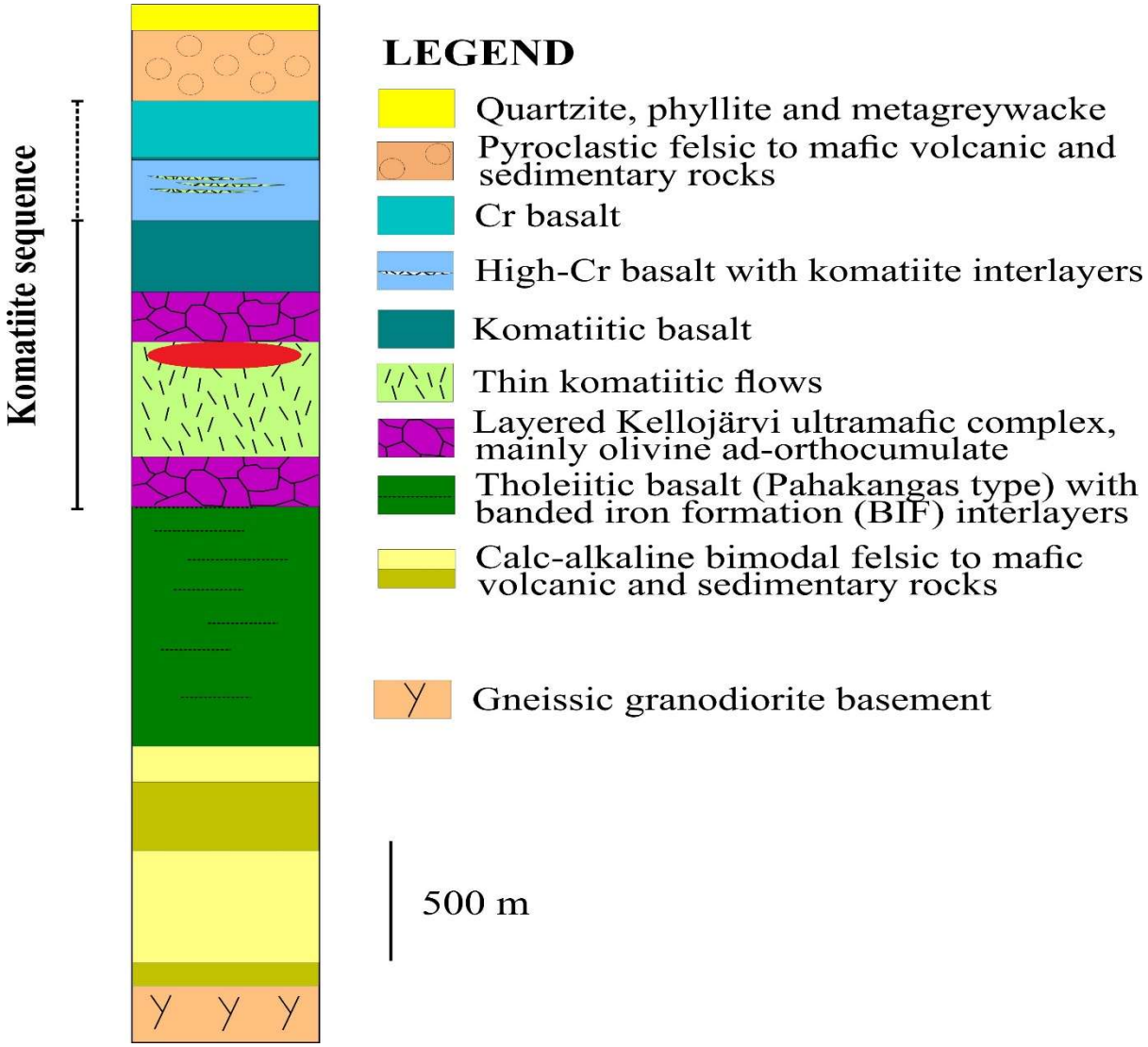

Figure 5. Generalized stratigraphic column of the Kuhmo greenstone belt in the Siivikkovaara area, Kuhmo. The position of the sulfide body in the stratigraphic column is marked in red (modified after Halkoaho et al. 2000).

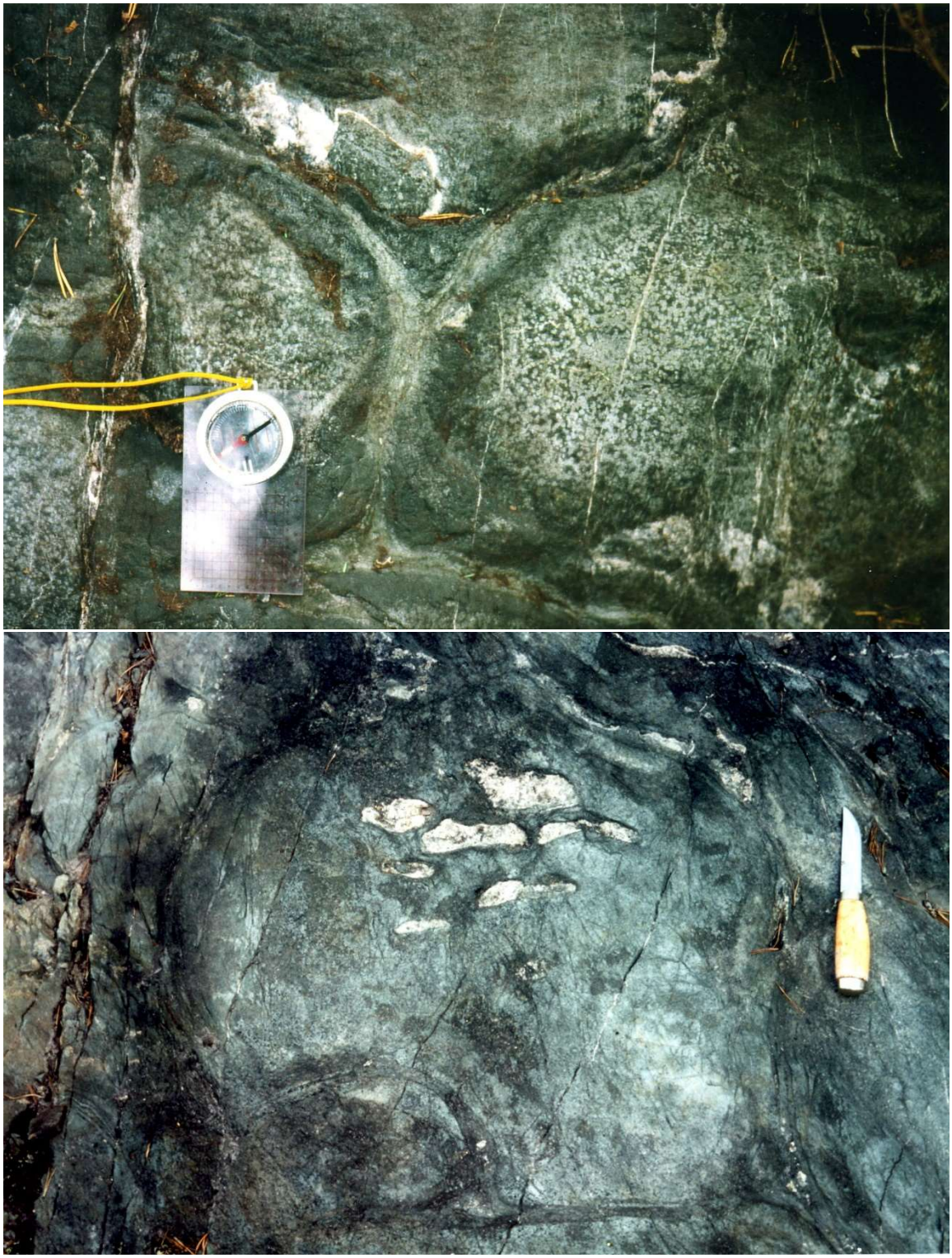

Figure 6. A. Variolitic pillow lava of komatiitic basalt, near the farmhouse of Viitaja (4455985/7126835). The length of the compass is 12.5 cm. B. Pillow lava structure in the high-Cr basalt, Mäkisensuo area (4455365/7128000). Some pillows contain drainage cavities (white inclusions) filled with quartz, and epidote±carbonate. The length of the knife is about 20 cm. Photos T. Halkoaho.

3.4. The Siivikkovaara Ni-Cu-Zn-Pb(-Au) deposit

The southern segment of the Kuhmo-Suomussalmi greenstone belt (Fig. 7) hosts a small Ni-Cu-Zn-Pb(-Au) sulfide enrichment associated with komatiites and pillow-textured komatiitic basalts (Fig. 8; see Vanne 1984). The mineralized body is about 50 m in diameter and is found at the fringe of a zone of tremolite rock that runs along the contact between komatiites and komatiitic basalts. The tremolite rocks are strongly depleted in Cr and may represent a fluid channel that fed an Archean black smoker on the ancient sea floor. The mineralized body might thus represent the subsurface section of the black smoker with characteristic geochemical and mineralogical traits related to relatively high-temperature hydrothermal alteration of the surrounding komatiites and komatiitic basalts.

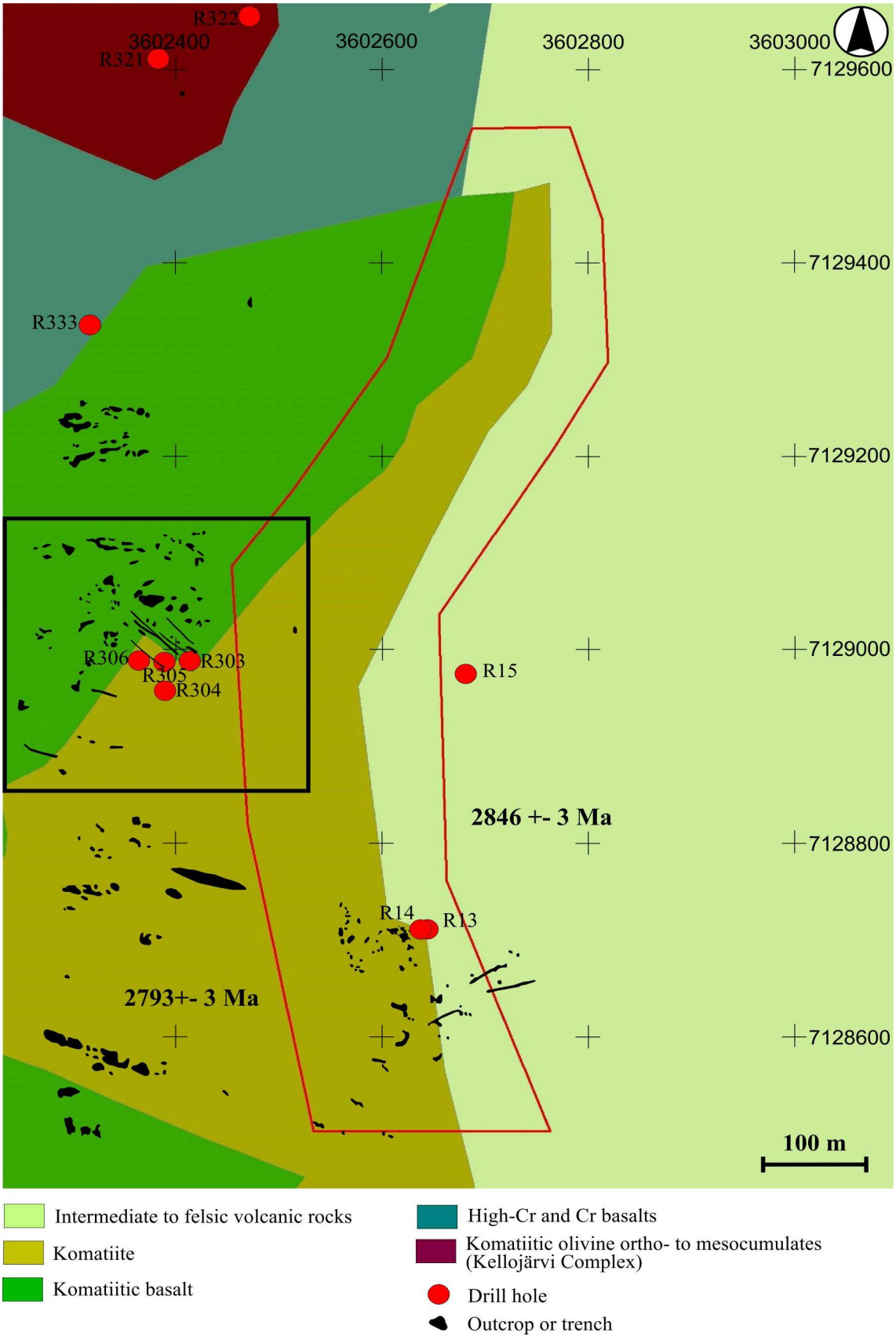

Figure 7. Sketch of the geology in the southern part of Kuhmo greenstone belt at the study area. Ages after Lehtonen et al. (2016). Modified after Halkoaho et al. (2016).

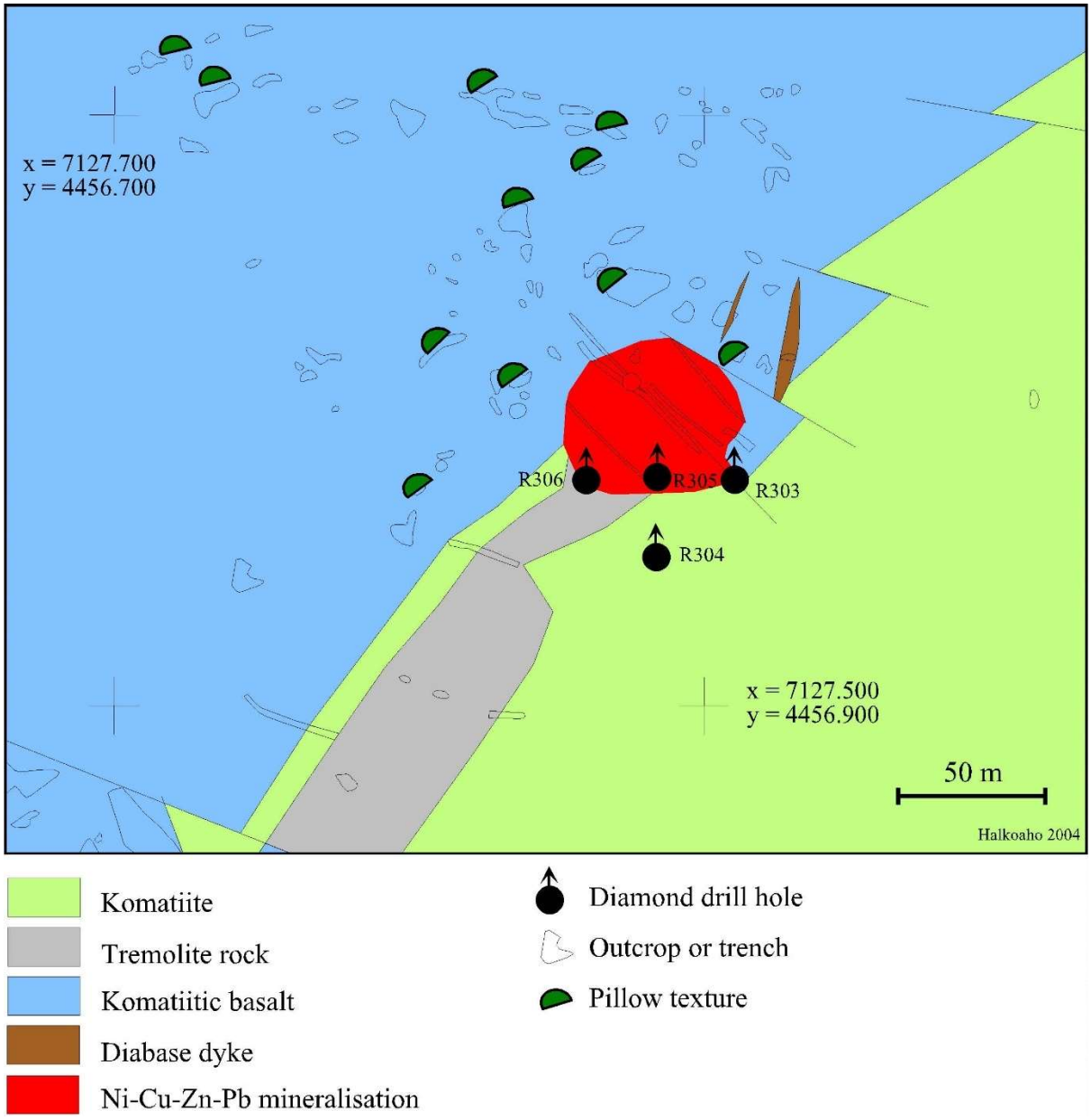

Figure 8. Geological map of the Siivikkovaara polymetallic deposit area, Kuhmo. Modified after Makkonen and Halkoaho (2007).

4. Previous work and scope of the present study

4.1. Background

Extensive efforts to understand the formation of komatiite-associated Ni-Cu-(PGE) sulfide deposits were carried out in the 1990's. In recent years, publishing on this topic has been declining. One of the important publications is the publication by Mercier-Langevin et al. (2012). This publication sums up the current knowledge in the literature and provides an in-depth perspective of the issues that are still to be resolved (Fig. 9).

Mercier-Langevin et al. (2012) reviewed komatiite-associated Ni-Cu-(PGE) sulfide deposits that illustrate the range of scales that must be taken into consideration when designing exploration strategies and targeting these deposits in their work entitled "A Special Issue on Archean Magmatism, Volcanism, and Ore Deposits: Part 1. Komatiite-Associated Ni-Cu-(PGE) Sulfide and Greenstone-Hosted Au Deposits". A number of different processes are important in the formation of magmatic Ni-sulfide deposits, determining the size of the deposits (Fig. 9). Ultramafic rocks are required in significant abundance and thickness to show the zones of high magma fluxes that are necessary for well-endowed belts and cratons according to Barnes and Fiorentini (2012). Vent-proximal areas with felsic rocks may also be associated with VMS that can provide S for sulfide saturation (Fiorentini et al. 2012). Country rocks can also act as contaminant and external source of S, but also as traps and/or barriers to magma delivery (Fig. 9), thus affecting the evolution of komatiitic systems (e.g., Heggie et al. 2012a, b). The post-magmatic evolution of Ni sulfide deposits during deformation and metamorphism is also critical to recognize (Collins et al. 2012). Understanding the metallogenic processes in Archean greenstone belts and comparing them to younger deposits formed in modern tectonic settings can provide further insights to the geologic processes during the Archean Eon.

Heggie et al. (2012a) argued that the rate of discovery of new deposits has been declining for the past 40 years because the deposits are challenging exploration targets due to their small size and lack of prominent alteration associated with the mineralizations. One of the methods used in exploration is lithogeochemistry of the chalcophile elements. These elements are closely related with the ore-forming process of these deposits (Lesher et al. 2001).

Heggie et al. (2012b) indicated that the spatial distribution of the chalcophile element signatures associated with mineralization provides valuable information into both magmatic and ore-forming processes. Chalcophile element is solid indicator to constrain Ni ore-forming

systems. Quantitative analysis of the magnitude of chalcophile element ore-forming signatures and constraining the spatial distribution of the signatures within dynamic subvolcanic-volcanic settings establishes the functionality of chalcophile element-based vectors towards locating the possible sulfide deposit.

Fiorentini et al. (2012) discussed another way for possible Ni exploration using sulfur isotopic data. They investigated the camp to district scale features that characterize the Agnew-Wiluna greenstone belt in Western Australia. Their work provides insights for application of sulfur isotopic data, which link these greenstone belt characteristics into a new ore-forming model, applicable to exploration in a great variety of scales.

Sulfur isotope data are an important means to identify the source of sulfur. The source of sulfur can be either the mantle or the crust, for nickel sulfides associated with komatiites and komatiitic basalts (Naldrett 1973, 1981, Naldrett and Turner 1977). Komatiites require a near-surface crustal sulfur source to form nickel sulfide mineralization. Regarding the concentration of PGEs in primitive komatiites, Fiorentini et al. (2010b) supported this idea, which based on PGE concentrations of komatiites, indicates that these magmas most likely reached surface and erupted sulfide undersaturated. Thus, to form a PGE rich deposit, external sources of PGE-rich sulfide are required. Bekker et al. (2009) used multiple sulfur isotope systematics concerning the S source of komatiite-hosted Ni-Cu-(PGE) deposits in the Norseman-Wiluna and Abitibi greenstone belts. The study confirmed that the S for these deposits was derived from country rock sulfide and not from mantle. Overall, sulfur isotopes are the key to understanding the source of the sulfur but utilization of this method in magmatic systems should be applied with caution. This is due to the fact that, isotopic signatures of crustal assimilation can be altered if silicate melt-sulfide melt mass ratios (R factor) are high enough.

Ikehata et al. (2014) described the mineralogy and geochemistry of the hydrothermal minerals in the seafloor hydrothermal mineralization of active hydrothermal fields in the southern Mariana Trough. Sulfur isotopic compositions of the study show a similar diversity with a mid-ocean ridge range for some of the samples and an island-arc range for another group of samples. These isotopic signatures may also be used in the thesis to specify the possible geotectonic setting of the mineralization, if the black smoker setting is independently constrained. The hydrothermal minerals from the Southern Mariana Trough show variable $\delta^{34}S$ values ranging from +0.8 to +8.5 ‰ (Ikehata et al. 2014).

Addressing these questions will broaden our knowledge on the formation of the komatiite-hosted sulfide ores. This is not important only for science, as deeper understanding of ore forming processes for komatiite-hosted Ni sulfide ores will help us define new metallogenic provinces to identify new deposits to secure the supply of commodities.

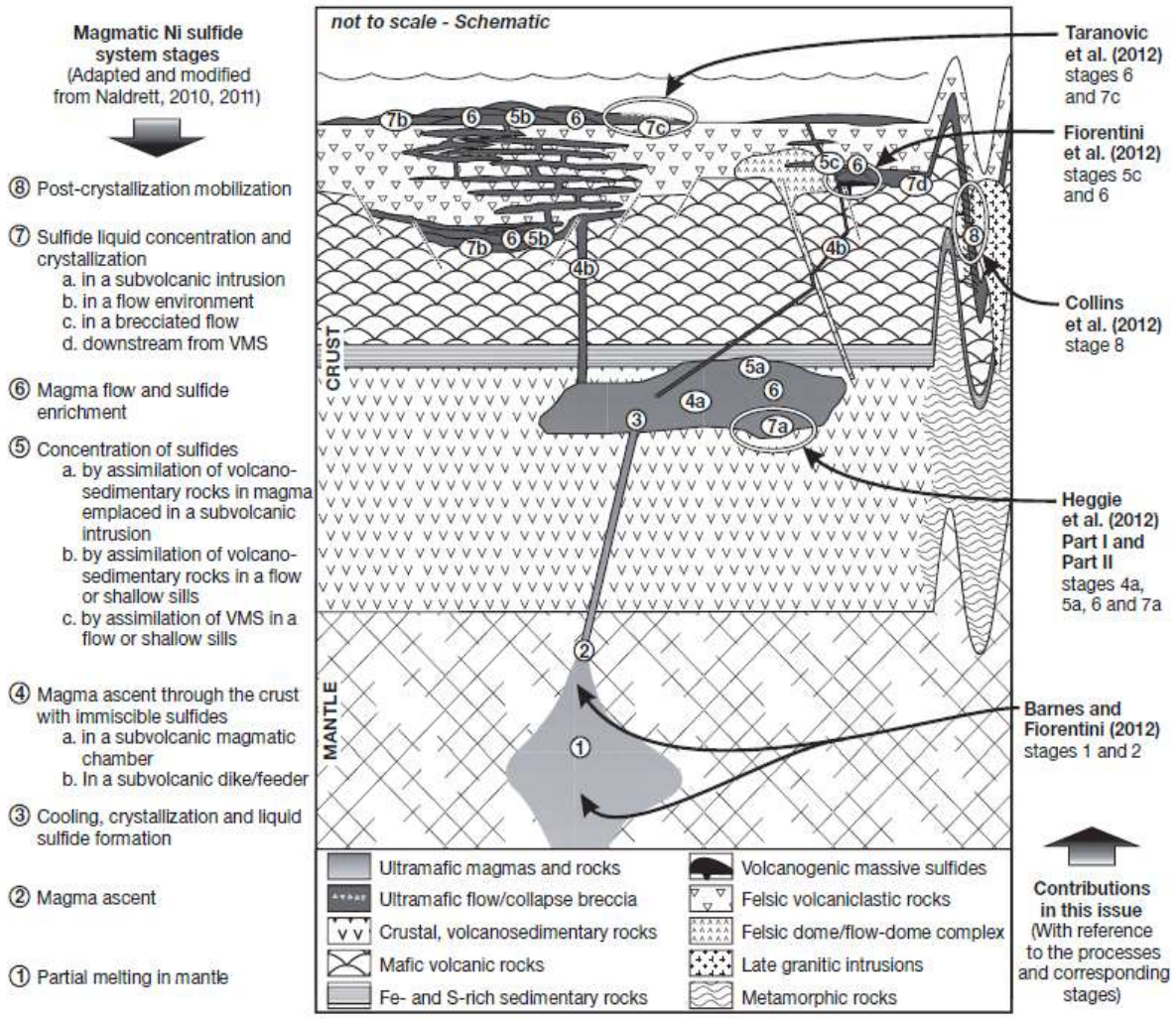

Figure 9. Schematic representation of the different types of a magmatic Ni sulfide system adapted from Naldrett (2011) and Houlé and Lesher (2011). The figure illustrates the contributions present in the literature and to which stage they refer.

4.2. Hypotheses and objectives

The goal of this thesis is to examine the Siivikkovaara Ni-Cu-Zn-Pb mineralized sulfide body, which is hosted by komatiite and komatiitic basalt in the Kuhmo greenstone belt, eastern Finland. The main hypothesis is that:

- The formation of the Siivikkovaara sulfide body may be linked to processes similar to those observed in modern black smokers. This hypothesis will be studied by analysing the hydrothermal alteration processes involved in the formation of the sulfide body. The isotope composition of sulfur ($\delta^{34}S$ values) and trace element of the sulfides in the mineralized body have been measured in order to assess mass contributions from the komatiites and komatiitic basalts surrounding the body and from pre-existing seawater, thus providing a potential link to the modern analogue.

In addition to the main hypothesis above:

- According to (Mercier-Langevin et al. 2012), the source of sulfur in komatiite-hosted sulfide ores and how specific sulfur sources influence the formation of komatiite-hosted sulfide deposits need to be studied in more detail utilizing the isotopic composition of sulfur ($\delta^{34}S$ values). The data in the current study will be used to make a contribution to this end.

As stated above, one of the issues discussed in this study, is whether the mineralized body can be related with processes inherent in modern black smokers. Archean volcanic-hydrothermal systems precipitated most sulfides in the discharge zone near the sea floor in an anoxic, sulfate-limited ocean, consistent with observations from Archean VMS deposits (Hannington et al. 1999). These processes are similar to modern hydrothermal vents. Thus, volcanic hydrothermal sulfide accumulations associated with active volcanism would have been the most abundant source of crustal sulfur during the Archean.

Therefore, emplacement of komatiite magmas in environments where submarine hydrothermal sulfides were relatively abundant in syngenetic or slightly older volcanic sequences appears to be the key to formation of komatiite-hosted Ni-Cu-(PGE) deposits in the Agnew-Wiluna greenstone belt. The geological setting of the Kuhmo greenstone belt can be related with the Agnew-Wiluna greenstone belt and thus studies from similar formations will be a guideline for the research that will be carried out in my thesis.

5. Materials and Methods

The mineralized Siivikkovaara body has been penetrated by four deep drill holes with depths varying from 64.5 to 117.55 m. Drill core material has been recovered from the Loppi drill core repository of the Geological Survey of Finland (GTK) (Appendix 1). Field work was carried out during October 2019 to sample the tremolite rock present in the area to further examine the relationship of the komatiite and komatiitic basalt and the Siivikkovaara mineralization.

Drill core material has been recovered from the Loppi drill core repository of the GTK. During the sampling, emphasis was given to ensure an adequate protolith-mineralized rock sample set for analysis of the alteration mass budget Silicates and sulfides from the mineralized body have been analysed using optical mineralogy. Whole-rock, major and trace element geochemical analyses have been carried out in order to examine the geochemical signatures of the komatiite/komatiitic basalt protolith vs. the mineralized body. The isotope composition of sulfur ($\delta^{34}S$ values) and trace elements values of the sulfides in the mineralized body have been measured in order to assess mass contributions from the komatiites and komatiitic basalts surrounding the body and from pre-existing sea water. The expected values of the $\delta^{34}S$ in ancient seafloor hydrothermal systems, prior to 2.4 Ga (the onset of oxygen in the atmosphere), show minor variations and cluster near 0‰. The near 0‰ $\delta^{34}S$ values would be another indicator of the Archean origin of the mineralization.

The results of this study will also have effects beyond academia. Further understanding of Archean komatiite hosted sulfide deposits can have profound effects on their exploration strategies. Thus, new frontiers in ore forming processes can specify new metallogenic provinces, which are needed in order to satisfy out ever increasing demand in commodities hosted by Archean komatiite sulfide deposits.

The isotope composition of sulfur of the sulfides in the mineralized body has been measured in the current study to assess mass contributions from the komatiites and komatiitic basalts surrounding the body and from pre-existing sea water.

5.1. Petrography

All thin sections were produced at the GTK's thin section lab in Kuopio. The mineralogy of the samples has been studied using optical microscopy for silicates and sulfides (Table 1).

Table 1. Thin sections with sulfide minerals, studied under reflective light microscope.

Sample code	Thin section ID	Sulfides
M52/4411/83/303_4.65m	190040	Chalcopyrite, pyrrhotite, pentlandite, sphalerite
M52/4411/83/304_34.80-35.00m	190047	Chalcopyrite, pyrrhotite, pentlandite
M52/4411/83/304_36.1m	190048	Chalcopyrite, pyrrhotite, pentlandite
M52/4411/83/304_36.4m	190049	Chalcopyrite, pyrrhotite, pentlandite, sphalerite
M52/4411/83/304_37.5m	190050	Chalcopyrite, pyrrhotite, pentlandite, sphalerite
M52/4411/83/305_9.55m	190056	Chalcopyrite, pentlandite, sphalerite
M52/4411/83/305_12.30m	190057	Chalcopyrite, pyrrhotite, pentlandite, sphalerite
M52/4411/83/305_15.00m	190058	Chalcopyrite, pentlandite, sphalerite
M52/4411/83/306_3.80m	190061	Chalcopyrite, pyrrhotite, pentlandite, sphalerite, violarite
M52/4411/83/306_14.90-15.0m	190062	Chalcopyrite, pyrrhotite, pentlandite, sphalerite, violarite

5.2. Geochemistry

The major and trace element geochemistry of the rocks has been analysed using X-ray fluorescence (XRF), Graphite furnace atomic absorption spectroscopy (GFAAS), Inductively coupled plasma - optical emission spectrometry (ICP-OES) and Inductively coupled plasma - mass spectrometry (ICP-MS) from major and trace elements (Appendix 3). All analyses were carried out in Labtium Oy laboratories in Kuopio and Sodankylä. X-ray fluorescence (XRF) analyses for major and selected trace elements were done using method 175X (https://labtium.fi/wpcontent/uploads/2017/07/Labtium_Sample_preparation_and_analytical_

methods.pdf). In these methods the analyses are made on pressed powder pellets. Trace element geochemistry analyses have been carried out using ICP-MS. REE element analyses were done using method 308M (https://labtium.fi/ wpcontent/ uploads / 2017 / 07 / Labtium_Sample_preparation_and_analytical_methods.pdf). This method is a destructive analytical method using HF–$HClO_4$digestion. Method 705U (https://labtium.fi/ wpcontent/ uploads/ 2017/07/ Labtium_Sample_preparation_and_analytical_methods.pdf) with GFAAS was used for the precious metals (Au, Pd, Pt) and whole PGE-group analyses. Carbon was determined by carbon analyser combustion technique (method 811L). ICP-OES analytical technique308P(https://labtium.fi/wpcontent/uploads/2017/07/Labtium_Sample_preparation_and_analytical_methods.pdf) was used to analyse the samples for Co, Sc, V, Y and Zr, also using HF–$HClO_4$ digestion. All compositions have been plotted against chondrite-normalized REE (Boynton 1984) diagrams and multi-element diagrams (Sun 1982 and Barnes et al. 1988). Plotting the geochemical results on these diagrams is a key method to understand the relative enrichment or depletion of the mineralized samples in chemical elements relative to reference values.

5.3. Isotope and trace element geochemistry

5.3.1. Multicollector LA-ICP-MS S^{34} analysis

Sulfur is a useful tool in isotope geochemistry. It is the most abundant element of sulfide minerals and provides insights into the origins of these minerals through its stable isotopes, with variations in the isotopic composition of sulfide minerals and related compounds caused by the process of fractionation at focus. These variations form because of differences in temperature, oxidation and reduction reactions that fractionate the different isotopes of sulfur. Sulfur has stable isotopes of ^{32}S, ^{33}S, ^{34}S and ^{36}S. Here, I will use $\delta^{34}S$ (Equation 1) to examine the connection between modern black smokers and the Siivikkovaara mineralized body.

The isotope composition of sulfur ($\delta^{34}S$) in the sulfides of the mineralized body was measured to assess mass contributions from the komatiites and komatiitic basalts surrounding the body and from pre-existing sea water. Sulfur isotopes analysis of sulfide minerals was performed using a Nu Plasma HR multicollector ICP-MS at the Geological Survey of Finland in Espoo mounted to a Photon Machine Analyte G2 laser microprobe (Table 2). Samples were ablated in He gas (gas flows = 0.4 and 0.1 l/min) within a HelEx ablation cell (Müller et al. 2009). S isotopes were analysed at medium resolution. During the ablation the data were collected in

static mode (^{32}S, ^{34}S). Single spot samples were ablated at a spatial resolution of 30 micrometers, using a fluence of 1.5 J/cm^2 and at 5 Hz on thin sections. The total S signal obtained was between 0.5 and 2.0 V. Under these conditions, after a 20 s baseline, 50-60 s of ablation is needed to obtain an internal precision of $^{34}S/^{32}S \leq \pm 0.000005$ (1 SE). One pyrite standard has been used for external standard bracketing (PPP-1, Gilbert et al. Journal of Analytical Atomic Spectrometry, 2014) and the house standards Py 2 have been used for quality control. The in-house pyrite standard Py 2 have been previouly measured by gas mass spectrometry. For a $\delta^{34}S_{CDT}$(‰) reference value of -0.3 ± 0.3 ‰ (1σ) we have found an average value of -0.2 ± 0.3 ‰ (1σ, n=4). One Chalcopyrite (Cpy1) in house standard while another one has been used for quality control. The in-house chacopyrite standard Cpy 2 has been previouly measured by gas mass spectrometry. For a $\delta^{34}S_{CDT}$(‰) reference value of -0.7 ± 0.5 ‰ (1σ) we have found an average value of -0.8 ± 0.2 ‰ (1σ, n=8).

Table 2. MC-ICP-MS instrumentation for S isotope analyses

Instrument	Nu Plasma HR multicollector ICPMS
Laser type	Photon Machine Analyte G2 laser microprobe
Energy density	1.5 J/cm^2
Repetition rate	5Hz
Gas flow (He)	0.4 and 0.1 l/min
Pulse duration	20 s baseline, 50-60 s of ablation
Spot diameter	30μm

Multicollector ICP-MS (MC-ICP-MS) allows for simultaneous collection of all stable sulfur isotopes, decreasing the effect of fluctuations in the plasma on the measured. Isotopic compositions are usually reported using the δ notation (‰) in the general form:

Equation 1:

$$\delta^{34} S_{sample} = \left(\left(R_{sample}/R_{CDT}\right) - 1 \right) \times 1000$$

$R_{sample} = {}^{34}S/{}^{32}S$

The isotopes that are commonly measured are ^{34}S and ^{32}S, simply because these are the two most abundant of the four sulfur isotopes, thus the term $R = {}^{34}S/{}^{32}S$. All $\delta^{34}S$ values are reported relative to the CDT standard, or Cañon Diablo Troilite (Ault and Jensen 1963) by the standard equation 1 defining delta.

5.3.2. LA-ICP-MS sulfide trace element analysis

Trace element analysis was carried out using the Coherent GeoLas MV 193 nm laser connected to an Agilent 7900s ICP mass spectrometer at the Environmental and Mineralogical Laboratories (HelLabs) at the Department of Geosciences and Geography, University of Helsinki. Laser ablation was performed with a constant 10 Hz pulse rate with an energy fluence of 7 J/cm^2 and a spot diameter of 30-44 μm depending on the material analysed. The ablated material was transported using a constant He gas flow at 1.050 l/min and mixed with Ar 850 ml/min in a cyclone coaxial mixer prior to entering the ICP torch to be ionized. The ions are then sampled, accelerated and focused before being separated and analysed in the quadrupole mass spectrometer. A set of 42 isotopes was analysed with the dwell time for each mass set at 10 ms. All analysed samples were normalized to Fe^{57} as internal standard. The isotopes of chalcopyrite, pyrrhotite, pentlandite and sphalerite were calculated to USGS sulphide standard MASS-1 as an external standard, the remaining elements were calculated using BHVO-2G as an external standard. The instrument was calibrated using SRM NIST610, analysing SRM NIST612 as unknown. For the analysis period of our samples, the standard error is <5 % for most elements with the exception of Sc (7%) and MREE and HREE (<10%). Repeated analysis of MASS-1 (n=8) corrected using BHVO-2G have errors of less than 3 % for Mn, Fe, Co, Ni, Cu, and Pb (<5%) relative to accepted values published in GEOREM. The reproducibility for Al, Ti, Cr, Mn, Co, Ni, Cu, Zn, Ga, Ge, Mo, Sn, Ta, and Pb elements is <5%. We note however, that few accepted published values are available for MASS-1 (GEOREM) and generally our reproducibility and accuracy for BHVO-2G measured as unknown is better than 7% for most elements.

The measured elements were normalized to Fe^{57}. The Se/Fe, Co/Fe, Ni/Fe and Ge/Fe ratios are reasonably constant. Results indicate that Fe is a much more suitable choice as internal standard compared to S. As observed by Gilbert et al. (2014), significant fractionation of S relative to Fe occurs in all sulfides during LA-ICP-MS analyses. Due to machine problems we could not analyse the major element compositions of the sulphides not allowing for an external standardization. Hence, we are limiting our in-situ dataset to trace element ratios rather than concentrations.

Table 3. LA-ICP-MS instrumentation for trace element analysis

Instrument	Agilent 7900s ICP-MS
Laser type	Coherent GeoLas MV 193 nm laser
Energy density	7 J/cm^2
Repetition rate	10 Hz
Gas flow (He, Ar)	1.050, 0.850 l/min
Pulse duration	40 s background, 40 s of ablation
Spot diameter	30-44 μm

6. Results

6.1. Petrography of silicate minerals

All the studied rock types have undergone a degree of metamorphism but in some cases, the primary textures can still be observed in thin sections, e.g. variolitic texture (Fig. 11). The main mineral assemblages of the studied komatiites (Fig. 12), komatiitic basalts (Figs. 10, 11, 13), and tremolite rocks are: actinolite, plagioclase, tremolite and chlorite with carbonate minerals, biotite, tourmaline and epidote as accessory mineral phases. Veining is a major feature in many thin sections. Veins are mostly comprised of carbonate minerals and plagioclase. Veining in the samples occurred in more than one event due to the crosscutting of the veins (Fig. 10). In places, some textural characteristics give the impression of them being the recrystallization products of pyroxene grains. Tourmaline is main mineral phase in one of the thin sections studied (Fig. 13). Opaque minerals are present as weak sulfide dissemination.

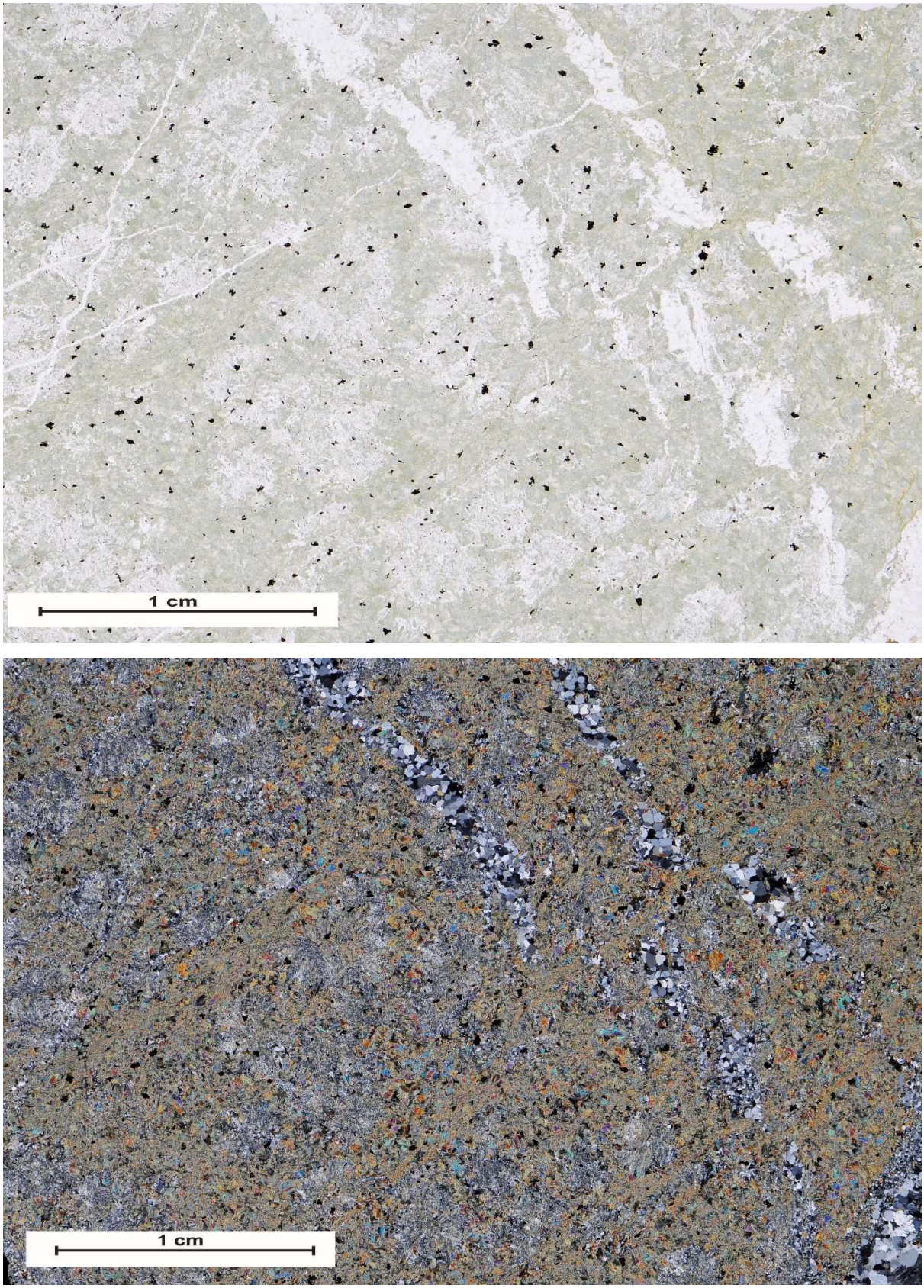

Figure 10. Photomicrograph of fine-grained komatiitic basalt. In this sample veining is a profound characteristic of the komatiitic basalt. Sample code: M52/4411/83/305_60. Mineral assemblage of the sample is comprised of actinolite, plagioclase, and opaque minerals. Upper image in plane-polarized light, lower in cross-polarized light.

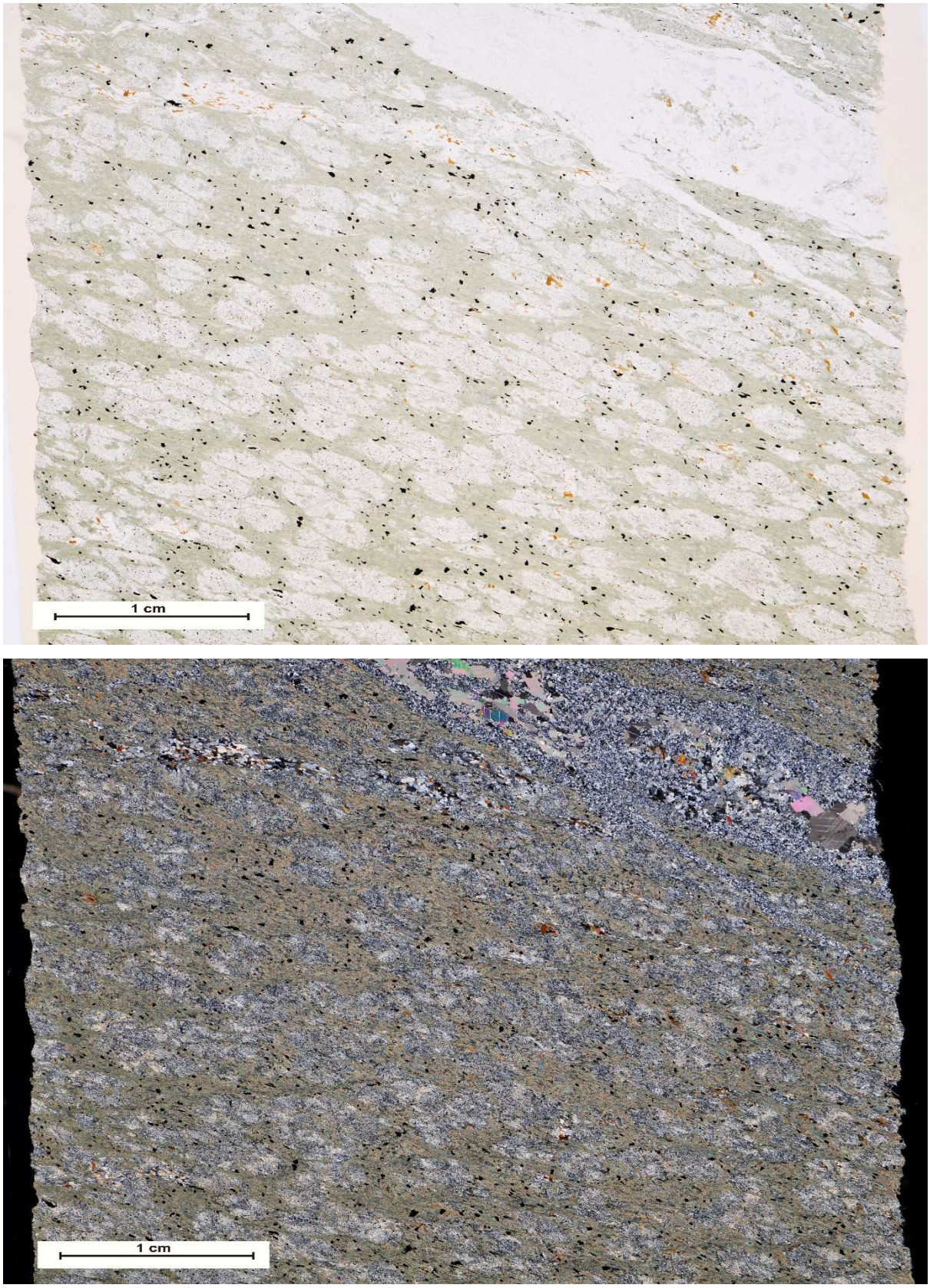

Figure 11. Photomicrograph of fine-grained komatiitic basalt with variolitic texture. Sample code: M52/4411/83/306_88.30. Mineral assemblage of the sample is comprised of actinolite, plagioclase, carbonate minerals, biotite, chlorite and opaque minerals. Upper image in plane-polarized light, lower in cross-polarized light.

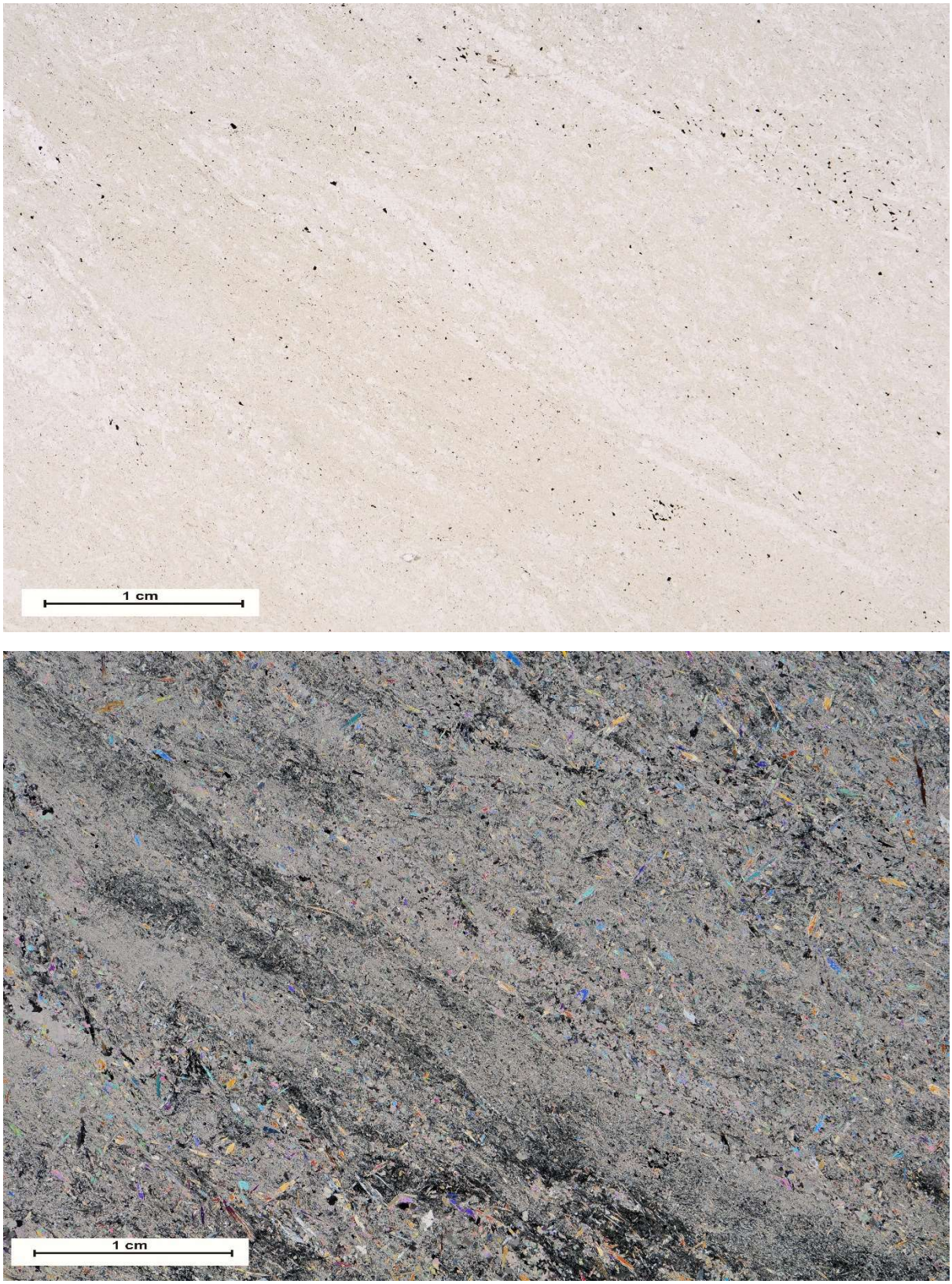

Figure 12. Photomicrograph of fine-grained komatiite. Sample code: M52/4411/83/304_33.15. Mineral assemblage of the sample is comprised of actinolite, chlorite and opaque minerals. Upper image in plane-polarized light, lower in cross-polarized light.

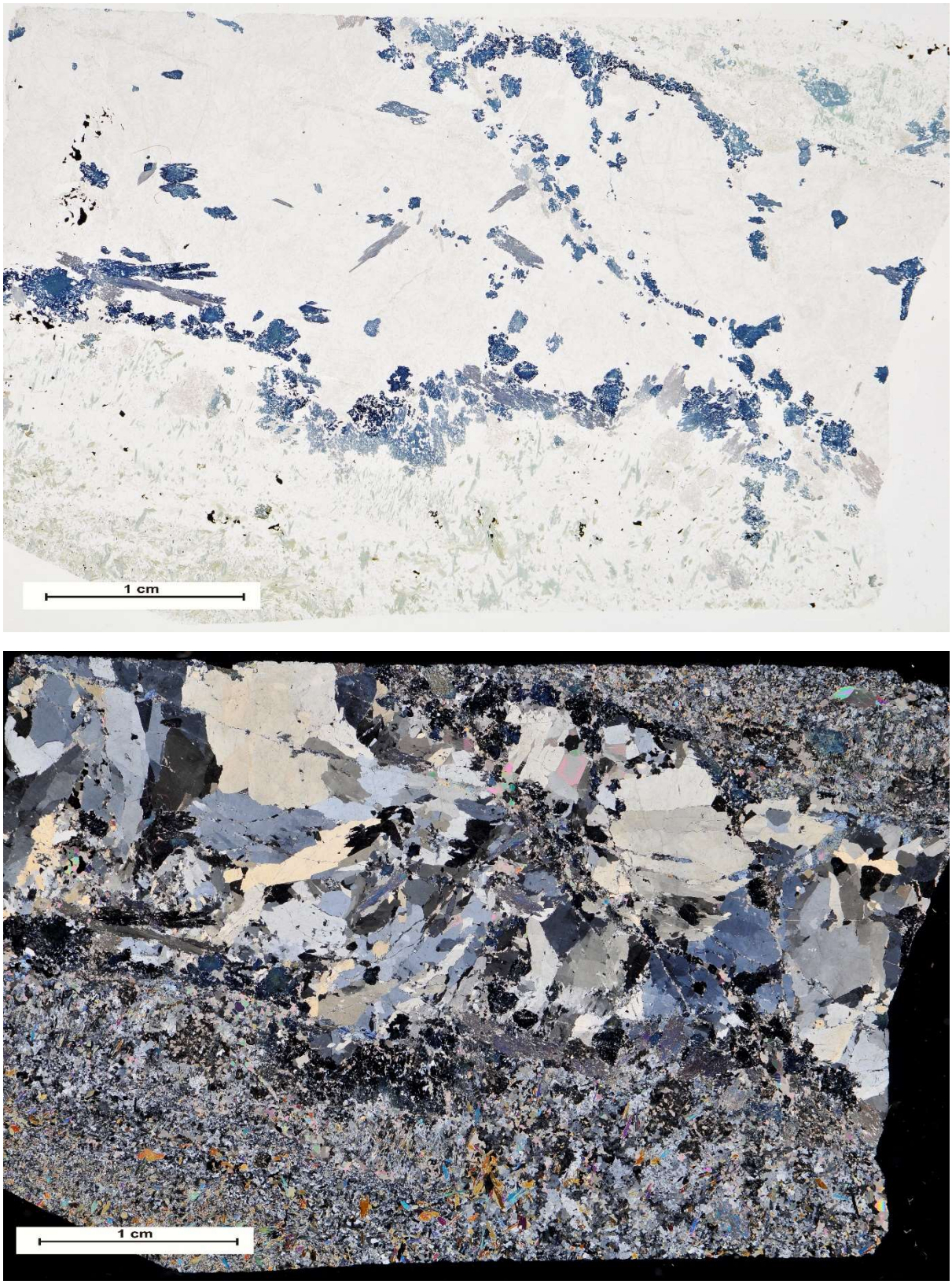

Figure 13. Photomicrograph of komatiitic basalt, with coarse grained tourmaline bearing vein. Sample code: M52/4411/83/303_71. Mineral assemblage of the sample is comprised of plagioclase, epidote, actinolite, tourmaline, garnet, carbonate and opaque minerals. Upper image in plane-polarized light, lower in cross-polarized light.

6.2. Petrography of sulfide minerals

Ten thick sections (Table. 1) with sulfide bearing phases were studied. Textural types range from traces of small disseminated grains to large sulfide grains. Chalcopyrite and pyrrhotite are the main sulfide phases in the studied samples. Pentlandite, sphalerite and violarite are present as accessory phases. Violarite is a supergene sulfide mineral associated with the weathering and oxidation of primary pentlandite nickel sulfide ore minerals (Figs. 14, 18). Intergrowths of chalcopyrite, pyrrhotite, pentlandite and sphalerite are common and can be observed in many samples (Figs. 15, 16, 17). The grain size of the sulfides has great variation in size, from disseminated μm size to macroscopic sulfides. The majority of sulfides are found in association with chalcopyrite and as individual grains composed of the mentioned sulfide phases.

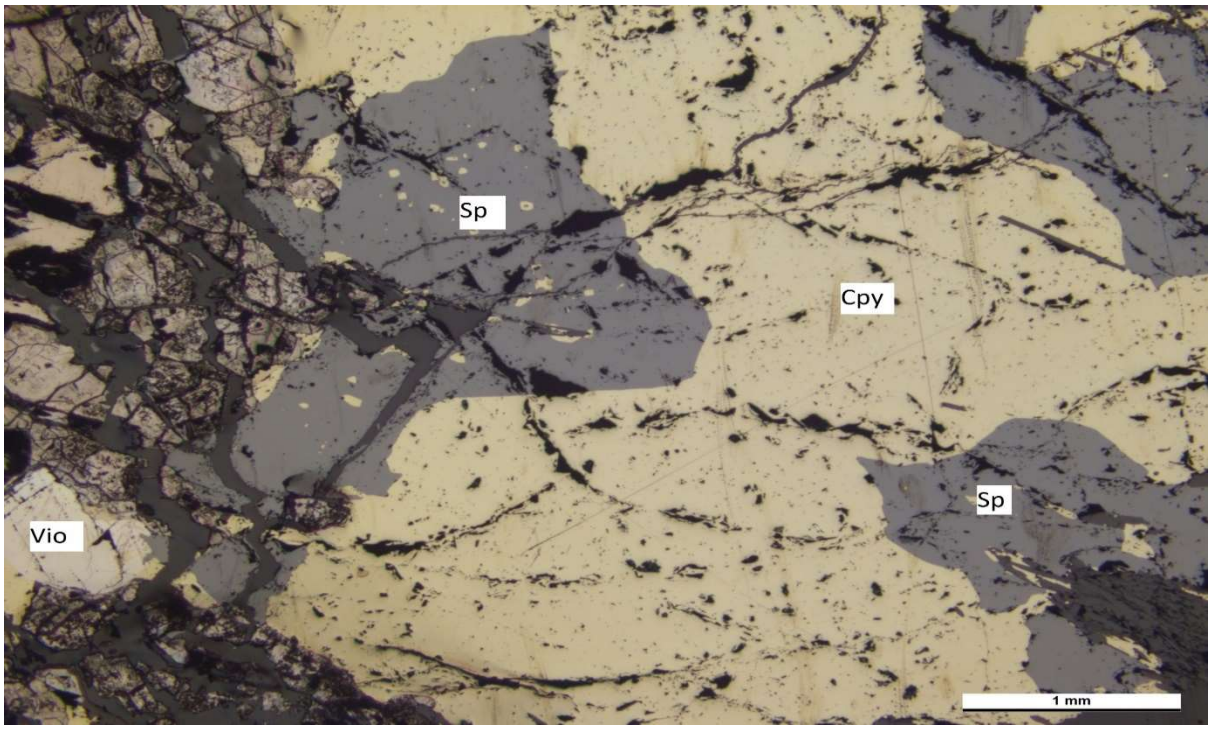

Figure 14. Photomicrograph under reflective light of fractured of chalcopyrite, sphalerite and secondary violarite in sample M52/4411/83/303_4.65m. cpy = chalcopyrite, sp = sphalerite, vio = violarite.

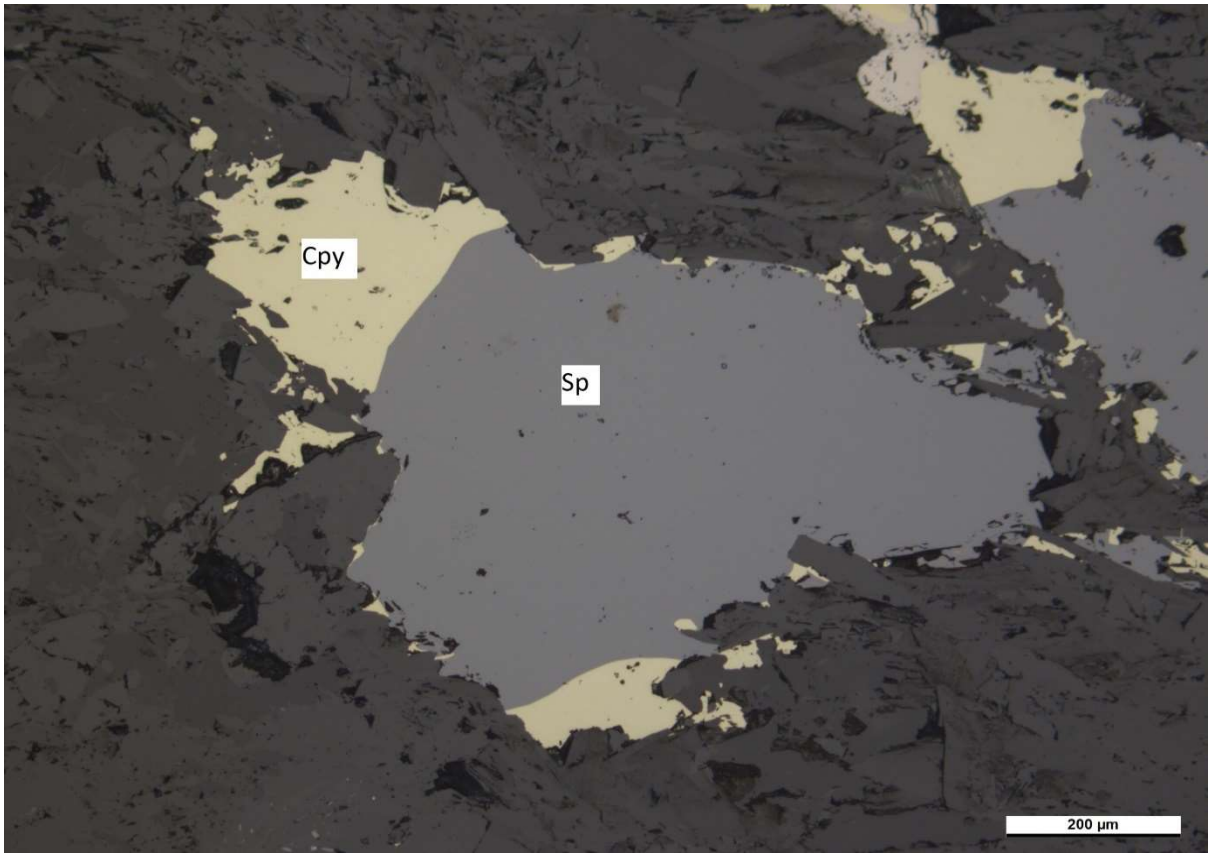

Figure 15. Photomicrograph under reflective light of chalcopyrite and sphalerite in sample M52/4411/83/303_4.65m. cpy = chalcopyrite, sp = sphalerite.

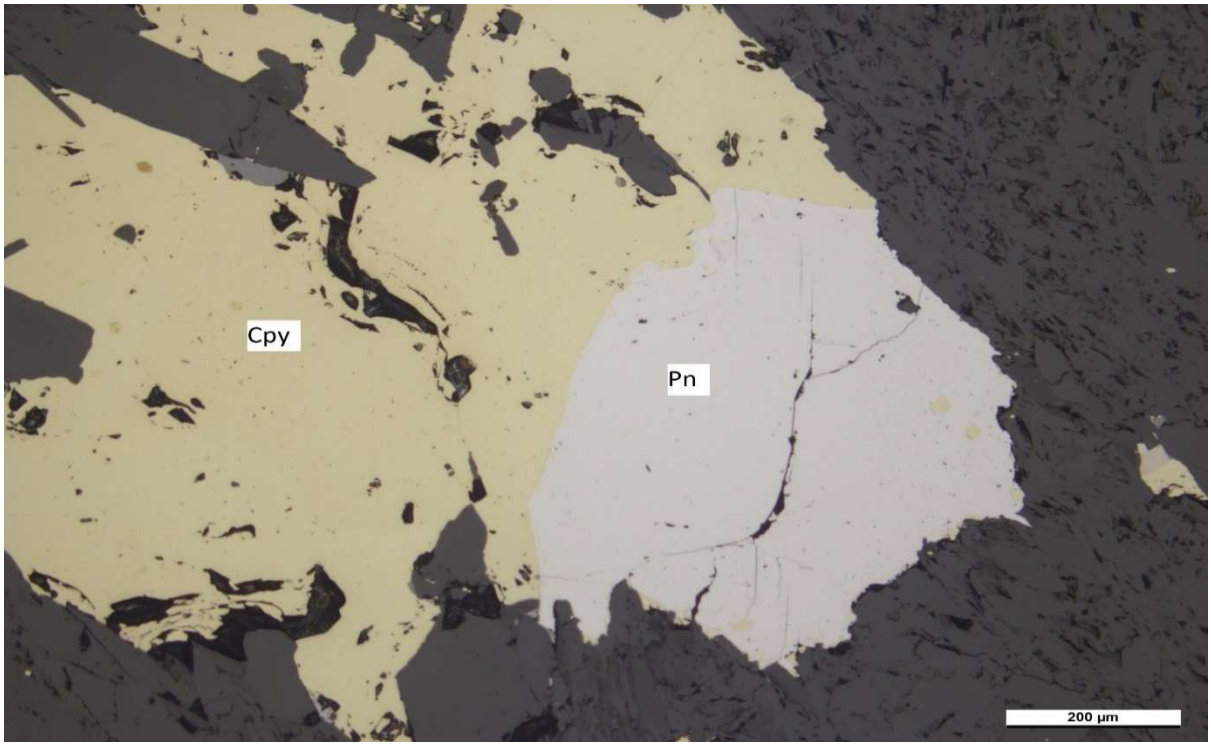

Figure 16. Photomicrograph under reflective light of chalcopyrite and pentlandite in sample M52/4411/83/303_4.65m. cpy = chalcopyrite, pn = pentlandite.

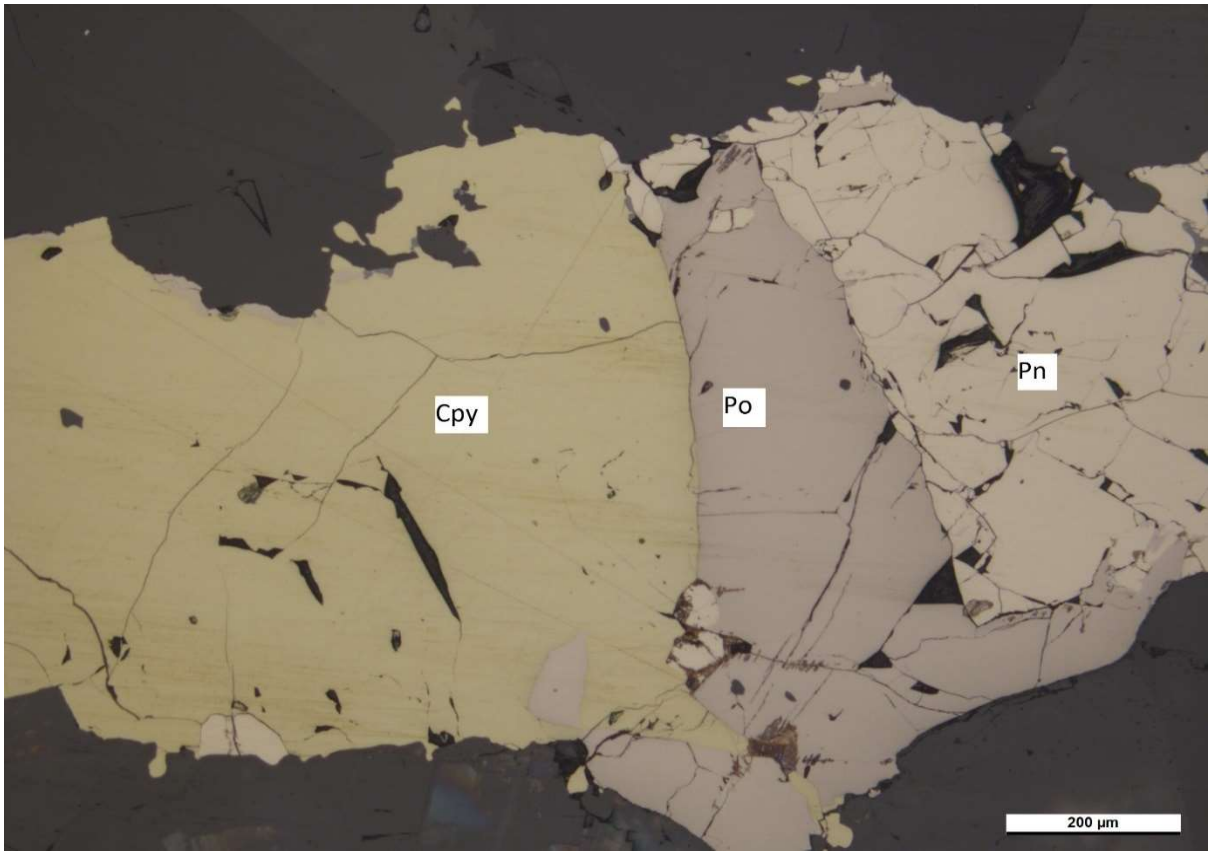

Figure 17. Photomicrograph under reflective light of chalcopyrite, pyrrhotite and pentlandite in sample M52/4411/83/304_34.80-35.00m. cpy = chalcopyrite, po = pyrrhotite, pn = pentlandite.

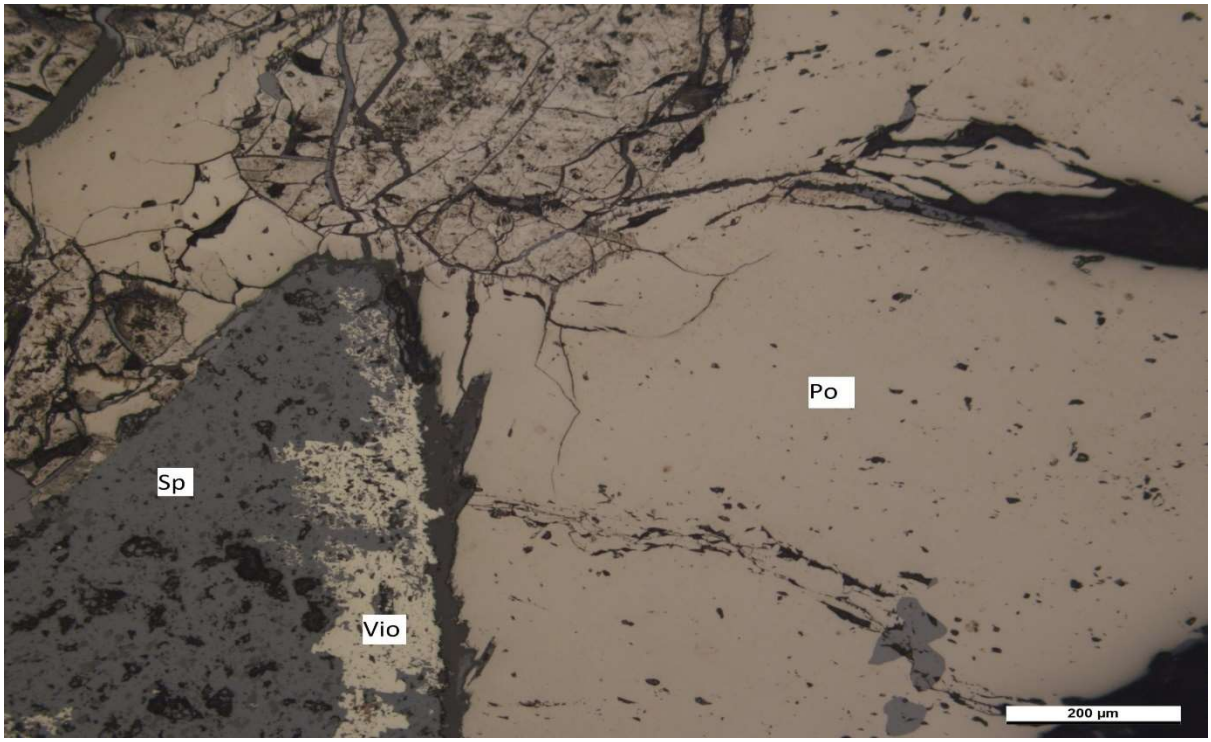

Figure 18. Photomicrograph under reflective light of fractured of pyrrhotite, sphalerite and secondary violarite in sample M52/4411/83/306_14.90-15.0m. po= pyrrhotite, sp = sphalerite, vio = violarite.

6.3. Mineral chemistry

6.3.1. LA-ICP-MS sulfide trace element geochemistry

A total of 119 points were analysed. In the absence of internal standards, we used ratios to present our data (Appendix 2). The sulfide phases analysed in the LA-ICP-MS where chalcopyrite, pyrrhotite, pentlandite and sphalerite. Typical time–signal diagrams for the sulfides are presented below in Figs. 19, 20, 21, 22.

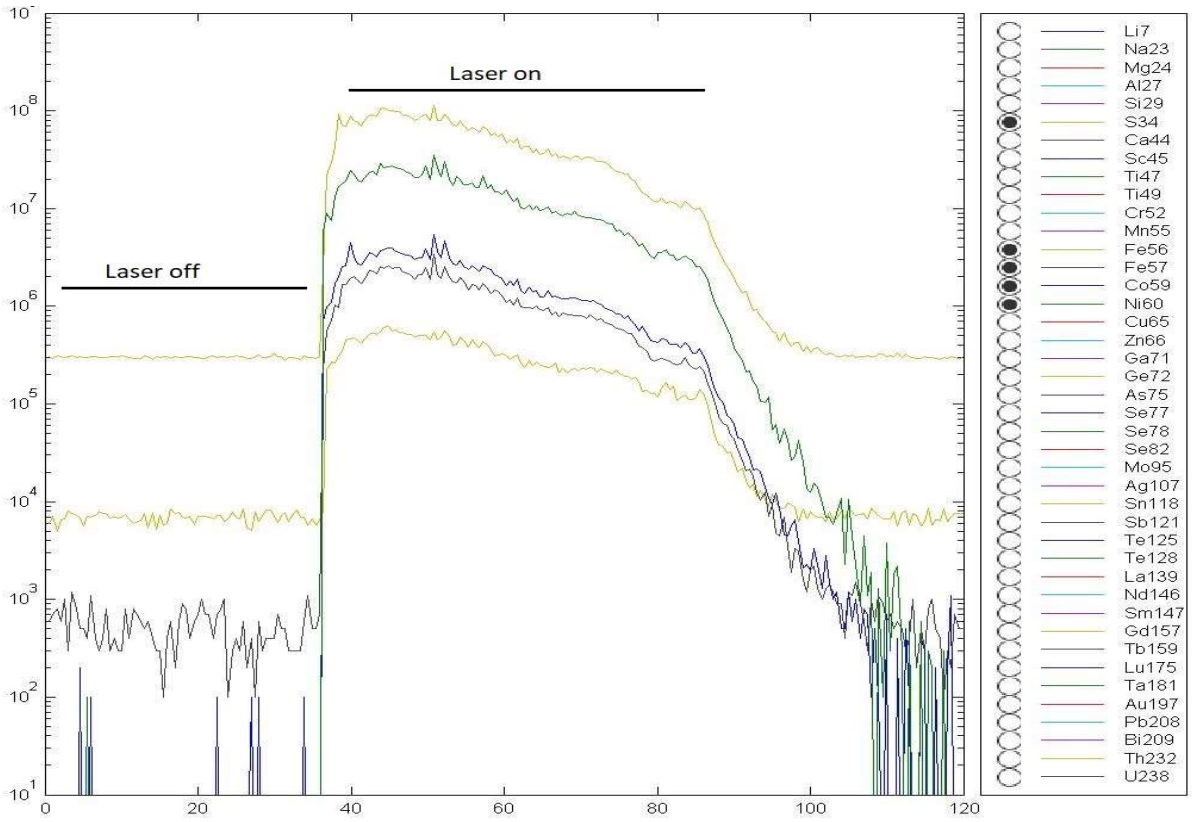

Figure 19. Typical examples of time(s) – signal(counts) diagrams showing trace element distribution in pentlandite. Spikes in the patterns are small inclusions in the minerals. Elements in the presented diagram are S^{34}, Fe^{56}, Fe^{57}, Co^{59} and Ni^{60}.

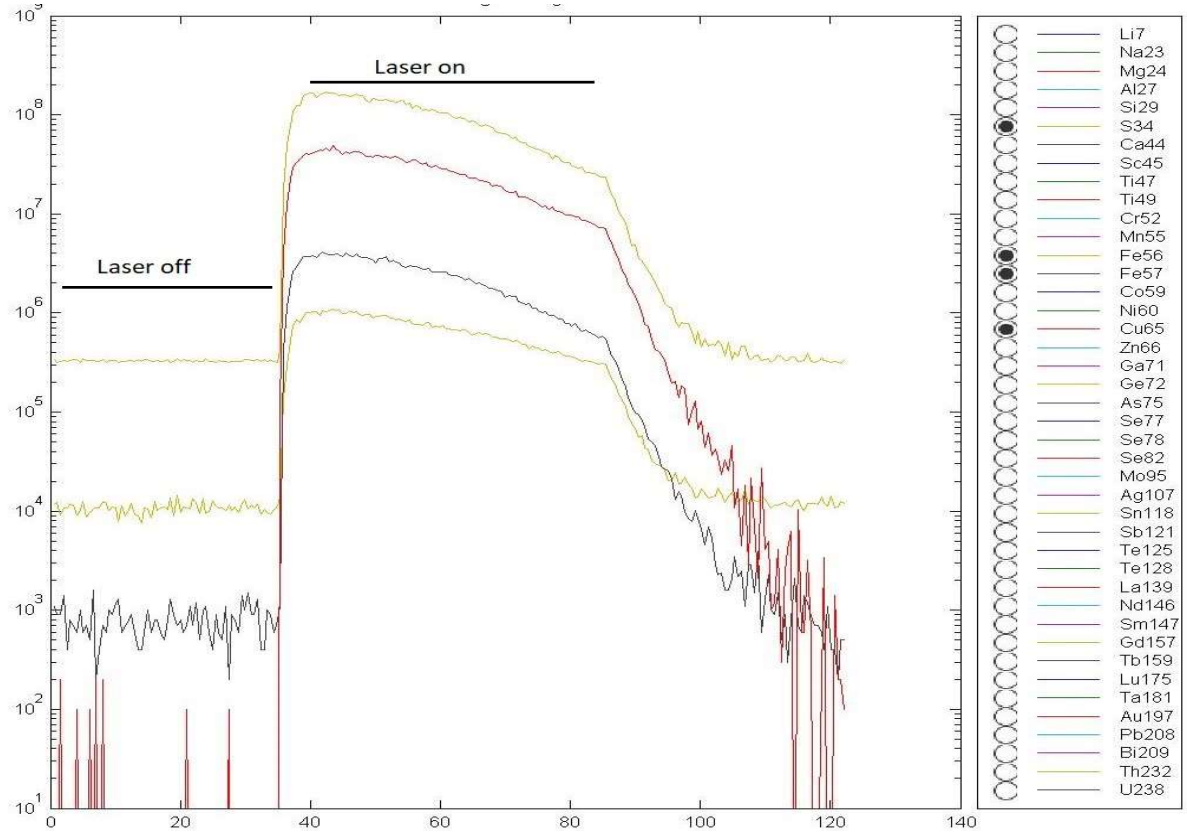

Figure 20. Typical examples of time(s) – signal(counts) diagrams showing trace element distribution in chalcopyrite. Elements in the presented diagram are S^{34}, Fe^{56}, Fe^{57} and Cu^{65}.

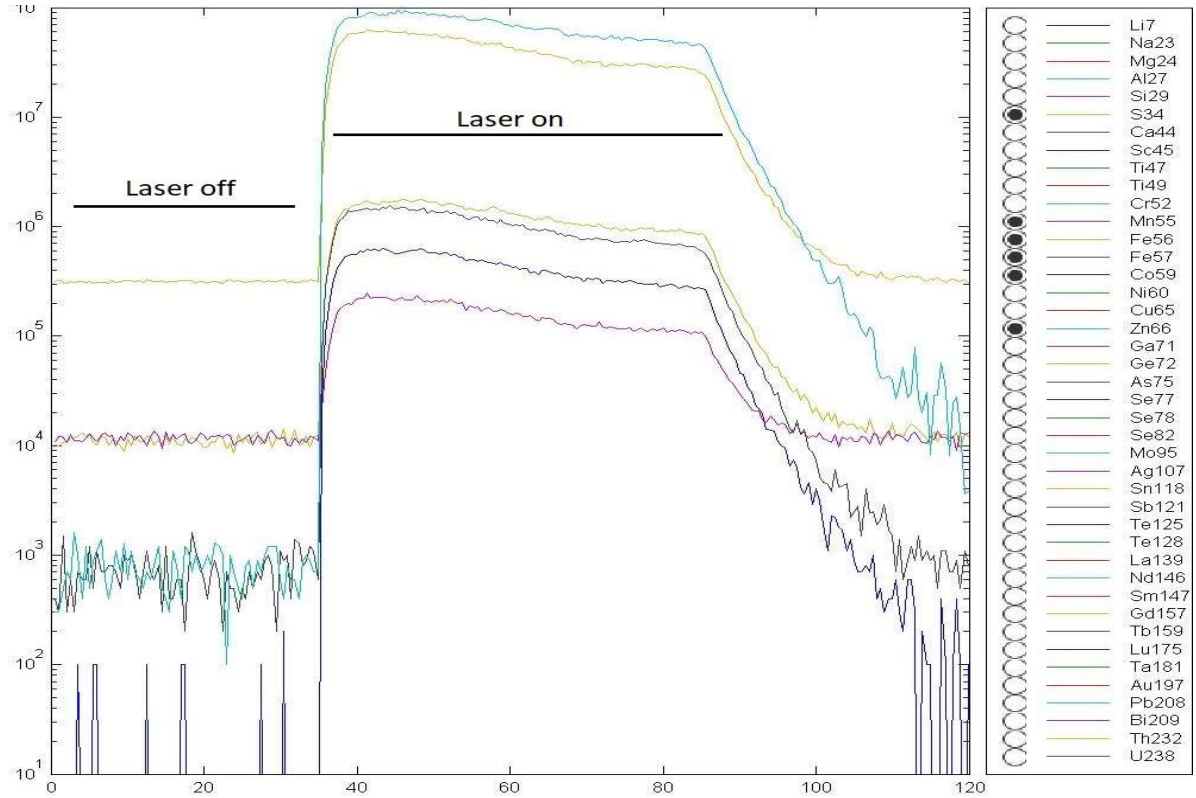

Figure 21. Typical examples of time(s) – signal(counts) diagrams showing trace element distribution in sphalerite. Elements in the presented diagram are S^{34}, Mn^{55}, Fe^{56}, Fe^{57}, Co^{59} and Zn^{66}.

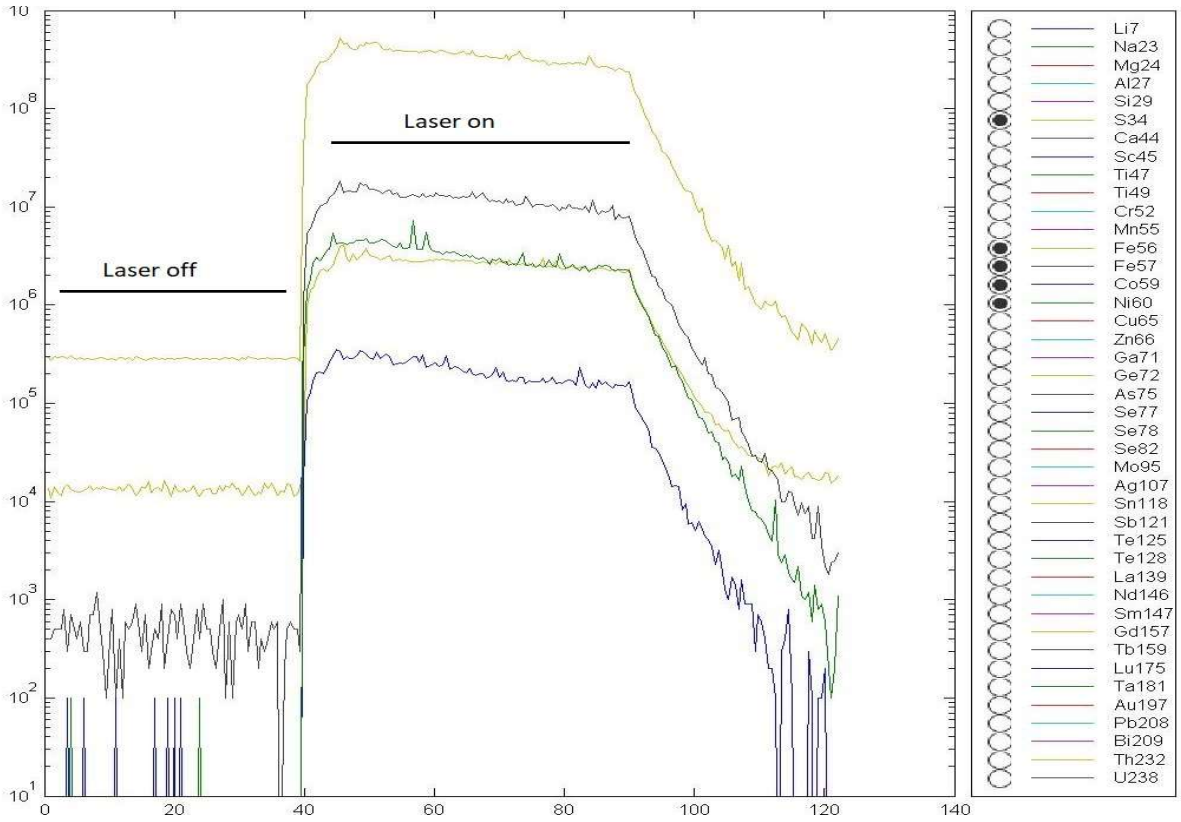

Figure 22. Typical examples of time(s) – signal(counts) diagrams showing trace element distribution in pyrrhotite. Elements in the presented diagram are S^{34}, Fe^{56}, Fe^{57}, Co^{59} and Ni^{60}.

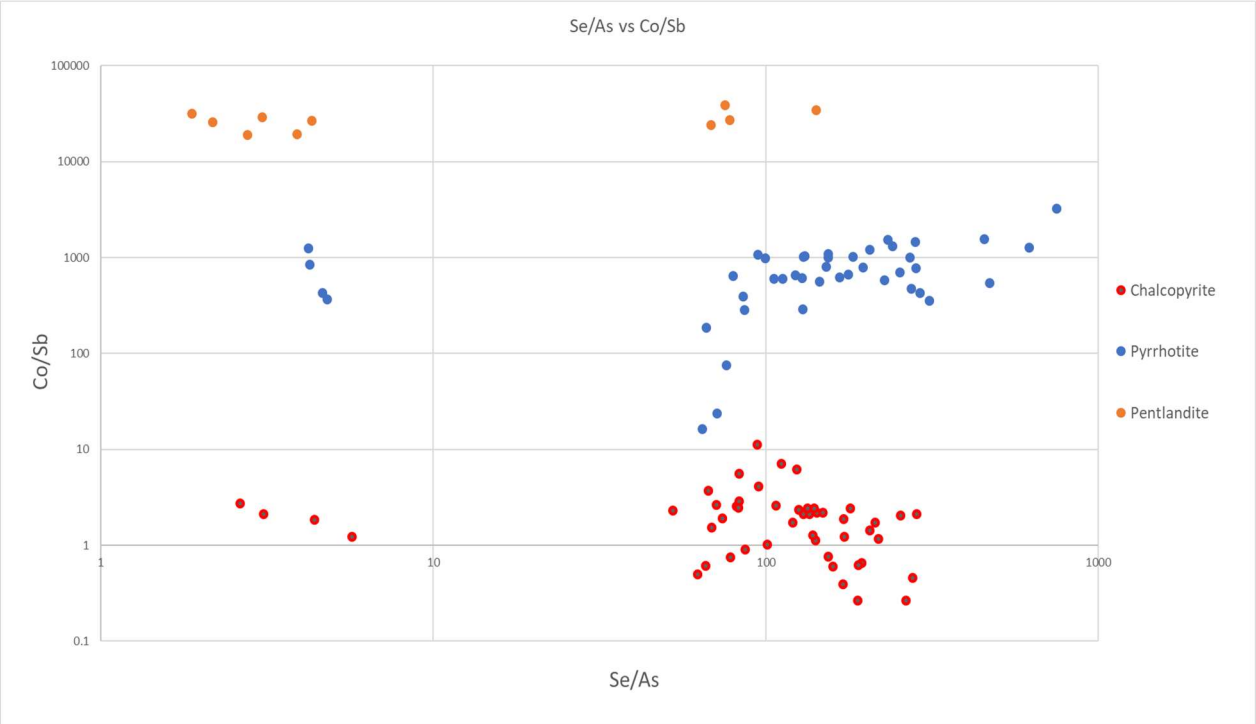

Figure 23. Diagram based on the sulfide trace element chemistry ratio of Se/As vs. Co/Sb.

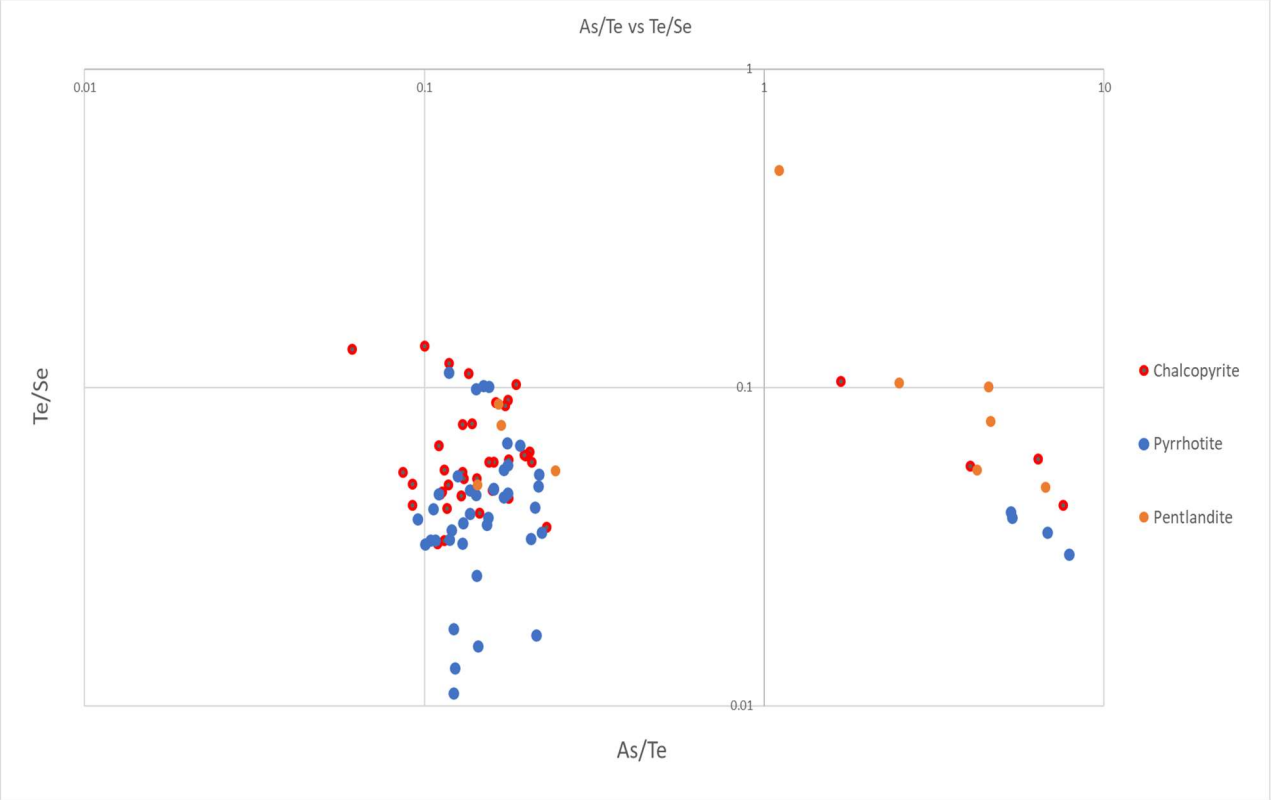

Figure 24. Diagram based on the sulfide trace element chemistry ratio of As/Te vs. Te/Se.

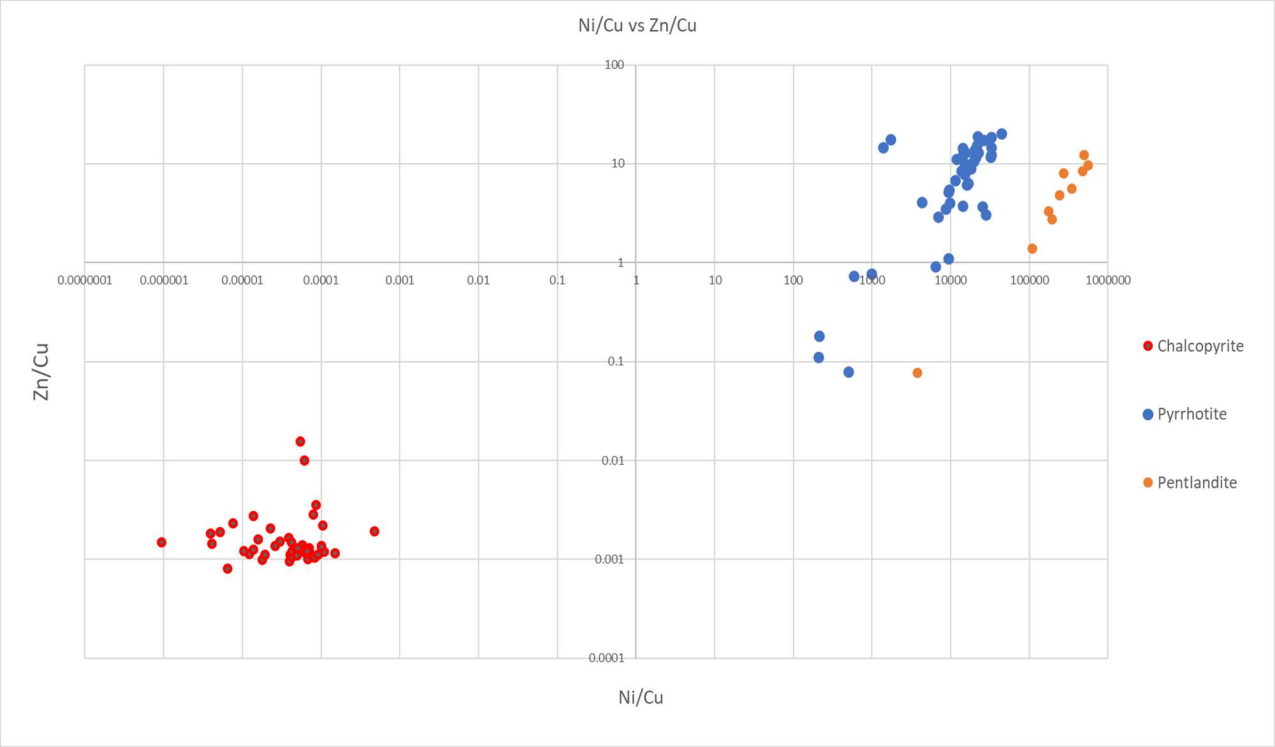

Figure 25. Diagram based on the sulfide trace element chemistry ratio of Ni/Cu vs. Zn/Cu.

In chalcopyrite, Co, Ni, Zn, As, Se, Ag, Sn, Sb, Au, Pb, and Bi values are mainly above the limits of detection and display variations. Relatively high Co, As, Se, Sn, Sb, and Bi values are not related to inclusions and reflect chalcopyrite compositions. Although many chalcopyrite grains have high Ni or Pb concentrations, the extreme values in these elements (i.e. thousands of ppm) are related to pentlandite and sphalerite inclusions. Cr, Mn, and Mo values are in general equal or below the limits of detection. Variations in concentrations of Cr, Mn, Sr and Mo in chalcopyrite can be attributed to oxide and silicate inclusions.

In pyrrhotite, Co, Ni, Se, Pb, Ag and Bi values are mainly above the limits of detection and display variations. Relatively high Co, Se, and Bi values are not related to inclusions and reflect pyrrhotite compositions. Cr, Mn, Sn, Sb, and Mo values are in general equal or below the limits of detection. Variations in concentrations of Cr, Mn, Sn, Sb, and Mo in pyrrhotite can be attributed to oxide and silicate inclusions.

In pentlandite, Co, Ni, Ti, Se, Te, Pb, and Bi values are mainly above the limits of detection and display variations. Relatively high Co, Se, and Bi values are not related to inclusions and reflect pentlandite compositions. Cr, Mn, and Mo values are in general equal or below the limits of detection.

The binary diagram Se/As vs. Co/Sb (Fig. 23) shows that the majority of the pyrrhotite and pentlandite grains in this study have relatively high ratios of Co/Sb. Chalcopyrite has low ratio of Co/Sb. Se/As ratios of all three minerals analysed are plotted in a similar pattern.

The binary diagram As/Te vs. Te/Se (Fig. 24) shows that the majority of the studied samples have relatively low ratios of As/Te and Te/Se.

The binary diagram Ni/Cu vs. Zn/Cu (Fig. 25) shows that pyrrhotite and pentlandite grains in this study have high ratios of Ni/Cu. Chalcopyrite has the lowest ratio of both Ni/Cu and Zn/Cu.

6.4. Geochemistry

The geochemical data are utilized and plotted according to the main rocks examined (See Materials and Methods). The studied komatiitic lithofacies are divided into cumulates, non-cumulus rocks and komatiitic basalts, based on geochemistry. This division follows the geochemical criteria as follows: MgO > 28 wt.% = komatiitic cumulates, 28 wt.% > MgO > 18 wt.% = komatiites and MgO < 18 wt.% komatiitic basalts. All major element oxides have been normalized to 100 wt.% volatile-free.

6.4.1. Major element geochemistry

Komatiites in the current study are classified by their MgO and SiO_2 contents (Fig. 30) to komatiites and komatiitic basalts (Le Bas 2000, Le Maitre et al. 2002). SiO_2 content of the studied samples varies largely between 45–57 wt.%.

According to classifications of komatiite by Nesbitt et al. (1979), the studied komatiites and komatiitic basalts are Aluminum-Undepleted Komatiites (AUKs) (Fig. 27). TiO_2 in komatiites ranges from ~0.2 – 0.45 wt.% and the more Ti enriched komatiitic basalts show Ti content from 0.35 – 0.75 wt.%. Komatiitic basalts show higher Al content than komatiites, with the highest values being ~15 wt.% Al_2O_3 (Fig. 27). The studied komatiites and komatiitic basalts show an average Al_2O_3/TiO_2 ratio of ~21 (Fig. 26). Tremolite rock is showing a depletion in Al_2O_3/ TiO_2 ratio with average values of ~15.

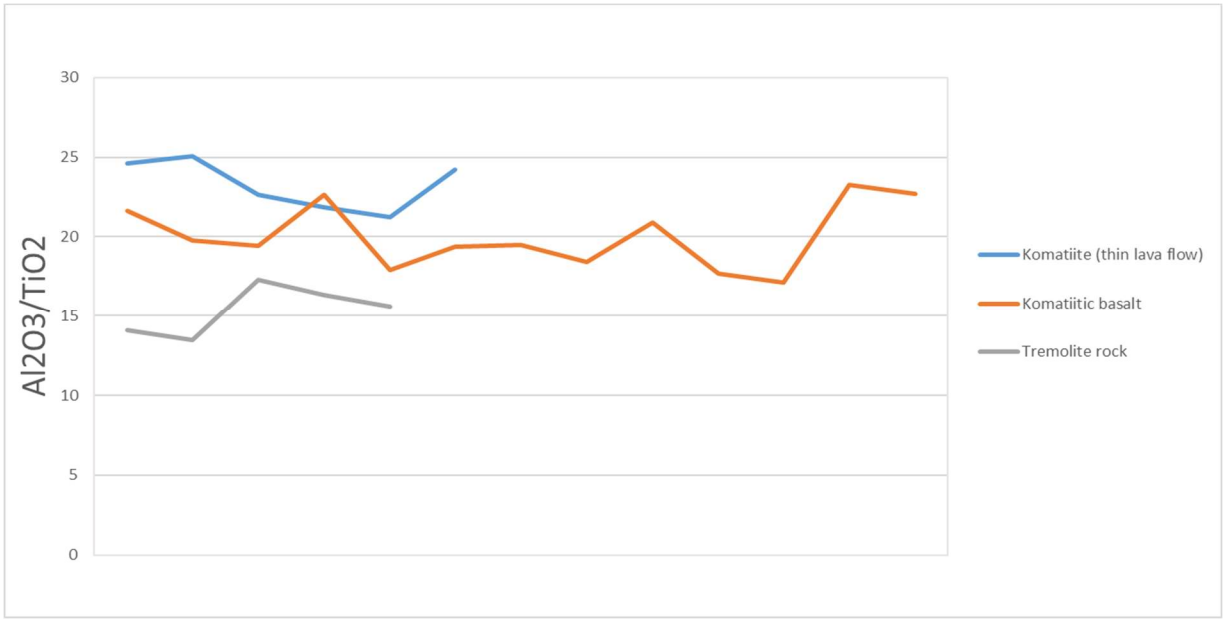

Figure 26. Al_2O_3/TiO_2 values of the studied samples.

The MgO content of the studied samples spans from 5 to 30 wt.% (Fig. 28) with compositions ranging from komatiitic basalt to komatiitic cumulates. Komatiites show the highest MgO content with MgO up to 30 wt.% (Figs. 28, 29, 30). Komatiitic basalt group MgO values mostly cluster around 10 wt.%. Lower MgO content can be attributed to proximity to the sulfide body (See Appendix 1 and 3). High SiO_2 may be related to hydrothermal input or later metamorphic processes.

The analysed samples were plotted in the Jensen cation diagram (Jensen 1976) and fall in the komatiite, komatiitic basalt and high Mg tholeiites (Fig. 31). Samples that plot in the high Mg tholeiites field are from the komatiitic basalt group.

The tremolite rock is depleted in almost all elements used here, compared to the komatiites and komatiitic basalts, except MgO. Tremolite rock has a MgO content of ~ 15 wt.%, whereas the komatiitic basalt MgO content clusters near 10 wt.%. The most noteworthy characteristic is the strong depletion in Al_2O_3 (Fig. 27 and Fig. 29).

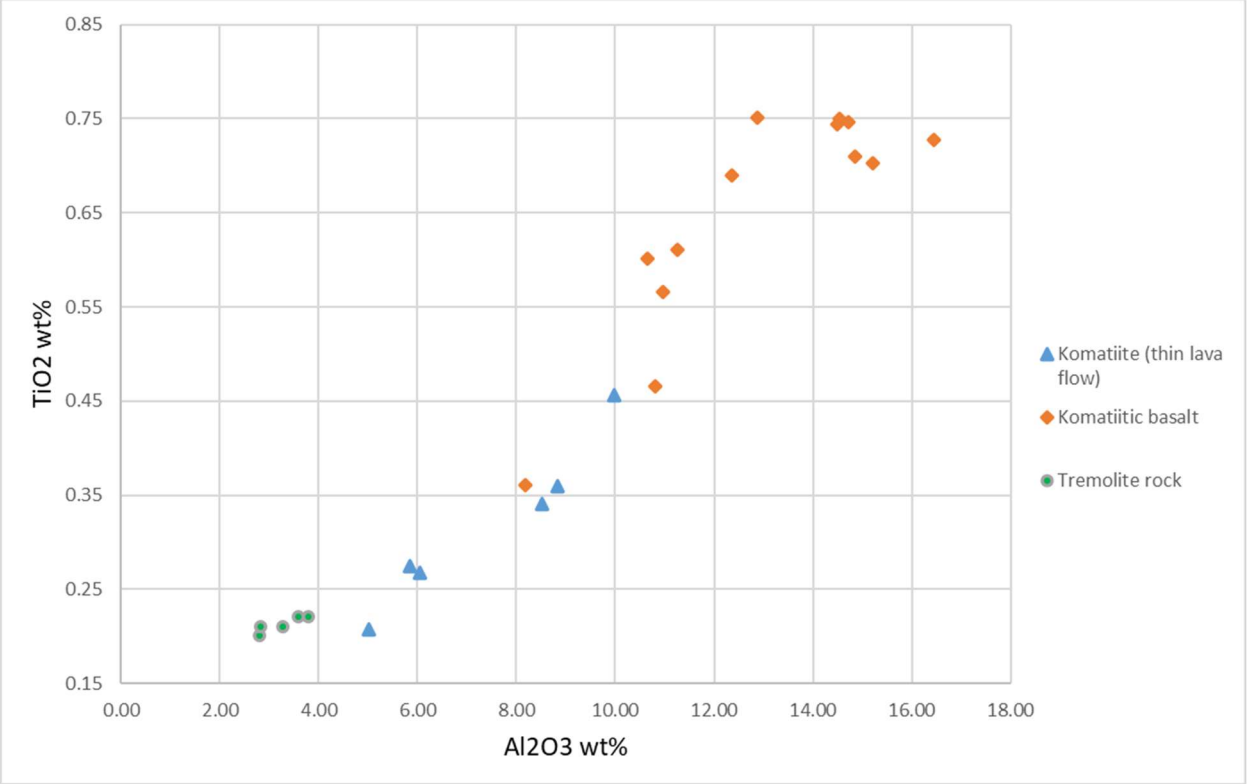

Figure 27. Al_2O_3 vs. TiO_2 diagram of the studied samples. Samples are categorized on the basis the rock type.

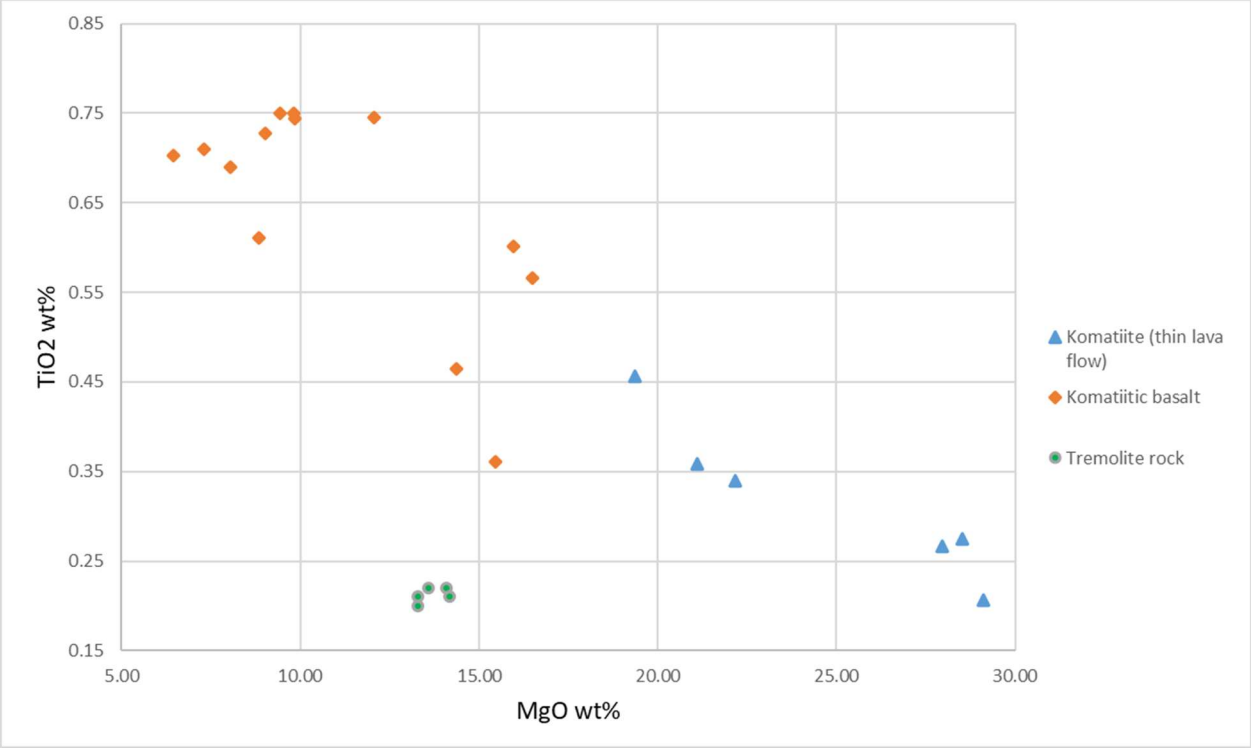

Figure 28. MgO vs. TiO_2 diagram of the studied samples. Samples are categorized on the basis the rock type.

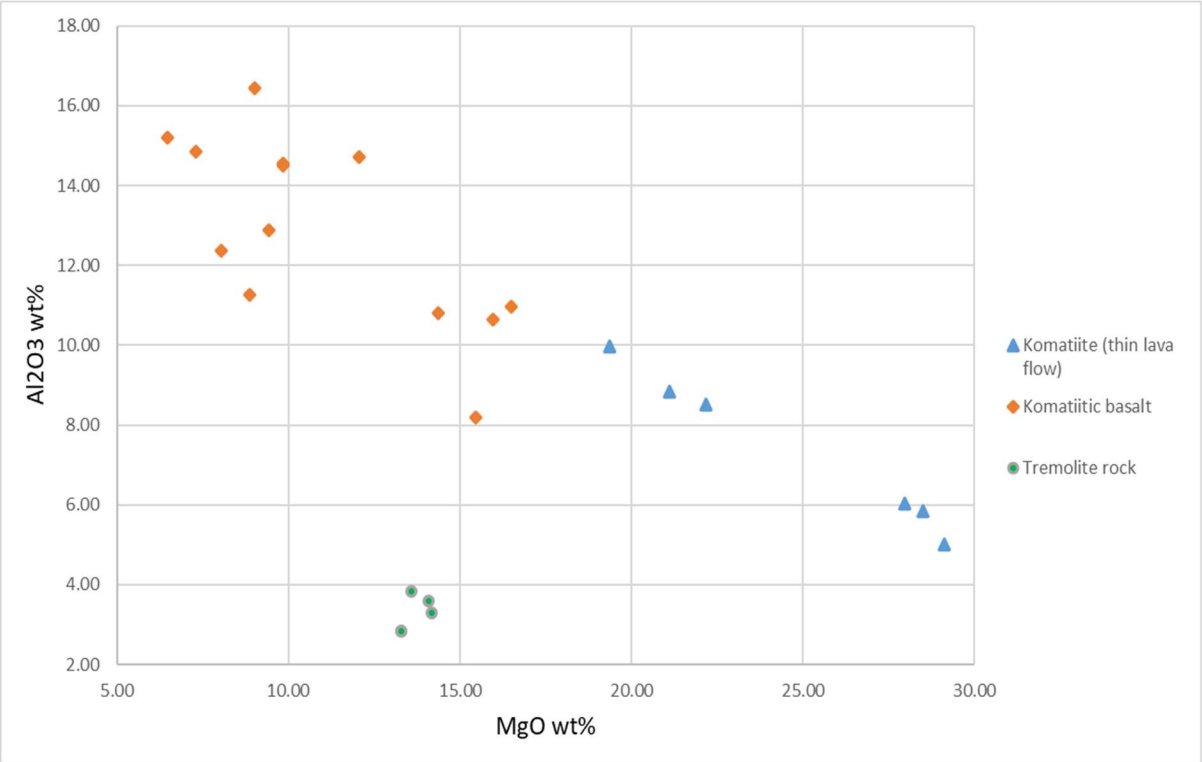

Figure 29. MgO vs. Al_2O_3 diagram of the studied samples. Samples are categorized on the basis the rock type.

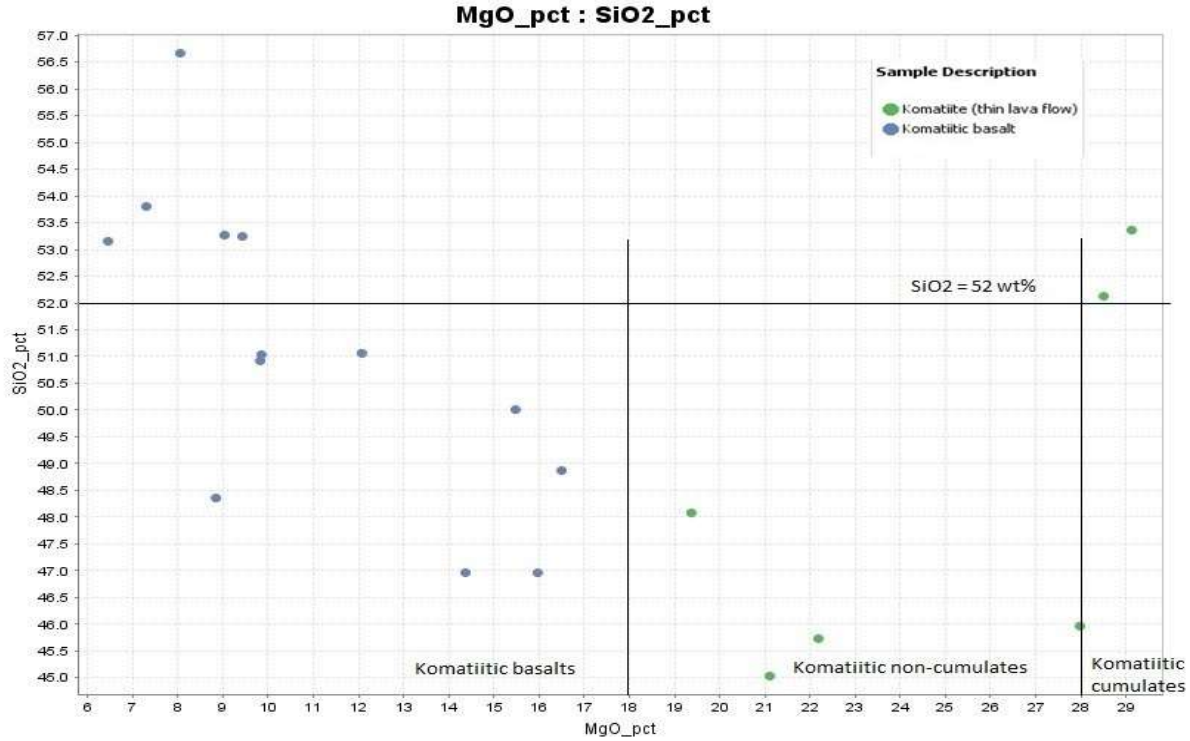

Figure 30. MgO vs. SiO_2 diagram of the komatiites and komatiitic basalts. The black lines mark the divide to komatiitic basalts, non-cumulus komatiites and cumulates by the MgO content. The horizontal black line represents the IUGS 52 wt.% SiO_2 upper limit for komatiites (see Le Bas 2000, Le Maitre et al. 2002) (pct = percentage).

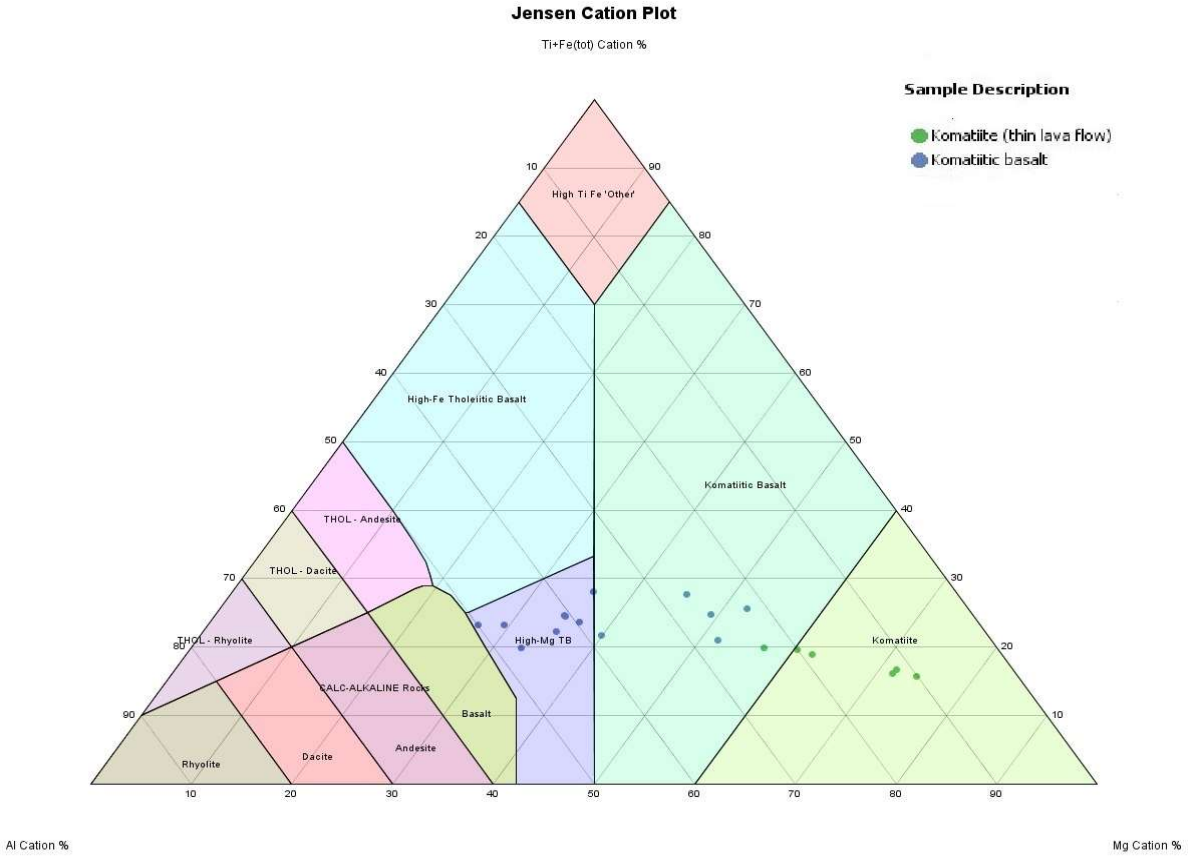

Figure 31. Komatiites and komatiitic basalts of the studied area in Jensen cation diagram (Jensen 1976).

6.4.2. Base metals and REE geochemistry

The Ni contents of the komatiite bodies and the tremolite rock display a great variability. Komatiitic basalt has the lower Ni content, with values bellow 200 ppm (Fig. 32). Komatiite has higher MgO/Ni and MgO/Cr (Fig. 32) ratios. In the Cr vs. Ni plot (Fig. 34), komatiite and komatiitic basalts plot in the komatiitic lithological envelope field and the mineralized body in the mineralized komatiite trend. The mineralized body and tremolite rock are showing a depletion in Cr content (Fig. 34) compared to komatiite.

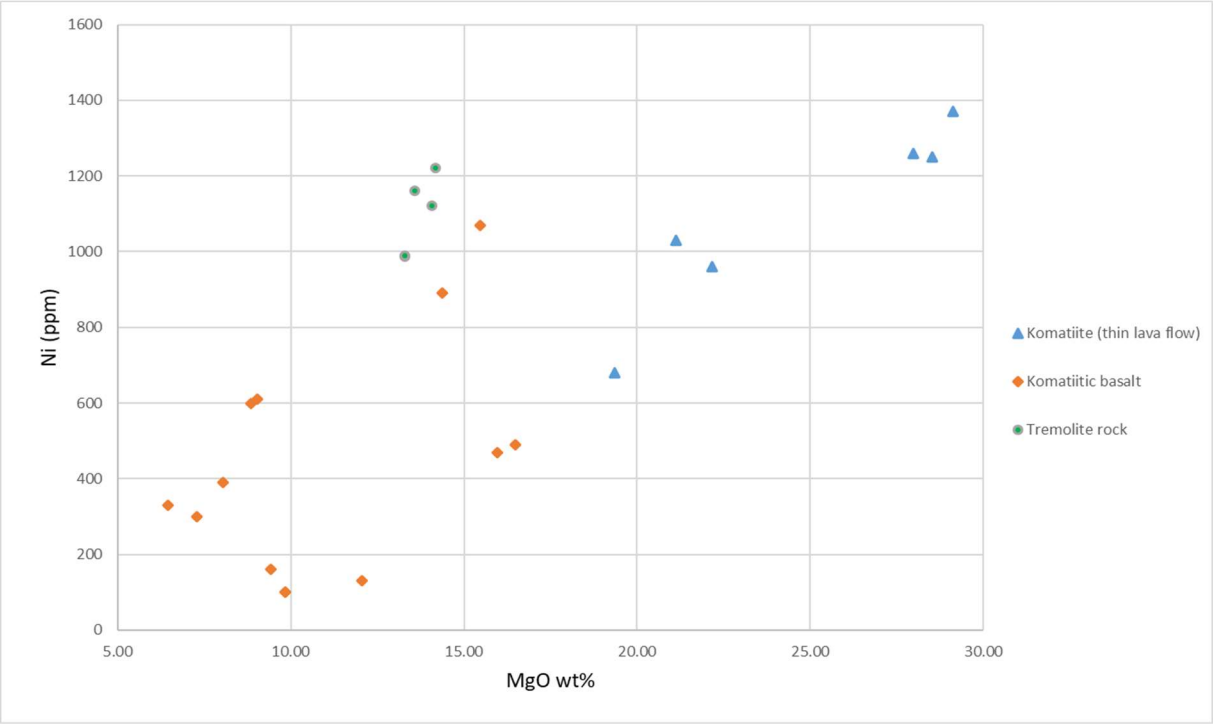

Figure 32. MgO vs. Ni-diagram of the studied samples. Samples are categorized on the basis the rock type.

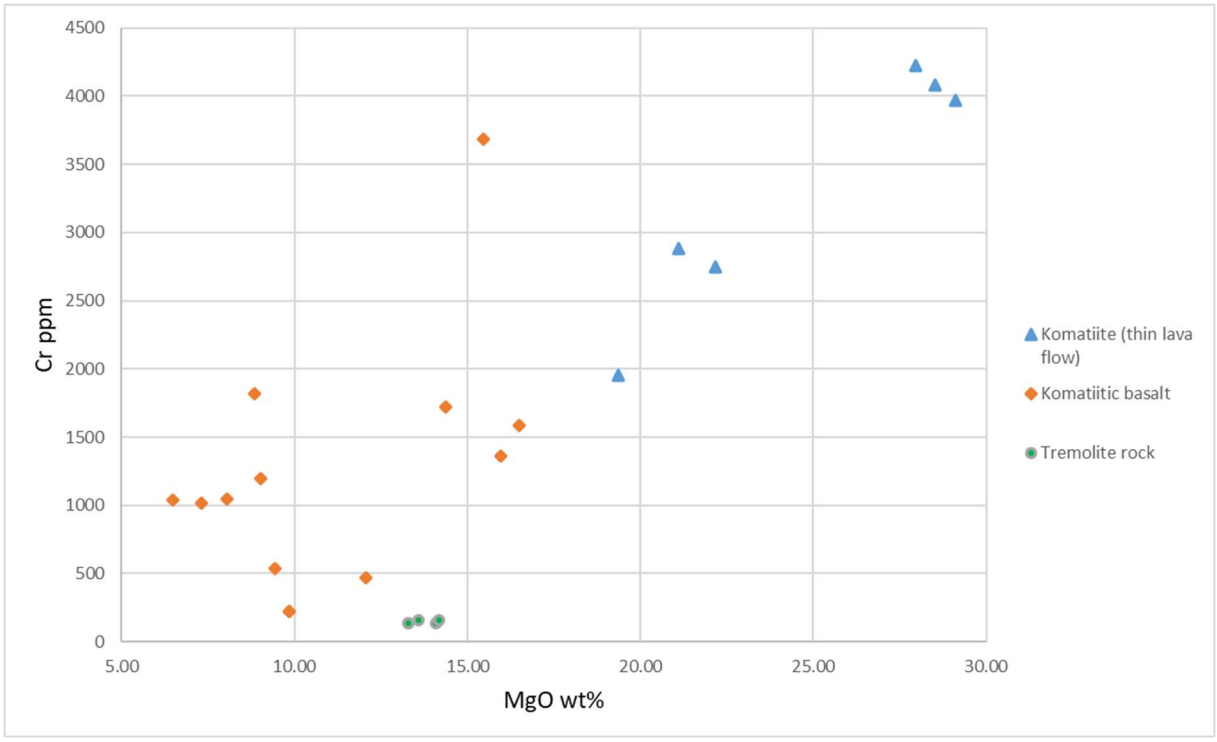

Figure 33. MgO vs. Cr-diagram of the studied samples. Samples are categorized on the basis the rock type.

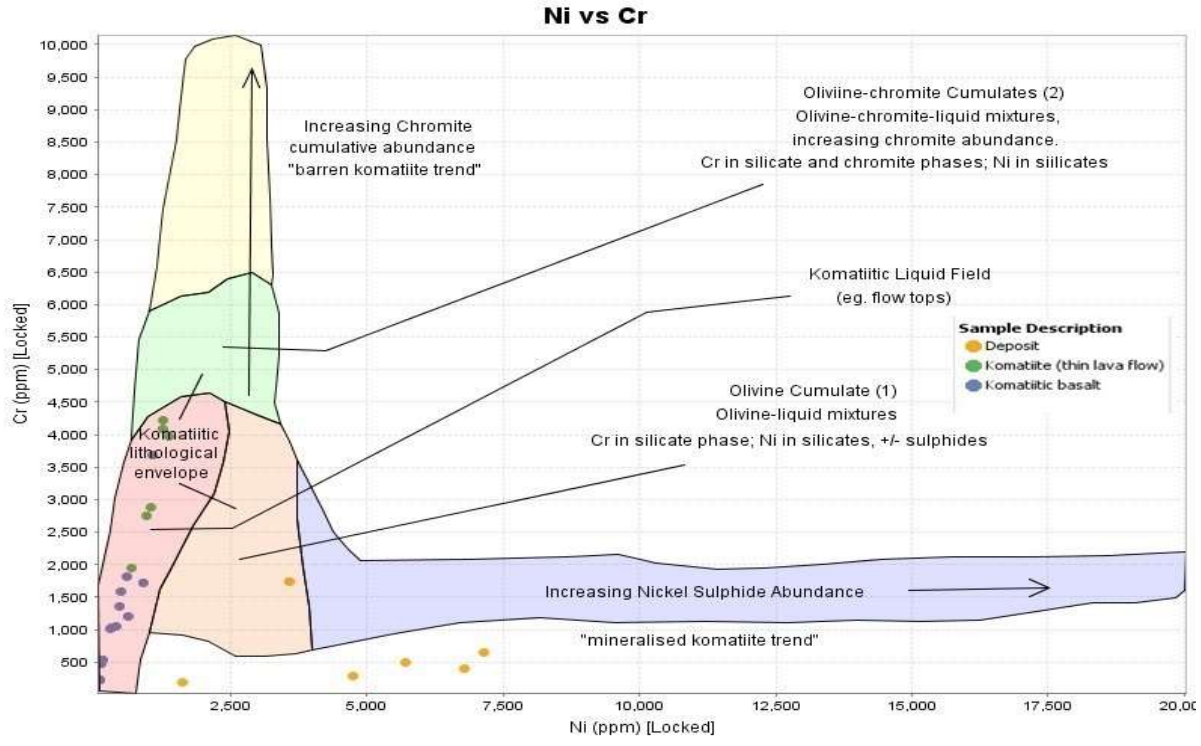

Figure 34. Ni vs. Cr plot of the whole-rock samples. Samples with low Cr and high Ni represent mineralized komatiite trend, along which Ni sulfide abundance increases. Samples with high Cr and low to moderate Ni represent the barren komatiite trend.

The whole-rock REE-patterns display a relative enrichment in REE compared to chondrite (Fig. 35). The samples are grouped in the graph based on the lithology. Komatiite basalt group shows the strongest enrichment in REE and the tremolite group has the weakest relative enrichment. A noteworthy characteristic of the REE-patterns is the depletion of Eu in the tremolite rock. The mineralized body plots between the komatiite and the komatiitic basalts, indicating some different formation processes due to the partitioning of the REEs in the deposit. No significant HREE and LREE distinction can be observed in the REE-patterns, although a slight LREE depletion is present.

In the Ni-PGE-Au-Cu graph (Fig. 36), a relative depletion in iridium-group platinum-group elements (IPGEs: Os, Ir, Ru) is clear from the pattern. On the other hand, palladium-group platinum-group elements (PPGEs: Rh, Pt, Pd) shows a strong enrichment relative to primitive mantle values. Ni, Cu and Au are also enriched relative to mantle values.

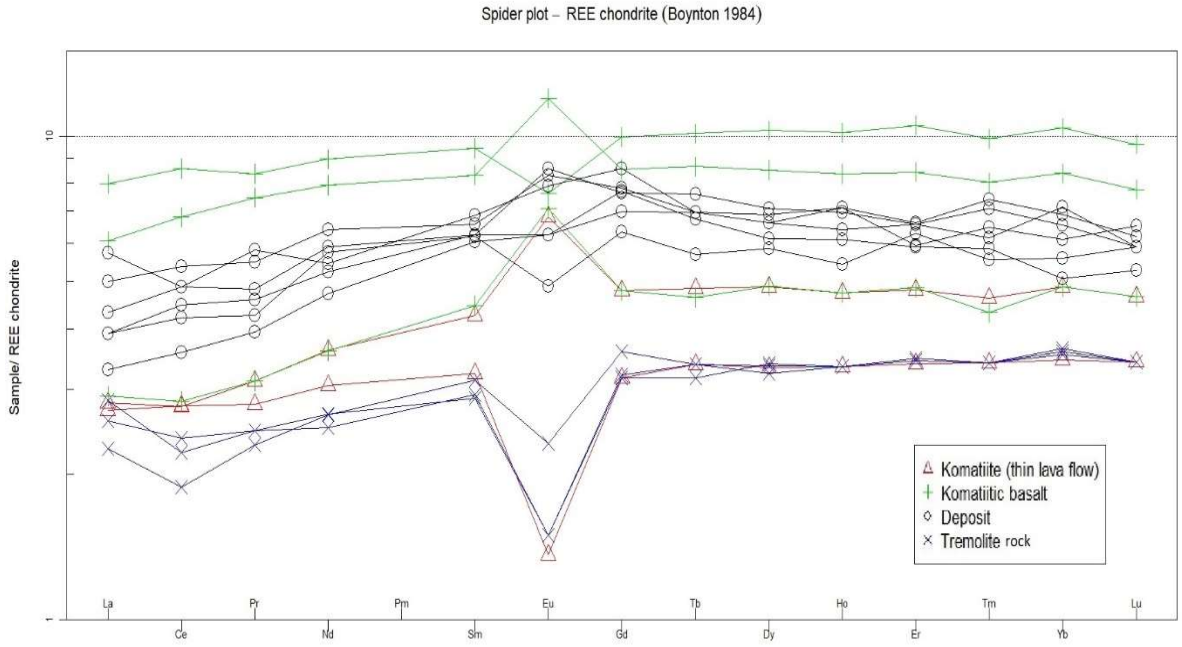

Figure 35. REE-patterns of the samples normalized to the chondritic composition of Boynton (1984).

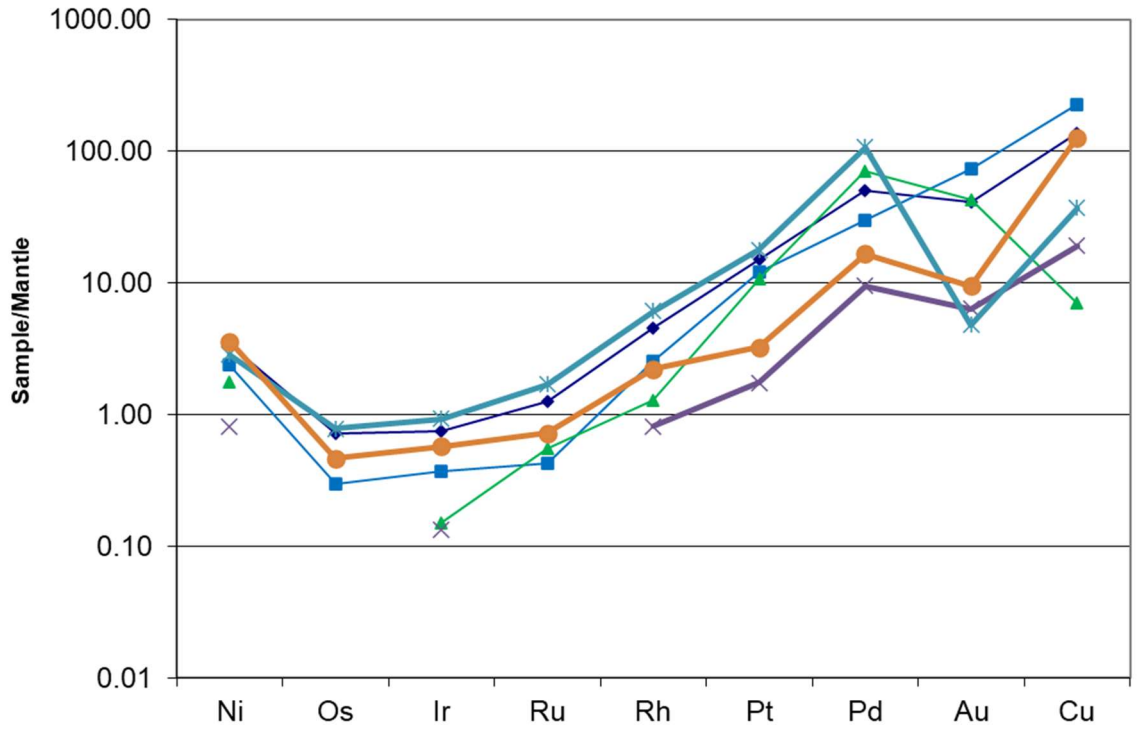

Figure 36. Primitive mantle-normalized chalcophile element patterns of the Siivikkovaara sulfide body (normalization after Sun 1982 and Barnes et al. 1988).

All samples show $(Gd/Yb)_N$ median values of ~ 1.012 (Fig. 37). $(Gd/Yb)_N$ =1 corresponds to C1 chondrite value. Mineralized body shows the highest $(Gd/Yb)_N$ values, with the highest value at ~1.52. On the other hand, tremolite rock is showing the lowest $(Gd/Yb)_N$ values. In $(La/Sm)_N$ values there is a range of values from ~0.6-0.9. $(La/Sm)_N$ =1 corresponds to C1 chondrite value. Tremolite rock has mildly depleted values with ~0.98 being the highest value, while the komatiite bodies exhibit values close to 0.9 and the mineralized body has depleted $(La/Sm)_N$ values bellow 1. Theoretically, komatiites that are contaminated with crustal contamination should be enriched in highly incompatible REE (La and Sm) compared to moderately incompatible REE (Gd and Yb). Samples are normalized to C1 chondrite after McDonough and Sun (1995).

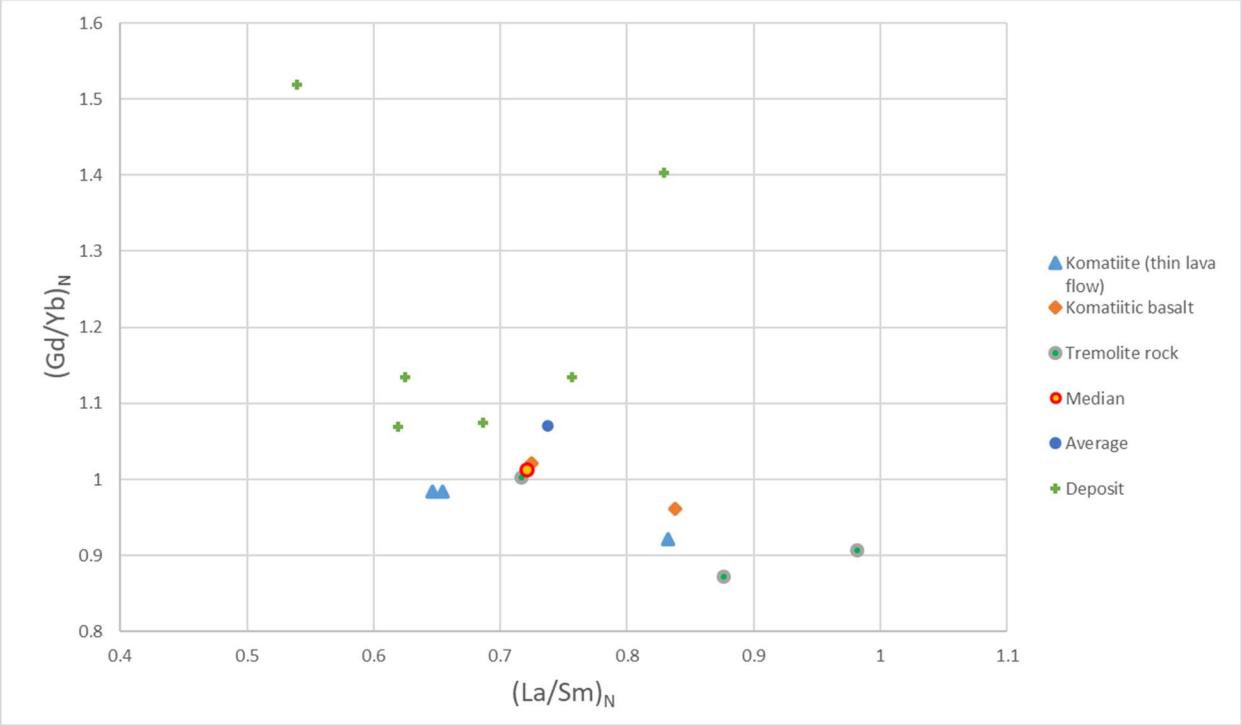

Figure 37. $(La/Sm)_N$ vs. $(Gd/Yb)_N$ plot of the studied samples. Enrichment in $(La/Sm)_N$ relative to $(Gd/Yb)_N$ have been attributed to crustal contamination. Chondrite values from McDonough and Sun (1995).

6.5. Isotope geochemistry

6.5.1. Multicollector LA-ICP-MS S^{34} analysis

The analysed mineral phases are chalcopyrite, pyrrhotite and sphalerite. A total of in-situ 47 isotope analyses on 10 samples were carried out. There are certain systematic differences between minerals. Chalcopyrite (Fig. 38) shows the lowest $\delta^{34}S$ values with an average value of -0.20‰. Pyrrhotite (Fig. 39) and sphalerite (Fig. 40) show small deviation in their $\delta^{34}S$ with an average of 1.01‰ and 1.04‰. The analysed minerals show an average $\delta^{34}S$ composition of 0.45‰.

Analytical uncertainties (2σ) for conventional techniques are ±0.1‰ for $\delta^{34}S$ (Seal 2006). The studied samples (Fig. 41) show an average 2σ of 0.27. Pyrrhotite is showing the highest 2σ values, with the highest value at 0.60 and sphalerite is showing the lowest 2σ values. Relatively high analytical uncertainties (2σ) can be attributed to the lack of pyrrhotite and sphalerite standards. Pyrrhotite that has the highest $\delta^{34}S$ values also shows the highest 2σ value.

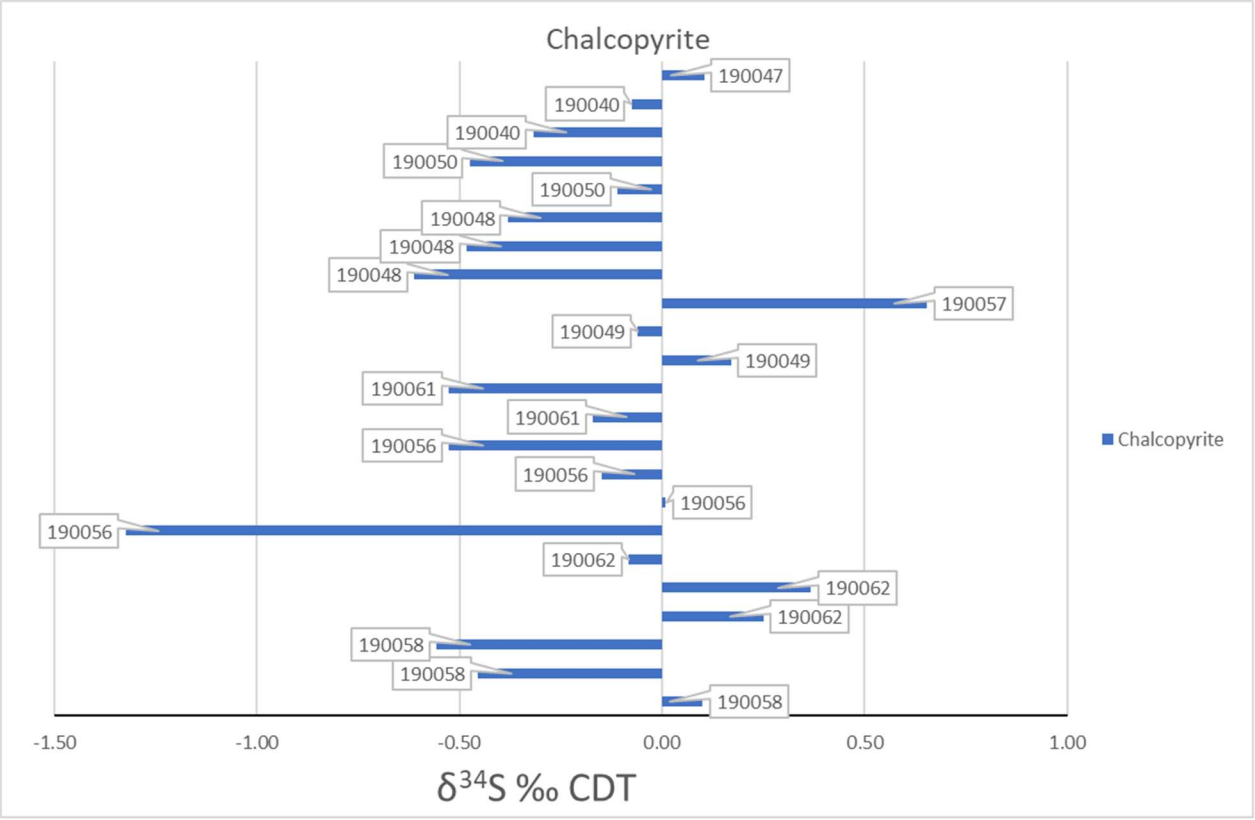

Figure 38. Sulfur isotope compositions ($\delta^{34}S$) of chalcopyrite. Data labels refer to sample codes.

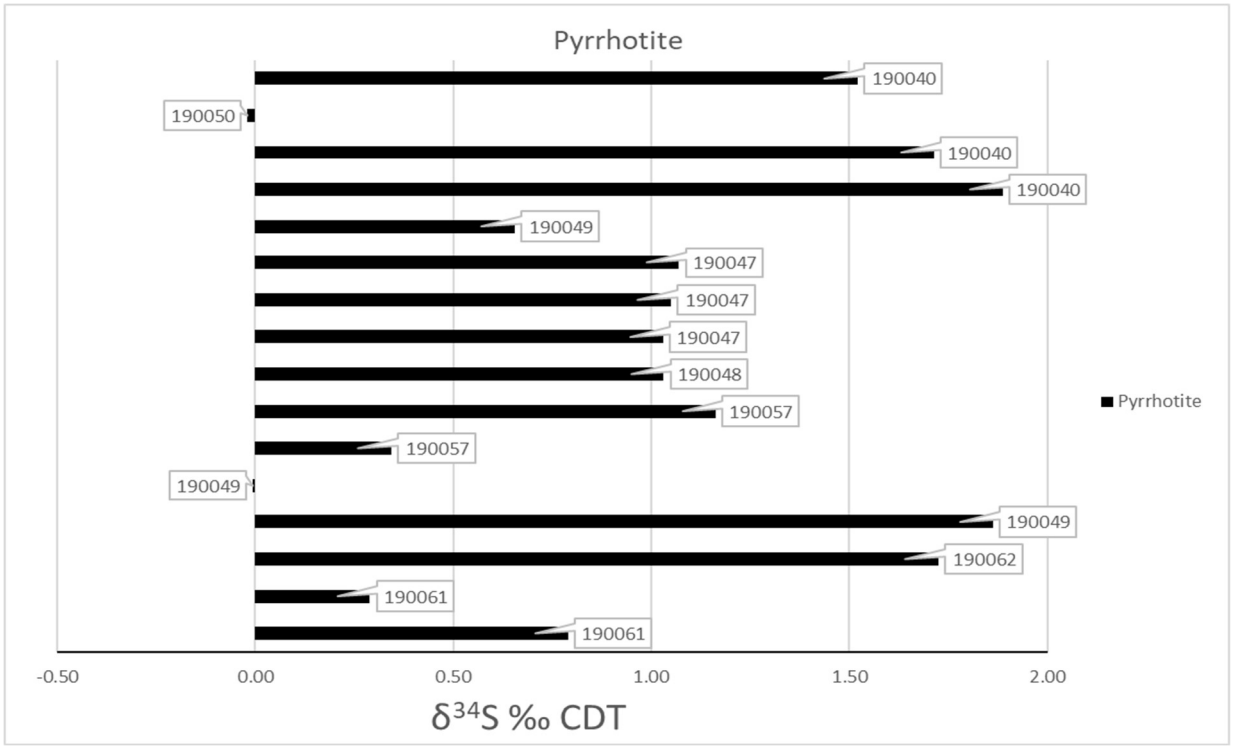

Figure 39. Sulfur isotope compositions ($\delta^{34}S$) of pyrrhotite. Data labels refer to sample codes.

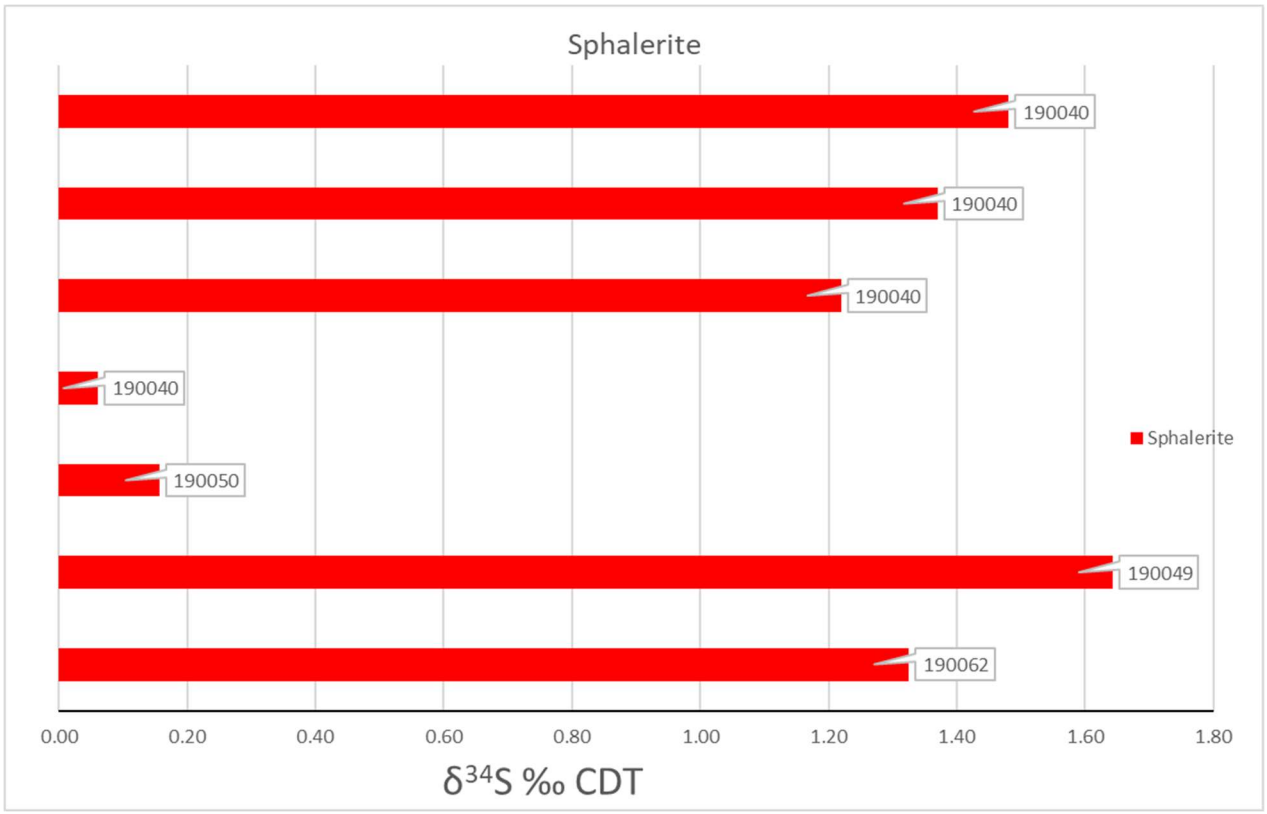

Figure 40. Sulfur isotope compositions ($\delta^{34}S$) of sphalerite. Data labels refer to sample codes.

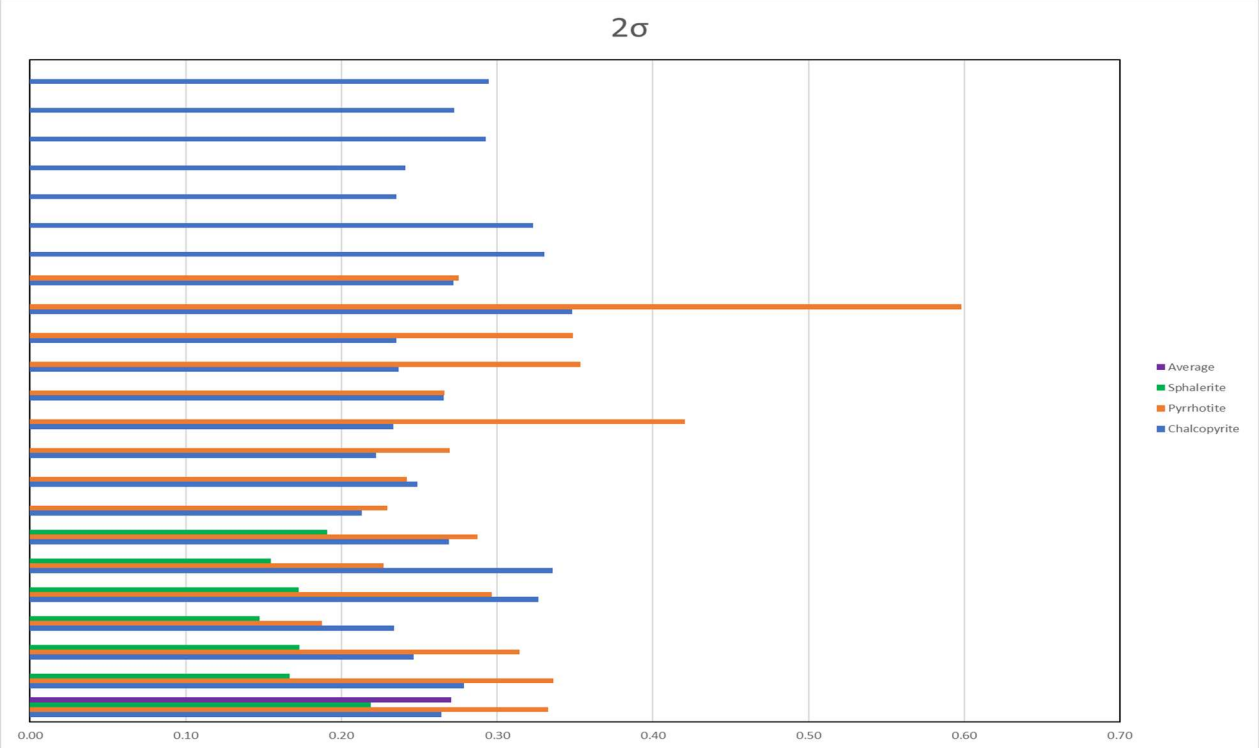

Figure 41. 2σ values of the analysed sulfides. Green colour is sphalerite 2σ, orange colour is pyrrhotite 2σ, blue colour is chalcopyrite 2σ and purple is the average 2σ value.

7. Discussion

7.1. The mission of the thesis

The aim of the following discussion is to focus on the key questions with respect to the formation processes that affected the studied mineralized body. The geochemical composition and petrology of komatiites, the $\delta^{34}S$ isotopic data and LA-ICP-MS trace element analysis of the sulfides are discussed with respect to the genetic features of the mineralization.

A number of komatiite-hosted Ni-Cu-PGE deposits have been discovered in Archean and Paleoproterozoic greenstone belts in eastern and northern Finland. Parental magma composition of these show variation from komatiitic basalt (Hietaharju and Peura-aho) to low-Mg komatiite (Vaara, Lomalampi, and Tainiovaara) and komatiite (Hotinvaara, Ruossakero, and Sarvisoaivi) (Konnunaho et al. 2015). Most of the deposits formed from Al-undepleted magma types and the studied komatiites are AUKs (See 6.4.1.). In the case of Ruossakero, Sarvisoaivi, and Hotinvaara deposits, the magma was Ti-depleted komatiite. Most of the ultramafic formations hosting the deposits have extrusive origin, but in some deposits, like Hotinvaara, Ruossakero, Sarvisoaivi, and Lomalampi cumulate bodies might represent sills. All komatiite-hosted Ni-Cu-PGE deposits in Finland belong to the type II komatiitic mineralization of Lesher and Keays (2002) and, in many cases, sulfides are associated with cumulates having low Cr contents (e.g., Vaara, Ruossakero, Tainiovaara, and Sarvisoaivi). The studied mineralization is showing Cr content in the komatiites, similar to the other deposits in Finland (Konnunaho et al. 2015). The deposits have been modified to various degrees by post-magmatic metamorphic processes. Emphasis in whole-rock geochemistry is given on the possible genetic implications from major element partitioning in the studied samples. Base metal, PGE and REE are focused on possible hydrothermal alteration processes that affected the mineralize body. Sulfur isotopic data are used to give insights into the source of sulfur in the system and LA-ICP-MS data processing and analyses are focused on the partitioning of trace elements in the sulfide minerals.

7.2. Genetic implications of komatiite formation from whole-rock geochemistry

Most of the komatiite-hosted Ni-Cu-PGE deposits in Finland show moderate Al_2O_3/TiO_2 of around 20 in their komatiite host-rocks, including the three major deposits within the Kuhmo greenstone belt (Vaara, Hietaharju, and Peura-aho) (Konnunaho et al. 2015). The studied komatiites have an average Al_2O_3/TiO_2 of ~21. The Hietaharju and Peura-aho deposits occur in the cumulate portions of lava flows generated from komatiitic basalt. The MgO content of the cumulates varies from 20–31 wt.%. Komatiitic basalts of the present study have lower MgO content that has values of 10-15 wt.%. The MgO content of the studied thin komatiite lava flows ranges between 19 and 28 wt.%. The Lomalampi, Vaara, and Tainiovaara deposits are associated with cumulates of low-MgO komatiitic flow units. The MgO content of thin komatiite lava flows ranges from 20–27 wt.%. Some komatiite MgO content exceeds 28 wt.% and thus the samples are plotted in the komatiitic cumulate field (Fig. 30). MgO and SiO_2 can be mobilized in hydrothermal systems. Given that, in (Fig. 30), those elements plot in the komatiite and komatiitic basalt field is an indicator that hydrothermal alteration did not affected the studied rocks. The lack of spinifex-textured rocks, flow-top units, and pristine magmatic silicate minerals such as olivine, are affecting the accurate estimation of the MgO contents of the komatiitic parental melts of the Ni-Cu deposits in Finland. Thus, the degree of post-magmatic modification of all the deposits has to be taken into consideration when studying these deposits.

Olivine-chromite cumulates crystallizing from Cr-saturated magmas along the solubility surface should have chromite/olivine ratios defined by the slope of that surface in Cr-MgO graph, and should hence define a roughly linear trend of positively correlating Cr and MgO forming an extension of the saturation surface trend (Barnes and Fiorentini 2012). This is referred to as the cotectic trend (Barnes 2007) and was labelled by (Barnes and Fiorentini 2012) as the “cotectic olivine-chromite cumulates” line. Cumulates of komatiitic basalt in the Hietaharju and Peura-aho areas have Cr contents of 0.2–0.65 wt.% (Konnunaho et al. 2015), while the Cr content in the studied komatiitic basalts varies between 0.1 and 0.25 wt.%. Komatiites in the present study have a Cr content of 0.28-0.62 wt.%. Thus, the studied komatiites show a positive correlation between MgO and Cr, following a cotectic olivine-chromite cumulate trend (Fig. 33). Given the above, these komatiitic rocks were derived from Cr-saturated magmas (cf. Barnes and Fiorentini 2012, Fig. 8.A). A noteworthy characteristic in the Cr content of the studied rocks, is the depletion of Cr of the tremolite rock and the

mineralization. Cr depletion is a characteristic of modern black smokers (Wang et al. 2017). Cr depletion in tremolite rock may be related with co-magmatic or post-magmatic modification.

The content of Ni shows a positive correlation with MgO, indicating Ni control by olivine in unmineralized samples, with S < 0.2 wt.% (Fig. 32). Konnunaho et al. (2015) reported that in the komatiitic basalts of Hietaharju and Peura-aho, Ni contents in unmineralized samples show values of around 500–1500 ppm. In the current study, Ni content of unmineralized samples ranges from 680 to 1370 ppm in komatiites and from 100 to 1070 ppm in komatiite basalts. Ni content of the mineralized body has highest values of ~7000 ppm. The tremolite rock is enriched in Ni relative to the komatiitic basalt with values of ~1000 to 1200 ppm.

7.3. Base metal, PGE and REE budget in hydrothermal ore forming processes

Ni and Cu whole-rock data show a positive correlation with sulfur concentration in the mineralized body (Fig. 42). This trend can be observed in almost all deposits. The exceptions are Ruossakero and Hotinvaara (Konnunaho et al. 2015), where there is no clear correlation between S and Ni or there are sample groups with different correlations. This feature has also been observed between S and Cu in Ruossakero and is likely related to different ore types within the deposit (variety of sulfide mineralogy and host rock types). Platinum and palladium show a positive correlation with S in most of the deposits, except for the Hotinvaara deposit.

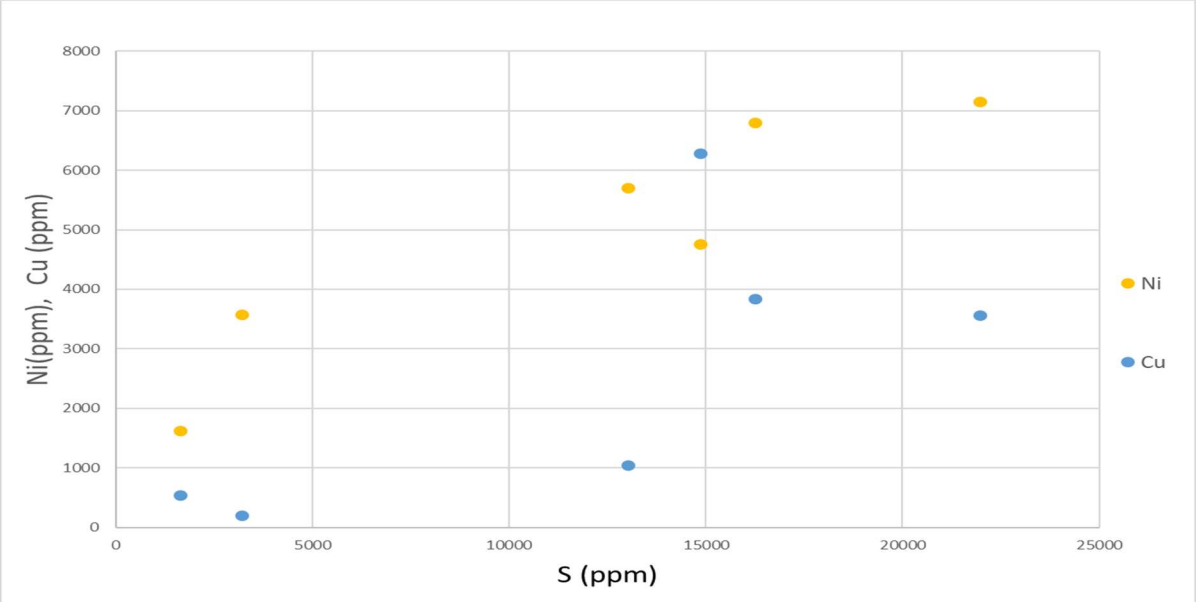

Figure 42. Ni and Cu vs. S whole-rock concentration of the mineralized body.

The Ni/Cu ratio in the Cu-enriched deposits is ~3–13 and in the Cu depleted deposit the values are ~15–36. The average Ni/Cu ratio of the studied samples is 5.17, thus the deposit is Cu-enriched. Lomalampi, Vaara, Peura-aho, and Hietaharju deposits are also enriched in Cu compared to the other deposits like Ruossakero, Sarvisoaivi, and Hotinvaara. The Cu-enriched deposits are also enriched in PGE, especially Pd and Pt. For deposits elsewhere (Naldrett 2004, Lesher 2007), low Ni/Cu (<6) is typical for Ni-Cu-(PGE) deposits in the Raglan and Delta Horizon areas of the Cape Smith Belt, Canada. Cu-enriched deposits (Hietaharju, Peura-aho, Vaara, and Lomalampi) contain a slightly higher amount of chalcopyrite than the other deposits (Konnunaho et al. 2015), an observation that is in accordance with the studied deposit, in which chalcopyrite is the main sulfide mineral. High-MgO komatiite hosted deposits tend to have high Ni and low Cu and thus high Ni/Cu ratio. Low MgO komatiite and komatiitic basalt hosted deposits (like Raglan and most of the Finnish deposits) tend to have higher Cu and thus lower Ni/Cu ratio.

In the Finnish komatiite-hosted Ni-Cu-PGE deposits, the average Pd and Pt contents vary in the range of 170–2160 and 300–1080 ppb, respectively (Konnunaho et al. 2015). Pt concentrations in the studied samples range from 16-163 ppb and Pd values from 41-470 ppb. Those concentrations, show a relative depletion in Pt and a relative enrichment in Pd of the deposit, compared to other similar deposit in Finland. The PGE data indicate magmatic origin for the Siivikkovaara deposit or at least that there was originally magmatic komatiite hosted Ni-Cu-PGE mineralization present. The PGE data indicate magmatic origin for the Siivikkovaara deposit or at least that there was originally magmatic komatiite hosted Ni-Cu-PGE mineralization present. PGE's are usually very low in VMS deposits.

According to Konnunaho et al. (2015), the highest average Pd + Pt concentrations are found in the Peura-aho (3240 ppb), Hietaharju (1080 ppb), Vaara (960 ppb), and Lomalampi (580 ppb) deposits (Fig. 43). Those deposits represent PGE enriched deposits. Analyses of the studied samples shows an average Pd + Pt value of 300 ppb. Given the results, the mineralization represents an enriched body in Pd + Pt, relative to the majority of deposits in Finland. Pt/Pd and Pd/Ir average ratios in the studied deposit are 0.5 and 138 respectively. Average Pt/Pd is ~0.4 in all Finnish deposits (Konnunaho et al. 2015). Generally, komatiite-hosted Ni-Cu-PGE deposits in the world are enriched in Pd over Pt, and have a Pt/Pd ratio similar to that in most Finnish deposits (Lesher and Keays 2002, Fiorentini et al. 2010a). The average Pd/Ir in all Finnish deposits is ~20 and in the current study, we present a value of 138. This value indicates

a significant enrichment in Pd, compared to other deposits in Finland. This is in accordance with the primitive mantle-normalized chalcophile element pattern of the sulfide body (Fig. 36), which shows that the deposit has a significant enrichment in PPGEs compared to primitive mantle values.

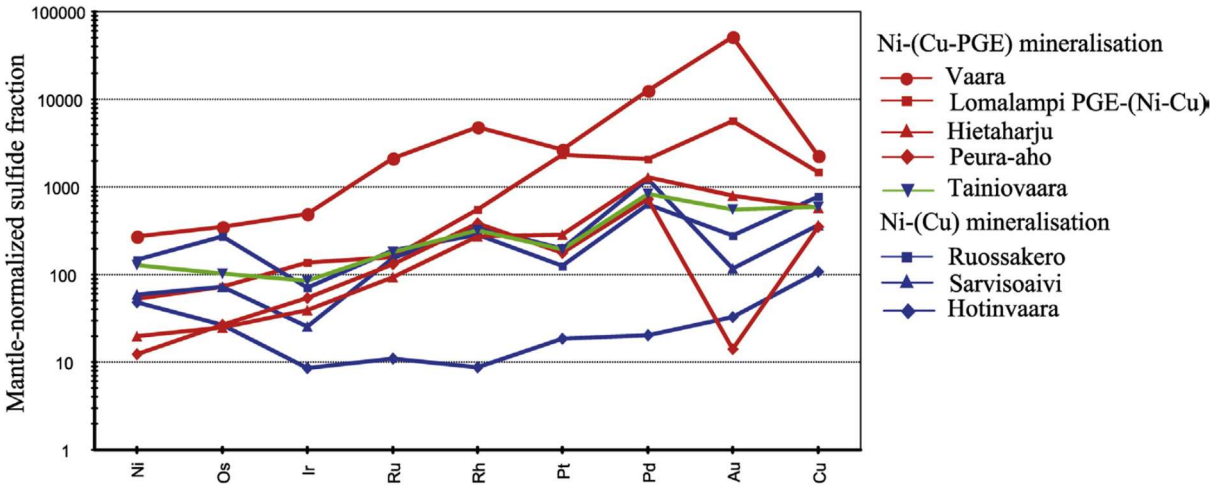

Figure 43. Primitive mantle-normalized chalcophile element patterns by Konnunaho et al. (2015). Metal contents normalized to 100% sulfide.

Elevated LREE contents in komatiitic rocks are often considered a consequence of crustal contamination, a crucial process for formation of Ni-Cu-(PGE) mineralizations in mafic-ultramafic systems.

The REE content of the samples was examined from this perspective. Jahn et al. (1980), Lesher et al. (2001) and Barnes et al. (2004) discussed that rocks with very high MgO and initially low LREE concentrations are more susceptible for mobility of these elements during alteration. Thus, distinguishing between contamination and alteration effects is essential but not easy, given the age of the rocks and their post-magmatic modification. When the REE content of all four groups is considered (Fig. 35), a significant enrichment with similar trends on REE plot can be seen and thus these blocks are genetically related to each other. Even though the REE patterns are enriched relative to chondrite values, no LREE enrichment compared to HREE is observed and the average values of La/Yb are ~1.0. This feature suggests a rather primitive and uncontaminated magma for the studied samples. Elevated $(La/Sm)_N$ has been considered a strong indicator of crustal contamination (e.g., Jahn et al. 1980, Hanski et al. 2001, Lesher et al. 2001, Barnes et al. 2004). Samples presented in the current study are depleted in $(La/Sm)_N$ relative to chondrite value (Fig. 37). This feature also suggests a rather primitive and

uncontaminated magma for the studied samples. The primitive and uncontaminated magma suggests that the deposit was formed in a magmatic environment that cannot be related with VMS-like setting.

The way that the trends are plotted for each group can be attributed to alteration due to the sulfide body being plotted in between the komatiitic basalt and the komatiite. Fluids affected both komatiitic basalts and komatiites and enriched the mineralization in REE. Another proof of alteration, is the behaviour of Eu and the depletion of the tremolite rock in REEs compared to all other groups. Eu^{2+} replaces Ca^{2+} in plagioclase (Hövelmann et al. 2010) and Eu is relatively enriched in the studied komatiitic basalts compared to the tremolite rock, due to the presence of plagioclase in the studied komatiitic basalts.

7.4. Source of sulfur

Sulfur isotope data from a variety of sulfide minerals from seafloor hydrothermal systems in mid-ocean ridge systems have $\delta^{34}S$ values that typically range between 0-6‰. In ancient seafloor hydrothermal systems, prior to 2.4 Ga (the onset of oxygen in the atmosphere) the $\delta^{34}S$ of hydrothermal sulfides show minor variations and cluster near 0‰. Uncontaminated mantle-derived magmas sulfur isotope composition ($\delta^{34}S$) has values from −2 to +2‰ (Ripley and Li 2003). Komatiite-hosted Ni-Cu-(PGE) deposits $\delta^{34}S$ value is generally close to zero or slightly positive (Ripley 1999, Lesher and Keays 2002). Finnish komatiite-hosted Ni-Cu-(PGE) deposits show $\delta^{34}S$ values between −0.7 to +15.0‰ with the Lomalampi deposit showing the highest values from +9.8–15.0‰ (Törmänen et al. 2015). These high S isotope values indicate a crustal component in the Lomalampi sulfides. On the other hand, Vaara and Hietaharju, located in the Suomussalmi greenstone belt, show the lowest $\delta^{34}S$ values between −0.7 and +2.7 ‰ (Konnunaho et al. 2013, unpublished data). In the country rocks that are sulfide-bearing, $\delta^{34}S$ ranges from −1.8 to +4.6 ‰ at Vaara and from −0.26 to 3.44 ‰ at Hietaharju. The Vaara and Hietaharju deposits show $\delta^{34}S$ values that overlap with the surrounding country rocks. Even though the values overlap with the surrounding country rocks, still are not distinguishable from uncontaminated mantle-sulfide composition (Konnunaho et al. 2015).

Magmatic sulfur is one of the principal reservoirs of sulfur and its $\delta^{34}S$ values cluster around 0‰ (Seal 2006, Thode et al. 1961, Ripley and Li 2003). Pristine MORBs have a $\delta^{34}S$ of 0.3 ±

0.5‰ (Sakai et al. 1984). Deviations between 2 and -2‰ are still regarded as representatives of a magmatic source. The magmatic sulfur could be precipitated directly from a mantle-derived source or could be remobilized from magmatic rocks and precipitated by a subsequent magmatic event.

The analysed minerals (Figs. 38, 39, 40) show an average $\delta^{34}S$ composition of 0.45‰. This value does not reveal a specific source for the sulfur in the studied deposit, other than that the source of sulfur is positively magmatic.

7.5. Trace element partitioning in sulfides

Selenium is concentrated in similar proportions in pyrrhotite, pentlandite, and chalcopyrite ratios (Figs. 23, 24). All three have Se concentrations of approximately 100-200 ppm, and plot with the same trend on the diagrams that include Se in their ratios.

Cobalt and Ni display different behaviour on the three analysed mineral patterns (Fig. 25). Pentlandite and pyrrhotite have Ni/Cu ratios that are significantly higher of those of chalcopyrite. Furthermore, Co and Ni are preferentially concentrated in pentlandite with values of up to 10,000 ppm for Co. Cu, Ag, and Zn partition into chalcopyrite, which exhibits a strong enrichment in Cu and Ag. In contrast, pyrrhotite and pentlandite exhibit a negative Cu anomaly and have lower Ag values.

Semi-metals (i.e., Te, Sb, Bi, As) are not compatible and the three mineral phases contain low concentrations and thus ratios of semi-metals and these elements do not correlate with each other or with other elements. Chalcopyrite displays the most enriched concentrations and highest ratios in semi-metals. Depletion in As is yet another indicator of magmatic origin of the deposit.

The overall partitioning of trace elements in the sulfide minerals of the Siivikkovaara mineralized body shows similarities to magmatic deposits. A more robust analysis of sulfide trace element geochemistry is highly recommended, based on internal standardization derived from electron microprobe analysis (EMPA).

8. Conclusions

This thesis examines potential hydrothermal alteration processes evolved in the formation of the Siivikkovaara Ni-Cu-Zn-Pb(-Au) deposit. It is the one of the few studies known in the literature to integrate the trace element chemistry of sulfides and sulfur isotopes together. I establish that the most likely formation of the mineralized body cannot be linked to modern black-smoker setting. The main outcome of the thesis can be summarized as follows:

- The source of sulfur is magmatic but cannot be related to a more specific geological setting. No great variations attributed to contamination by country rocks were found in the sulfur isotopic data.

- Enrichment in some elements may be attributed to co-magmatic and later post-magmatic modification of the mineralization and remobilization of the elements.

- MgO and SiO_2 can be mobilized in hydrothermal systems. The fact that (in Fig. 30), these elements plot in the komatiite and komatiitic basalt field is a further indicator that hydrothermal alteration did not affect the studied rocks.

- The komatiitic rocks of the studied samples were derived from Cr-saturated magmas.

- Cr depletion in tremolite rock may be related with alteration processes during metamorphism or co-magmatic and post-magmatic modification.

- The PGE data indicate a magmatic origin for the Siivikkovaara deposit or at least that there originally was a magmatic komatiite hosted Ni-Cu-PGE mineralization present. PGEs are usually very low in VMS deposits.

- REE data suggest a rather primitive and uncontaminated magma for the studied samples. Alteration and contamination have modified the incompatible element abundances (e.g. LREE) and a slight depletion in LREE can be observed.

- The studied komatiites are principally AUK type, which seems to be favorable for komatiite-hosted sulfide deposits globally and in Finland.

- The sulfide mineral compositions of the mineralized body exhibit similarities to sulfide minerals derived from primitive magmas.

- Pyrrhotite and pentlandite in the Siivikkovaara deposit contain significant amounts of Co. Chalcopyrite is enriched in Ag and Zn relative to pyrrhotite and pentlandite.

Acknowledgements

First of all, I would like to thank and express my gratitude to my Supervisor, Professor Tapani Rämö for providing me this unique opportunity to work with him. He has been a mentor throw out my M.Sc. studies. During work on this project he has been the most crucial factor to completing this difficult work. Special mention must go to Doc. Tapio Halkoaho, who came up with the project. His expertise of the area, his overall help and the field work we carried out together was an unforgettable experience. Professor Christoph Beier carried out the LA-ICP-MS analyses, which was a challenging analytical work, and I thank him not just for this, but for his important comments and help for the completion of this work. Dr. Tuomo Törmänen played a major role with his expertise in the field of VMS deposits and I am grateful for the cooperation we had, especially in the processing the data sets. Dr. Yann Lahaye is thanked for his analyses for sulfur isotopes at the GTK facilities in Espoo. I must also thank all of my professors during my studies for giving me the knowledge that I now possess.

Apart from my professors, I thank all of my friends and colleagues at the Department of Geoscience and Geography for the support we gave to each other all these years and for all the interesting conversations we had in our common love in Geology. My friend and colleague Nikos Karampelas is thanked for his help with the tremolite rock thin sections. I must also thank my friends and colleagues Keith and Letizia for our time together in Helsinki. Special mention must go to my best friends, Marco for making my first year in Finland such a great experience and Savvas and Alexis for being beside me all these years.

Last, but most important, I thank with all my heart, my family. They are my cornerstone for achieving everything that I have achieved so far, with their immeasurable support that they showed me. Without them nothing would be possible.

References

1. Arndt, N.T., Lesher C.M., Barnes S.J. 2008. Komatiite. Cambridge University Press.
2. Ault, W.U., Jensen, M.L. 1963. Summary of sulfur isotope standards. In: Biogeochemistry of Sulfur Isotopes. Jensen ML (Eds.) National Science Foundation, Symposium Proceedings, Yale University.
3. Barnes, S.J., Boyd, R., Kornelliussen, A., Nilssen, L-P., Often, M., Pedersen, R-B., and Robins, B., 1988. The use of mantle normalization and metal ratios in discrimination between the effects of partial melting, crystal fractionation and sulphide segregation on platinum group elements, gold, nickel and copper: examples from Norway. In: Prichard, H.M., Potts, P.J., Bowles, J.Fw., Cripp, S.J. (Eds.) Geoplatinum. Elsevier, London, 113-143.
4. Barnes, S.J. 2006. Nickel Deposits of the Yilgarn Craton: Geology, Geochemistry, and Geophysics Special Publication 13, Society of Economic Geologists, 13 –119.
5. Barnes, S.J., 2007. Cotectic precipitation of olivine and sulfide liquid from komatiite magma, and the origin of komatiite-hosted disseminated nickel sulfide mineralization at Mount Keith and Yakabindie, Western Australia: Economic Geology, 102, 299−304.
6. Barnes, S.J., Cruden, A.R., Arndt, N.T, Saumur, B.M. 2016. The mineral system approach applied to magmatic Ni–Cu–PGE sulphide deposits. Ore Geology Reviews, 76, 296-316.
7. Barnes, S. J. and Fiorentini, M. L. 2012. Komatiite Magmas and Sulfide Nickel Deposits: A Comparison of Variably Endowed Archean Terranes. Economic Geology, 107, 755–780.
8. Barnes, S.J., Hill, R.E.T., Perring, C.S., Dowling, S.E. 2004. Lithogeochemical exploration for komatiite-associated Ni sulfide deposits: Strategies and limitations. Mineralogy and Petrology, 82, 259-293.
9. Barnes, S.J., Wells, M.A., Verrall, M.R. 2009. Effects of magmatic processes, serpentinization, and talc-carbonate alteration on sulfide mineralogy and ore textures in the Black Swan disseminated nickel sulfide deposit, Yilgarn Craton. Economic Geology and the Bulletin of the Society of Economic Geologists, 104, 539-562.
10. Bedrock of Finland – DigiKP. Digital map database [Electronic resource]. Espoo: Geological Survey of Finland [9 May 2020], Version 2.2., available at: https://gtkdata.gtk.fi/Kalliopera/index.html
11. Bekker, A., Barley, M.E., Fiorentini, M., Rouxel, O.J., Rumble, D., Beresford, S.W., 2009. Atmospheric sulfur in Archaean komatiite-hosted nickel deposits: Science, 326, 1086–1089.
12. Boynton, W.V. 1984. Cosmochemistry of the rare earth elements, meteorite studies. In: Rare earth element geochemistry. Henderson, P. (Eds.), Elsevier, Amsterdam. 63-114.
13. Collins, J.E., Hagemann, S.H., McCuaig, T.C., Frost, K.M., 2012. Structural controls on sulfide mobilization at the Flying Fox Ni-Cu-PGE deposit, Forrestania greenstone belt, Western Australia: Economic Geology, 107, 859–879.
14. Fiorentini, M., Barnes, S. J., Lesher, C.M., Heggie, G., Keays, R.R., Burnham, O.M., 2010b. Platinum-group element geochemistry of mineralized and non-mineralized komatiites and basalts: Economic Geology, 105, 795–823.
15. Fiorentini, M., Beresford, S., Barley, M., Duuring, P., Bekker, A., Rosengren, R., Cas, R., Hronsky, 2012. District to camp controls on the genesis of komatiite-hosted nickel sulfide deposits, Agnew-Wiluna greenstone belt, Western Australia: Insights from the multiple sulfur isotopes: Economic Geology, 107.
16. Fiorentini, M.L., Beresford, S.W., Rosengren, N., Barley, M.E., McCuaig, T.C., 2010a. Contrasting komatiite belts, associated Ni-Cu-(PGE) deposit styles and assimilation histories: Australian Journal of Earth Sciences, 57, 543–566.
17. Gilbert, S.E., L.V. Danyushevs.ky, T. Rodermann, A. Shimizu, A. Gurenko, S. Meffre, H. Thomas, R.R. Large, D. Death, 2014. Optimisation of laser parameters for the analysis of sulphur isotopes in sulphide minerals by laser ablation ICP-MS. Journal of Analytical Atomic Spectrometry, 29, 1042–1051.
18. Halkoaho, T., Hokka, J. and Niskanen, M. 2016. Tutkimustyöselostus Kuhmon kaupungissa malminetsintälupa-alueella Mertaperä 1 (lupatunnus ML2013:0053) vuonna 2015 suoritetuista malminetsintätutkimuksista. (A research report of exploration studies concerning the exploration permit area of Mertaperä 1 (a permit number ML2013:0053) in Kuhmo during year 2015). Geological Survey of Finland, archive report, 86/2016. 19 http://tupa.gtk.fi/raportti/arkisto/86_2016.pdf
19. Halkoaho, T., Konnunaho, J. and Niskanen, M. 2018. The Ni-(Cu-PGE) potential of Kellojärvi komatiitic cumulate body – Prospectus. Geological Survey of Finland, 62/2018. 15, 1 App. http://tupa.gtk.fi/raportti/arkisto/62_2018.pdf

20. Halkoaho, T., Liimatainen, J., Papunen, H., Välimaa, J., 2000. Exceptionally Cr-richbasalts in the komatiitic volcanic association of the Archaean Kuhmo greenstonebelt, eastern Finland. Mineralogy and Petrology, 70, 105–120.
21. Halkoaho, T., Niskanen, M., 2009. Tutkimustyöselostus Kuhmon kaupungissaKellojärven Pärsämänsuon alueella suoritetuista nikkelimalmitutkimuksistavuosina 2007–2009. Geological Survey of Finland, Exploration ReportM19/4411/2009/70, 16 (in Finnish).
22. Halkoaho, T., Niskanen, M., 2012. Tutkimustyöselostus Kuhmon kaupunginKellojärven Pärsämänsuo 1 valtausalueella (kaivosrekisterinumero 8344/1)suoritetuista nikkelimalmitutkimuksista vuosina 2007–2011. Geological Survey of Finland, Exploration Report 64/2012, 18 (in Finnish).
23. Hannington, M.D., Bleeker, W., Kjarsgaard, L., 1999. The Giant Kidd Creek volcanogenic massive sulfide deposit, Western Abitibi subprovince, Canada: Economic Geology Monograph, 10, 163–224.
24. Hanski, E., 1980. Komatiitic and tholeiitic metavolcanics of the Siivikkovaara area in the Archean Kuhmo greenstone belt, eastern Finland. Geological Survey of Finland, Bulletin, 52, 67–100.
25. Hanski, E., Huhma, H., Rastas P., Kamenetsky, V.S., 2001. The Paleoproterozoic Komatiite Picrite Association of Finnish Lapland. Journal of Petrology, 42, 855–876.
26. Heggie, G.J., Fiorentini, M.L., Barnes, Stephen J., Barley, M.E., 2012a. Maggie Hays nickel deposit: Pt. 1. Stratigraphic controls on the style of komatiite emplacement in the 2.9 Ga Lake Johnston greenstone belt, Yilgarn Craton, Western Australia: Economic Geology, 107, 797–816.
27. Heggie, G.J., Fiorentini, M.L., Barnes, Stephen J., Barley, M.E., 2012b. Maggie Hays nickel deposit: Pt. 2. Nickel mineralization and the spatial distribution of PGE ore-forming signatures in the Maggie Hays Ni system, Lake Johnston greenstone belt, Yilgarn Craton, Western Australia: Economic Geology, 107, 817–833.
28. Herzberg, C., 1992. Depth and Degree of Melting of Komatiites. Journal of Geophysical Research, American Geophysical Union, 97, 4521–4540.
29. Hölttä, P., Balagansky, V., Garde, A. A., Mertanen, S., Peltonen, P., Slabunov, A., Sorjonen-Ward, P. Whitehouse, M., 2008. Archean of Greenland and Fennoscandia. Episodes 31 (1).
30. Hölttä, P., Heilimo, E., Huhma, H., Juopperi, H., Kontinen, A., Konnunaho, J., Lauri,L., Mikkola, P., Paavola, J., Sorjonen-Ward, P., 2012. Archaean complexes of the Karelia Province in Finland. Geological Survey of Finland, Special Paper 54, 9–20.
31. Hölttä, P., Heilimo, E., Huhma, H., Kontinen, A., Mertanen, S., Mikkola, P., Paavola, J.,Peltonen, P., Semprich, J., Slabunov, A., Sorjonen-Ward, P., 2014. The Archaean Karelia and Belomorian Provinces, Fennoscandian Shield. In: Dilek, Y., Furnes,H. (Eds.), Evolution of Archean Crust and Early Life. Science and Business Media, Dordrecht, 55–102.
32. Hölttä, P., Huhma, H., Mänttäri, I., Paavola, J., 2000. P–T–t development of Archaean granulites in Varpaisjärvi, Central Finland II: dating of high-grade metamorphisms with the U–Pb and Sm–Nd methods. Lithos, 50, 121–136.
33. Hövelmann, J., Putnis, A., Geisler, T., Schmidt, C.B., Golla-Schindler, U., 2010. The replacement of plagioclase feldspars by albite: observations from hydrothermal experiments. Contributions to Mineralogy and Petrology, 159, 43–59.
34. Houlé, M.G., Lesher, C.M., 2011. Komatiite-associated Ni-Cu-(PGE) deposits, Abitibi greenstone belt, Superior province, Canada: Reviews in Economic Geology, 17, 89−121.
35. Hronsky, J.M.A., Schodde, R.C., 2006. Nickel exploration history of the Yilgarn Craton: From the Nickel Boom to today: Society of Economic Geologists Special Publication 13, 1−11.
36. Huhma, H., Mänttäri, I., Peltonen, P., Kontinen, A., Halkoaho, T., Hanski, E., Hokkanen,T., Hölttä, P., Juopperi, H., Konnunaho, J., Layahe, Y., Luukkonen, E., Pietikäinen,K., Pulkkinen, A., Sorjonen-Ward, P., Vaasjoki, M., Whitehouse, M., 2012a. The age of the Archaean greenstone belts in Finland. Geological Survey of Finland, Special Paper, 54, 74–175.
37. Hyppönen, V., 1983. Pre-Quaternary rocks of the Ontojoki, Hiisijärvi and Kuhmomap-sheet areas. Geological Map of Finland 1:100 000, explanation to the maps of Pre-Quaternary rocks, sheets 4411, 4412 and 4413. Geological Survey of Finland, 60 (in Finnish with English summary).
38. Ikehata, K., Suzuki, R., Shimada, K., Ishibashi, J., Urabe, T. 2014. Mineralogical and Geochemical Characteristics of Hydrothermal Minerals Collected from Hydrothermal Vent Fields in the Southern Mariana Spreading Center. Subseafloor Biosphere Linked to Hydrothermal Systems, 275-287. doi:10.1007/978-4-431-54865-2_22
39. Jahn, B-M., Auvray, B., Blais, S., Capdevila, R., Cornichet, J., Vidal, F., Hameurt, J., 1980. Trace element geochemistry and petrogenesis of Finnish greenstone belts. Journal of Petrology 21, 201-244

40. Jahn, B–M., Gruau, G., Glickson, A.Y. 1982. Komatiites of the Onverwacht Group, South Africa, REE geochemistry, Sm/Nd age and mantle evolution. Contributions to Mineralogy and Petrology 80, 25–40.
41. Jensen, L.S., 1976. A new cation plot for classifying subalkalic volcanic rocks: Ontario Department of Mines, Miscellaneous Paper 66.
42. Käpyaho, A., Hölttä, P., Whitehouse, M.J., 2007. U–Pb zircon geochronology of selected Archaean migmatites in eastern Finland. Geological Survey of Finland, Bulletin, 79 (1), 95–115.
43. Konnunaho J., Halkoaho T., Hanski E., Törmänen T., 2015. Chapter 3.2 - Komatiite-Hosted Ni-Cu-PGE Deposits in Finland, (Eds.): Wolfgang D. Maier, Raimo Lahtinen, Hugh O'Brien, Mineral Deposits of Finland, Elsevier, 93-131, ISBN 9780124104389, https://doi.org/10.1016/B978-0-12-410438-9.00004-2.
44. Konnunaho, J. 2016. Komatiite-hosted Ni-Cu-PGE deposits in Finland: Their characterization, PGE content, and petrogenesis. Academic dissertation, Geological Survey of Finland, Espoo.
45. Konnunaho, J., Hanski, E., Bekker, A., Halkoaho, T., Hiebert, R., Wing, B. 2013. The Archean komatiite-hosted, PGE-bearing Ni–Cu sulfide deposit at Vaara, eastern Finland: Evidence for assimilation of external sulfur and post-depositional desulfurization. Mineralium Deposita, 48, 967-989.
46. Kontinen, A., Paavola, J., Lukkarinen, H., 1992. K–Ar ages of hornblende and biotite from Late Archaean rocks of eastern Finland – interpretation and discussion of tectonic implications. Geological Survey of Finland, Bulletin, 363, 31.
47. Korsman, K., Koistinen, T., Kohonen, J., Wennerström, M., Ekdahl, E., Honkamo, M., Idman, H. Pekkala, Y. (Eds.) 1997. Suomen kallioperäkartta/Bedrock map of Finland 1:1 000 000. Espoo: Geological Survey of Finland.
48. Kozhevnikov, V.N., Brezhnaya, N.G., Presnyakov, S.L., Lepekhina, E.N., Antonov, A.V., Sergeev, S.A., 2006. Geochronology (SHRIMP II) of zircons from Archean strato-tectonic associations of Karelian greenstone belts: significance for stratigraphic and geodynamic reconstructions. Stratigraphy and Geological Correlation, 14, 240–259.
49. Lahtinen, R., Korja, A., Nironen, M., 2005. Palaeoproterozoic tectonic evolution. In: Lehtinen, M., Nurmi, P.A., Rämö, O.T. (Eds.), Precambrian Geology of Finland—Key to the Evolution of the Fennoscandian Shield. Elsevier, Amsterdam, 481–532.
50. Lauri, L.S., Andersen, T., Hölttä, P., 2011. Evolution of the Archaean Karelian Provincein the Fennoscandian Shield in the light of U–Pb zircon ages and Sm–Nd andLu–Hf isotope systematics. Journal of Geological Society, London, 167, 1–18.
51. Le Bas, M.J. 2000. IUGS Reclassification of the High–Mg and Picritic Volcanic Rocks. Journal of Petrology, 41, 1467–1470.
52. Le Maitre, R.W. (Eds.), Streckeisen, A., Zanettin, B., Le Bas, M.J., Bonin, B., Bateman, P., Bellieni, A., Dudek, A., Efremova, S., Keller, J., Lameyre, J., Sabine, P.A., Schmid, R., Sorensen, H., Wolley, A.R. 2002. Igneous rocks A Classification and Glossary of Terms, 2nd edition. Cambridge University Press, Cambridge. 236p.
53. Lehtonen, E., Heilimo, E., Halkoaho, T., Käpyaho, A., Hölttä, E., 2016. U–Pb geochronology of Archaean volcanic-sedimentary sequences in the Kuhmo greenstone belt, Karelia Province – Multiphase volcanism from Meso- to Neoarchaean and a Neoarchaean depositional basin? Precambrian Research, 275, 48–69.
54. Lesher, C.M., Barnes, S.J. 2008. Komatiite-associated Ni–Cu–PGE deposits. In Arndt, N.T., Lesher C.M., Barnes S.J. 2008 (Eds.). Komatiite, Cambridge University Press, 295-327.
55. Lesher, C.M., 2007. Ni-Cu-(PGE) deposits in the Raglan area, Cape Smith Belt, New Québec: Geological Association of Canada, Mineral Deposits Division Special Publication, 5, 351−386.
56. Lesher, C.M., Burnham, O.M., Keays, R.R., Hulbert, L. 2001. Trace-element geochemistry and petrogenesis of barren and ore-associated komatiites. Canadian Mineralogist, 39, 673–696.
57. Lesher, C.M., Burnham, O.M., Keays, R.R., Barnes, S.J., and Hulbert, L., 2001. Trace-element geochemistry and petrogenesis of barren and ore associated komatiites: Canadian Mineralogist, 39, 673−696.
58. Lesher, C.M., Keays, R. 2002. Komatiite-associated Ni-Cu-PGE deposits: Geology, mineralogy, geochemistry and genesis. The Geology, Geochemistry Mineralogy and Mineral Beneficiation of Platinum Group Elements, 54.
59. Luukkonen, E., 1988. The structure and stratigraphy of the northern part of the late Archaean Kuhmo greenstone belt, eastern Finland. Geological Survey of Finland Special Paper, 4, 71–96.

60. Luukkonen, E., Halkoaho, T., Hartikainen, A., Heino, T., Niskanen, M., Pietikäinen, K., Tenhola, M. 2002. Itä-Suomen Arkeeiset alueet –hankkeen (12201 ja 2015000) toiminta vuosina 1992 – 2001 Suomussalmen, Hyrynsalmen, Kuhmon, Nurmeksen, Rautavaaran, Valtimon, Lieksan, Ilomantsin, Kiihtelysvaaran, Enon, Kontiolahden, Tohmajärven ja Tuupovaaran alueella. Geological Survey of Finland, unpublished report M 19/4513/2002/1.265 (in Finnish).
61. Maier, W.D., Peltonen, P., Halkoaho, T., Hanski, E., 2013. Geochemistry of komatiites from the Tipasjärvi, Kuhmo, Suomussalmi, Ilomantsi and Tulppio greenstone belt, Finland: implications for tectonic setting and Ni sulphide prospectivity. Precambrian Research, 228, 63–84.
62. Makkonen, H., Halkoaho, T. 2007. Whole rock analytical data (XRF, REE, PGE) for several Svecofennian (1. 9 Ga) and Archean (2. 8 Ga) nickel deposits in eastern Finland. Geological Survey of Finland, archive report, M19/3241/2007/32. 49 p., 13 App. http://tupa.gtk.fi/raportti/arkisto/m19_3241_2007_32.pdf
63. Mänttäri, I., Hölttä, P., 2002. U–Pb dating of zircons and monazites from Archeangranulites in Varpaisjärvi central Finland: evidence for multiple metamorphism and Neoarchean terrane accretion. Precambrian Research, 118, 101–131.
64. McDonough, W., Sun, S.S. 1995. The composition of the Earth. Chemical Geology. 67. 1050-1056.
65. Mercier-Langevin, P., Houle, M. G., Dube, B., Monecke, T., Hannington, M. D., Gibson, H. L., Goutier, J. 2012. A Special Issue on Archean Magmatism, Volcanism, and Ore Deposits: Part 1. Komatiite-Associated Ni-Cu-(PGE) Sulfide and Greenstone-Hosted Au Deposits: Preface. Economic Geology, 107(5), 745-753. doi:10.2113/econgeo.107.5.745.
66. Mikkola, P., Huhma, H., Heilimo, E., Whitehouse, M., 2011. Archean crustal evolution of the Suomussalmi district as part of the Kianta complex, Karelia: constraints from geochemistry and isotopes of granitoids. Lithos 125, 287–307.
67. Müller, W., M. Shelley, Miller, P., Broude, S. 2009. "Initial performance metrics of a new custom-designed ArF excimer LA-ICPMS system coupled to a two-volume laser-ablation cell. Journal of Analytical Atomic Spectrometry, 24, 209-214
68. Mutanen, T., Huhma, H., 2003. The 3.5 Ga Siurua trondhjemite gneiss in the ArchaeanPudasjärvi Granulite Belt, northern Finland. Geological Society of Finland, Bulletin, 75, 1–68.
69. Naldrett, A.J., 1973. Nickel sulfide deposits—their classification and genesis, with special emphasis on deposits of volcanic association. Canadian Institute of Mining and Metallurgy CIM Bulletin, 66, 45–63.
70. Naldrett, A.J., 1981. Nickel sulfide deposits: Classification, composition, and genesis: Economic Geology 75th Anniversary Volume, 628–685.
71. Naldrett, A.J. 2004. Magmatic Sulfide Deposits: Geology, Geochemistry, and Exploration. Springer, Berlin. https://doi.org/10.1007/978-3-662-08444-1
72. Naldrett, A.J.,2011. Fundamentals of magmatic sulfide deposits: Reviews in Economic Geology, 17, 1−50.
73. Naldrett, A.J., and Turner, A.R., 1977. The geology and petrogenesis of a greenstone belt and related nickel sulfide mineralisation at Yakabindie, Western Australia: Precambrian Research, 3, 43–103.
74. Nesbitt, R. W., Jahn, B.M., Purvis, A. C. 1982. Komatiites: An early Precambrian phenomenon. Journal of Volcanology and Geothermal Research, 14, 31–45.
75. Nesbitt, R.W., Sun, S.S. 1976. Geochemistry of Archaean spinifex–textured peridotites and magnesian and low–magnesian tholeiites. Earth and Planetary Science Letters, 31,433-453.
76. Nesbitt, R.W., Sun, S.S., Purvis A.C. 1979. Komatiites: Geochemistry and Genesis. Canadian Mineralogist, 17, 165–186.
77. Nisbet, E.G., Walker, D. 1982. Komatiites and the structure of the Archaean mantle. Earth and Planetary Science Letters, 60, 105-113.
78. Papunen, H., 1960. Havaintoja Siivikkovaaran alueen kallioperästä Kuhmon pitäjänVieksin kylässä. Unpublished M.Sc. Thesis. Department of Geology, University of Helsinki, 56 (in Finnish).
79. Papunen, H., Halkoaho, T., Luukkonen, E., 2009. Archaean evolution of the Tipasjärvi-Kuhmo-Suomussalmi Greenstone Complex, Finland. Geological Survey of Finland, Bulletin, 403.
80. Piirainen, T., 1988. The geology of the Archaean greenstone–granitoid terrain in Kuhmo, eastern Finland. In: Mattila, E. (Eds.), Archaean geology of the Fennoscandian Shield. Geological Survey of Finland Special Paper, 4, 39–51.
81. Puchtel, I.S., Hofmann, A.W., Amelin, Y.V., Garbe-Schönberg, C.-D., Samsonov,A.V., Shchipansky, A.A., 1999. Combined mantle plume-island arc model forthe formation of the 2.9 Ga Sumozero-Kenozero greenstone belt, SE Baltic Shield: isotope and trace element constraints. Geochimica et Cosmochimica Acta, 63,3579–3595

82. Ripley, E.M., Li, C. 2003. Sulfur isotope exchange and metal enrichment in the formation of magmatic Cu-Ni-(PGE) deposits. Economic Geology, 98, 365–641.
83. Ripley, E.M., 1999. Systematics of sulfur and oxygen isotopes in mafic igneous rocks and related Cu-Ni-PGE mineralization. In: Keays, R.R., Lesher, R.R., Lightfoot, P.C., Farrow, C.E.G. (Eds.), Dynamic processes in magmatic ore deposits and their application in mineral exploration. Geological Association of Canada, Short Course Notes, 13, 133–158.
84. Robb, L. 2005. Introduction to ore-forming processes. Blackwell, 368.
85. Sakai, H. Des Marais, D.J. Ueda, A. Moore, J.G. 1984. Concentrations and isotope ratios of carbon, nitrogen, and sulfur in ocean-floor basalts. Geochimica et Cosmochimica Acta, 48, 2430–2441.
86. Samsonov, A.V., Bogina, M.M., Bibikova, E.V., Petrova, A.Y., Shchipansky, A.A., 2005. The relationship between adakitic, calc-alkaline volcanic rocks and TTGs: implications for the tectonic setting of the Karelian greenstone belts, Baltic Shield. Lithos 79, 83–106.
87. Seal, R.R. II. 2006. Sulfur Isotope Geochemistry of Sulfide Minerals. Reviews in Mineralogy and Geochemistry 12. 61, 633-677.
88. Slabunov, A.I., Lobach-Zhuchenko, S.B., Bibikova, E.V., Sorjonen-Ward, P., Bal-agansky, V.V., Volodichev, O.I., Shchipansky, A.A., Svetov, S.A., Chekulaev,V.P., Arestova, N.A., Stepanov, V.S., 2006. The Archaean nucleus of the Baltic/Fennoscandian Shield. In: Gee, D.G., Stephenson, R.A. (Eds.), European Lithosphere Dynamics. Geological Society of London, Memoir, 32,627–644.
89. Sorjonen-Ward, P., Luukkonen, E., 2005. Archean rocks. In: Lehtinen, M., Nurmi, P.A., Rämö, O.T. (Eds.), The Precambrian Geology of Finland-Key to the Evolution of the Fennoscandian Shield. Developments in Precambrian Geology, Elsevier, Amsterdam, 14, 19–99.
90. Stone, W.E, Archibald, N.J. 2004. Structural controls on nickel sulfide ore shoots in Archaean komatiite, Kambalda, WA: The volcanic trough controversy revisited. Journal of Structural Geology, 26, 1173-1194.
91. Sun, S.S., Nesbitt, R.W. 1978. Petrogenesis of Archean ultrabasic and basic volcanics: evidence from the rare elements. Contributions to Mineralogy and Petrology. 65, 301–325.
92. Sun. S.S., 1982. Chemical composition and origin of the Earth's primitive mantle. Geochimica et Cosmochimica Acta, 46, 179-192.
93. Svetov, S.A., Svetova, A.I., 2011. Archaean subduction: marker rock assemblagesand architecture. In: Proceedings of the All-Russian Conference convened to celebrate the 50th anniversary of the founding of the Institute of Geology, 24–26 May, Karelian Research Centre (KRC), Russian Academy of Sciences (RAS), Petrozavodks, 22–32.
94. Taranovic, V., Lesher, C.M., Houlé, M.G., Bédard, J.H., 2012. Physical volcanology and metallogenesis of komatiite-associated Ni-Cu-(PGE) mineralization in the C zone, Bannockburn Township, Ontario: Economic Geology, 107, 835–857.
95. Thode, H.G. Monster, J. Dunford, H.B. 1961. Sulphur isotope geochemistry. Geochimica et Cosmochimica Acta, 25, 159–174.
96. Törmänen, T, Konnunaho, J., Hanski, E, Moilanen, M., Heikura, P. 2015. The Paleoproterozoic komatiite-hosted PGE mineralization at Lomalampi, Central Lapland Greenstone Belt, northern Finland. Mineralium Deposita. 10.1007/s00126-015-0615-y.
97. Vaasjoki, M., Korsman, K., Koistinen, T., 2005. Overview. In: Lehtinen, M., Nurmi, P.A., Rämö, O.T. (Eds.), The Precambrian Geology of Finland—Key to the Evolution of the Fennoscandian Shield. Elsevier, Amsterdam, 1–18.
98. Vaasjoki, M., Taipale, K., Tuokko, I., 1999. Radiometric ages and other isotopic data bearing on the evolution of Archaean crust and ores in the Kuhmo Suomussalmi area, eastern Finland. Geological Survey of Finland, Bulletin, 71, 155–176.
99. Vanne, J. 1984. Tutkimustyöselostus Kuhmon kunnassa valtausalueella Siivikkovaara 1-5, kaiv.rek. n:o 2853/1-5 suoritetuista malmitutkimuksista. Geological Survey of Finland, unpublished report M 06/4411/-84/1/10 (in Finnish)
100. Wang Y., Han X., Petersen S., Frische M., Qiu Z., Li H., Honglin Li, Wu Z., Cui C., 2017. Mineralogy and trace element geochemistry of sulfide minerals from the Wocan Hydrothermal Field on the slow-spreading Carlsberg Ridge, Indian Ocean, Ore Geology Reviews, 84, 1-19, ISSN 0169-1368, https://doi.org/10.1016/j.oregeorev.2016.12.020.

APPENDIX 1: Drill core sample characterization, Siivikkovaara sulfide body.

Drill Core: 303			
Sample code	**Sample description**	**Section number**	**Petrography**
M52/4411/83/303_4.65m	Sulfides	190040	Chalcopyrite, pyrrhotite, pentlandite, sphalerite
M52/4411/83/303_15.00-15.40m	komatiitic basalt	190041	Actinolite, plagioclase, biotite, epidote, opaque minerals
M52/4411/83/303_52.10-52.30m	komatiitic basalt	190042	Chlorite, Actinolite, plagioclase, opaque minerals
M52/4411/83/303_71m	komatiitic basalt	Ku09071	Plagioclase, epidote, amphibole, tourmaline, garnet, carbonate minerals, opaque minerals
M52/4411/83/303_97.95-98.20m	komatiitic basalt	190043	Chlorite, actinolite
Drill Core: 304			
M52/4411/83/304_9.35-9.90m	komatiite	190044	Actinolite, chlorite, plagioclase, opaque minerals
M52/4411/83/304_18.90-19.25m	komatiite	190045	Actinolite, plagioclase, chlorite
M52/4411/83/304_32.95-33.30m	komatiite	190046	Actinolite, chlorite, plagioclase, opaque minerals
M52/4411/83/304_34.80-35.00m	Calcite mineralization	190047	Chalcopyrite, pyrrhotite, pentlandite
M52/4411/83/304_36.1m	Sulfides	190048	Chalcopyrite, pyrrhotite, pentlandite
M52/4411/83/304_36.4m	Sulfides	190049	Chalcopyrite, pyrrhotite, pentlandite, sphalerite
M52/4411/83/304_37.5m	Sulfides	190050	Chalcopyrite, pyrrhotite, pentlandite, sphalerite
M52/4411/83/304_38.1-38.5m	Tremolite schist, contact between mineralization and lower komatiite basalt	190051	Actinolite, chlorite, plagioclase, carbonate minerals, opaque minerals
M52/4411/83/304_39.6-39.9m	Tremolite schist, contact between mineralization and lower komatiite basalt	190052	Actinolite, chlorite, plagioclase, opaque minerals

M52/4411/83/304_55.7-56.05m	Mafic dyke	190053	Actinolite, plagioclase, opaque minerals
M52/4411/83/304_77.0-77.30m	komatiitic basalt	190054	Actinolite, plagioclase, biotite, opaque minerals
M52/4411/83/304_114.20-114.50m	komatiitic basalt	190055	Actinolite, plagioclase, biotite,
Drill Core: 305			
M52/4411/83/305_9.55m	Sulfides	190056	Chalcopyrite, pentlandite, sphalerite
M52/4411/83/305_12.30m	Sulfides	190057	Chalcopyrite, pyrrhotite, pentlandite, sphalerite
M52/4411/83/305_15.00m	Sulfides	190058	Chalcopyrite, pentlandite, sphalerite
M52/4411/83/305_14.45m	komatiitic basalt	0503044	Actinolite, chlorite, plagioclase, opaque minerals
M52/4411/83/305_38.80-39.30m	komatiitic basalt	190059	Actinolite, plagioclase, biotite, orthoclase, opaque minerals
M52/4411/83/305_60m	komatiitic basalt	Ku09072	Amphibole, plagioclase, opaque minerals
M52/4411/83/305_64.30-64.40m	komatiitic basalt	190060	Actinolite, plagioclase, biotite, opaque minerals
Drill Core: 306			
M52/4411/83/306_3.80m	Sulfides	190061	Chalcopyrite, pyrrhotite, pentlandite, sphalerite, violarite
M52/4411/83/306_11.25m		0503045	Actinolite, chlorite, plagioclase, carbonate minerals
M52/4411/83/306_14.90-15.0m	Calcite mineralization	190062	Chalcopyrite, pyrrhotite, pentlandite, sphalerite, violarite
M52/4411/83/306_34.30-34.80m	komatiitic basalt	190063	Actinolite, chlorite, plagioclase, carbonate minerals
M52/4411/83/306_50.80-51.40m	komatiitic basalt	190064	Actinolite, biotite, plagioclase, carbonate minerals
M52/4411/83/306_88.20-88.40m	komatiitic basalt with variolitic texture	190065	Actinolite, plagioclase, carbonate minerals, biotite, chlorite, opaque minerals

APPENDIX 2: LA-ICP-MS data on sulfides from the Siivikkovaara mineralized body.

File	Co59	Ni60	Cu65	Zn66	Ga71	As75	Se82	Mo95	Ag107	Sn118	Sb121	Te128	Pb208	Bi209
	µg/g	µg/g	µg/g	µg/g	µg/g	µg/g	µg/g	µg/g	µg/g	µg/g	µg/g	µg/g	µg/g	µg/g
190040_Chalco_8-1_sr.csv	0.075497	15.86609	277174.8	382.1423	0.105994	<0.6154	38.36903	<0.094273	215.3866	4.426984	<0.15188	<3.4956	0.888637	<0.017854
190040_Chalco2_sr.csv	0.719486	22.42896	285008.4	805.905	0.429578	<1.442	<75.6598	<0.23784	168.1636	6.902459	<0.31338	7.734567	1.262664	<0.049276
190040_Chalco3_sr.csv	0.567276	17.84219	278994.1	331.9891	0.282717	<0.62955	42.26175	<0.036195	110.8971	4.669065	<0.154	4.672835	1.260546	<0.017546
190040_Chalco4_sr.csv	0.353388	3.429833	278935.3	316.5383	0.335949	<0.6204	42.65751	<0.10931	120.6568	4.428117	0.230239	<3.8268	2.009276	<0.021336
19047_Chalco_2_sr.csv	0.326675	18.28238	272290.6	273.2371	0.014353	<0.50863	87.13284	<0.03403	24.31853	1.44922	<0.17321	<3.5093	1.320206	0.386357
19047_Chalco_4_sr.csv	0.145233	13.28528	280128.2	329.6893	<0.060708	<0.85317	66.90159	<0.041991	22.17461	1.479468	<0.19395	<4.1816	1.46575	2.216329
19047_Chalco_5_sr.csv	0.359328	20.37582	272956.4	296.6634	<0.045815	<0.68718	86.54043	<0.12028	20.7913	1.784838	<0.15325	<3.8818	1.269684	0.403587
190048_Chalco_6-1_sr.csv	0.350788	11.33008	279531.5	309.2441	<0.044456	34.38869	90.49788	<0.037542	38.89942	6.31466	<0.1286	5.377887	0.447646	0.341637
190048_Chalco_6-2_sr.csv	0.317257	10.8331	275406.9	261.3869	0.034631	33.29906	103.0656	<0.12077	33.8037	6.858875	<0.14995	<4.391	0.856825	0.463123
190048_Chalco_10-1_sr.csv	0.271697	10.79183	277817.7	457.4886	<0.070408	22.74237	129.5473	0.041788	32.31613	5.924401	<0.22331	13.52892	1.434574	14.79809
190048_Chalco_10-2_sr.csv	0.279955	11.96507	276595.3	294.7107	<0.05336	23.51485	103.1768	<0.037145	27.65237	5.445145	<0.15233	5.833361	1.186961	5.589114
190049_Chalc_3-2_sr.csv	0.441614	21.83345	264680.9	276.6349	<0.045031	<0.74642	106.5141	<0.037294	37.78489	5.624493	<0.20059	5.758594	1.10075	0.430188
190049_Chalc_4-1_sr.csv	0.611281	28.59797	269969.4	591.0583	<0.097764	<1.243	92.00165	<0.06583	41.35771	7.178002	<0.31879	12.39685	10.33808	1.34044
190049_Chalc_4-2_sr.csv	0.567379	29.88705	271041.5	321.6098	0.030613	<1.1262	135.6487	<0.054578	37.65979	5.943678	<0.33162	<4.932	1.903845	0.521577
190050_Chalco_2-1_sr.csv	0.625288	14.91227	274474.2	4303.569	<0.050837	<0.57317	111.5595	<0.10675	42.7087	6.43488	0.95063	<5.1545	10.95695	2.274236
190050_Chalco_2-2_sr.csv	0.234156	14.06511	278185.1	343.5883	0.064763	<0.62768	108.0719	<0.035876	40.89105	6.366524	<0.19089	<5.3337	1.038842	0.295188
190050_Chalco_3-1_sr.csv	0.300701	19.193	273074.7	355.4168	<0.055047	<0.63088	129.4154	<0.14621	40.97566	6.499648	0.208498	<5.4057	3.246894	0.740741
190050_Chalco_3-2_sr.csv	0.150578	12.49461	276070.5	324.6521	0.051015	<0.57335	108.6652	<0.037095	39.31418	6.031777	0.242916	<5.0867	3.067235	1.530034
190050_Chalco_6-1_sr.csv	0.29847	23.67702	275715.8	981.6351	<0.051119	<0.57048	150.7279	<0.10646	43.35436	6.361709	1.116016	<4.9791	12.5722	2.587554
190050_Chalco_6-2_sr.csv	0.356334	24.68138	272479.8	303.2732	0.066353	<0.50887	129.6576	<0.10193	39.84521	6.366618	<0.17291	5.527638	1.079102	0.369811
190050_Chalco_7-1_sr.csv	0.465851	37.64605	532881.1	650.9072	<0.10558	<0.91935	196.2898	<0.18899	81.04938	12.23237	0.268938	10.64069	2.75167	1.182587
190050_Chalco_7-2_sr.csv	0.437417	34.03606	538537	629.7456	0.083194	<0.91733	260.8367	<0.060007	78.27163	12.11218	<0.20693	<8.3982	1.185046	0.507829
190050_Chalco_8-1_sr.csv	0.204522	11.94359	278971.1	338.6213	0.074268	<0.47382	103.4296	0.03685	42.73512	6.569801	<0.17433	5.130731	0.884688	0.589614
190050_Chalco_8-2_sr.csv	0.377518	13.62619	279634.6	356.6166	<0.04111	<0.54633	97.93809	<0.036896	38.03916	6.072754	<0.15488	<5.008	0.885434	0.305469
190056_Chalc_3-1_sr.csv	0.380834	3.787035	272971	344.2733	0.222913	<0.6615	92.3821	<0.12673	31.4217	4.72704	<0.15667		8.370594	0.398778
190056_Chalc_3-2_sr.csv	0.202091	2.117375	281416.6	646.4319	0.138736	<0.85941	74.52723	<0.053209	41.41868	5.918298	<0.22311		2.548637	0.141546
190056_Chalc_4-1_sr.csv	0.052873	0.261031	278497.3	411.9829	0.167224	<0.55273	104.5798	<0.04578	36.49432	5.169661	<0.19906		5.816993	0.243406
190056_Chalc_4-2_sr.csv	0.309937	8.109071	271829.3	410.1672	0.140798	<0.60086	78.0783	<0.061227	23.26686	4.082662	0.147649		8.14781	0.284936
190056_Chalc_5-1_sr.csv	0.076905	1.10968	272521.2	390.0224	0.159734	<0.4463	123.4587	<0.039429	40.23633	4.656313	<0.16901		4.531403	0.438665
190056_Chalc_5-2_sr.csv	0.214235	6.375114	278592.2	572.739	0.191934	<0.70953	100.3185	<0.062214	42.94014	5.831	<0.18893		18.87834	0.731307
190058_Chalc_4-1_sr.csv	0.273365	4.276048	272303.7	430.2187	<0.040002	<0.61868	95.13114	0.431611	16.16505	0.209988	0.358901	<4.4868	5.577791	1.025938
190058_Chalc_4-2_sr.csv	0.285231	3.79561	274665.6	756.393	<0.054428	<0.63981	88.54136	<0.048831	16.05882	<0.1954	<0.22365	<5.8061	3.372715	0.645672
190058_Chalc_8-1_sr.csv	0.131504	2.863861	273307.1	331.1542	<0.055467	<0.72695	124.0312	<0.14385	16.53465	0.304838	0.33323	<5.6633	1.298038	0.241376
190058_Chalc_8-2_sr.csv	0.109785	1.418714	275036.9	519.1597	0.058199	<0.6532	104.2001	0.150837	11.2198	0.194919	<0.18257	<5.7163	1.773207	0.254572
190058_Chalc_6-2_sr.csv	0.191558	1.080126	277000.3	506.4027	<0.045725	<0.588	59.37666	0.940413	14.55843	0.468295	<0.18766	<4.5337	4.179465	0.886682
190061_Chalc_3-2_sr.csv	0.123281	1.767939	273186	218.2983	0.125088	<0.735	48.46491	<0.14703	1.37866	4.686646	<0.20103	<4.2488	0.938826	0.114365
190061_Chalco_1-1_sr.csv	0.743168	16.70874	268814.2	340.0767	0.220344	<1.2849	91.44531	<0.065362	60.80704	5.920825	<0.28058	10.88494	2.701014	0.645552
190061_Chalco_2-2_sr.csv	0.616684	6.937429	268688.4	368.0966	0.288663	0.875549	118.3962	0.057202	64.02936	5.439666	<0.28967	6.135147	1.497735	0.303393
190062_Chalco_2-1_sr.csv	0.570842	13.95892	277466.3	357.1337	0.145866	<0.85136	69.61934	<0.041627	100.151	1.968229	<0.22388	<4.233	1.037488	2.534286
190062_Chalco_3-1_sr.csv	0.718043	11.51957	274361.2	405.3392	0.101896	<0.94826	79.01648	<0.042622	96.05183	2.404713	<0.25001	<4.5901	1.167045	2.049812
190062_Chalco_4-1_sr.csv	1.450143	40.74342	272989.7	312.3902	0.179537	<1.2058	100.0747	<0.070498	95.49845	3.458799	<0.26001	6.087139	2.23013	6.144883
190062_Chalco_5-1_sr.csv	0.451059	4.895706	271660.4	269.1375	0.025545	<0.56639	75.46388	<0.060771	82.59297	1.837093	<0.18641	<3.5728	3.581448	1.470874
190062_Chalco_6-1_sr.csv	2.547271	123.4493	258755.9	498.196	<0.054971	<0.66893	62.98162	<0.04769	79.51886	2.229744	<0.22605	<4.853	5.998707	2.092663
190062_Chalco_8-1_sr.csv	0.462784	18.54807	277276.8	333.5019	0.099878	<0.65725	70.55573	<0.15892	98.78311	2.161367	<0.17832	4.113898	0.828896	6.016177
190062_Chalco_8-2_sr.csv	0.36291	13.49477	275406	302.2074	0.074089	0.59832	88.92223	<0.040695	102.3172	2.136522	<0.16505	4.585767	1.498662	4.913534
190062_Chalco_9-1_sr.csv	0.991684	28.03214	280299.5	385.0867	0.102232	<0.88836	84.66973	<0.047497	104.0425	2.644695	<0.24083	<5.0254	3.996819	1.723154
190062_Chalco_9-2_sr.csv	0.793488	16.80716	276660.3	2770.725	<0.057979	<0.63677	79.06179	<0.13097	100.3384	2.590093	0.129083	10.40561	2.62157	13.65955
190062_Chalco_10-1_sr.csv	0.356014	5.391297	279468.9	310.892	<0.063873	<0.87045	72.1822	<0.041793	94.58853	2.344577	<0.14505	<4.4328	4.015007	1.826796
190062_Chalco_10-2_sr.csv	1.028343	27.85797	276118.7	373.4039	0.093923	<0.70554	78.51068	0.0619	99.78813	2.343803	<0.14571	4.563029	1.135103	1.98038

File	Co59	Ni60	Cu65	Zn66	Ga71	As75	Se82	Mo95	Ag107	Sn118	Sb121	Te128	Pb208	Bi209
	µg/g	µg/g	µg/g	µg/g	µg/g	µg/g	µg/g	µg/g	µg/g	µg/g	µg/g	µg/g	µg/g	µg/g
190040_Pyrr_1-1_sr.csv	105.3524	12654.01	7.2704	126.3844	<1.2713	18.4229	1314.642	1.1152	2.7839	4.6402	4.4852	129.7491	10.28214	0.64966
190040_Pyrr_1-2_sr.csv	101.3308	12367.34	<8.8569	<128.7906	0.595768	<21.18	<1365.173	<1.4157	<3.6185	<5.3787	<6.2116	<137.0831	3.770774	<0.85561
19047_Pyrrh_1_sr.csv	214.4433	7600.685	7.664383	<5.8898	0.100535	<0.97124	96.64435	0.365421	<0.14632	<0.12122	<0.21924	<5.504	0.309342	0.309275
19047_Pyrrh_7_sr.csv	216.6978	10672.79	1.519695	<4.3566	<0.081044	<0.78464	101.8963	<0.046661	0.138365	<0.13922	<0.21182	<4.8968	0.462289	0.367171
19047_Pyrrh_8_sr.csv	235.4766	10551.09	0.634922	<3.992	<0.053289	<0.73675	96.41353	<0.17759	<0.090566	0.11041	<0.2292	<4.6125	0.342375	0.217969
19047_Pyrrh_9_sr.csv	110.0768	8886.334	1.029267	3.6056	<0.047008	0.7339	89.90515	0.064384	0.183383	<0.14496	0.1685	4.1613	0.245827	0.268214
190048_Pyrr_5-1_sr.csv	188.7306	8899.156	0.917291	<3.6597	0.052125	39.6066	168.4003	<0.17604	<0.14073	<0.19359	<0.22281	5.0275	0.182644	0.311565
190048_Pyrr_7-2_sr.csv	215.6262	9647.262	0.596742	3.6132	<0.068931	35.17139	147.9802	0.143843	0.248096	0.16968	0.17169	<5.1671	0.244218	0.390493
190048_Pyrr_9-1_sr.csv	72.10182	6175.116	0.448284	<3.7699	<0.05925	29.72438	142.341	0.074234	0.124897	<0.19921	<0.19654	<5.5425	0.124383	0.152193
190048_Pyrr_9-2_sr.csv	68.1584	5671.756	<0.37448	<3.7449	<0.05984	28.98884	134.701	0.106997	0.630639	<0.1905	<0.16051	<5.4526	0.318403	0.460621
190049_Pyrrh_3-1_sr.csv	161.4168	3244.501	0.750542	3.0413	<0.028881	0.56799	53.85525	0.076004	0.117823	0.166319	0.15047	2.6258	0.179757	0.243107
190049_Pyrr_2-2_sr.csv	98.52332	7053.121	0.494237	<7.0363	0.063307	<1.2986	112.0835	<0.18384	0.402665	<0.24133	<0.34709	<5.9658	0.438996	0.409563
190049_Pyrr_5-2_sr.csv	164.3847	6319.24	0.528577	<5.8684	<0.021162	<1.0903	158.1999	<0.16216	0.169343	<0.1324	<0.29334	<5.2918	0.66664	0.671363
190049_Pyrr_6-2_sr.csv	161.7093	6345.238	<0.43642	<5.5751	<0.057982	<1.1276	145.2609	<0.15256	0.158574	<0.13529	<0.26429	<5.0906	0.256944	0.340115
190049_Pyrr_7-2_sr.csv	177.8637	6465.918	<0.41681	<5.4108	<0.062023	<1.1284	126.7679	<0.056925	0.275685	<0.17699	<0.29855	<5.3202	0.523105	0.790938
190050_Pyrr_1-1_sr.csv	217.9604	9793.861	<0.43845	<8.2223	<0.062784	<1.0553	160.7115	0.083137	<0.1586	<0.22017	<0.27207	<8.4299	0.69067	0.651945
190050_Pyrr_1-2_sr.csv	203.818	9733.508	0.368423	<6.3742	0.027714	<0.77003	151.3525	0.073692	<0.13622	<0.21628	<0.25772	<6.9797	0.58596	0.557348
190050_Pyrr_4-1_sr.csv	118.4268	7465.402	<0.36462	<4.2244	0.020365	<0.65143	165.1517	<0.1125	0.145323	<0.14008	<0.16869	<5.4894	0.378662	0.437943
190050_Pyrr_4-2_sr.csv	111.1154	8164.649	0.87219	<4.5164	0.081097	<0.65406	149.0199	<0.041646	0.434503	<0.16586	<0.19277	<6.1645	1.164372	1.038647
190050_Pyrr_5-1_sr.csv	42.6647	3568.978	0.158916	2.0544	<0.021482	<0.29527	85.91057	<0.018854	0.117064	<0.067942	<0.10054	<2.8306	0.64901	0.53824
190050_Pyrr_5-2_sr.csv	73.85441	4008.549	<0.20564	<2.1698	<0.030159	0.28482	77.26314	0.086071	0.161705	0.075779	0.074198	2.9793	0.239435	0.196235
190050_Pyrr_9-1_sr.csv	203.2853	5895.573	<0.60975	<3.3171	<0.020245	<0.63331	147.7812	<0.17218	0.328699	<0.17517	<0.13392	<5.2641	0.313984	0.543971
190050_Pyrr_9-2_sr.csv	211.416	6335.199	<0.41367	<3.2269	<0.067862	<0.56154	157.7852	<0.040455	0.225795	<0.14461	<0.14661	<5.2075	0.340148	0.412612
190050_Pyrr_10-2_sr.csv	62.70233	6881.227	0.414331	<4.0111	<0.07909	<0.6384	198.2611	<0.045097	0.276242	<0.16079	<0.17787	<6.3549	0.45477	0.51264
190056_Pyrr_1-1_sr.csv	280.2965	12103.7	0.578845	<6.6536	<0.08562	0.8269	170.1658	0.048783	0.751591	<0.22468	0.23217		1.438261	<0.039578
190056_Pyrr_1-2_sr.csv	269.0819	11533.1	0.629712	5.5762	0.050026	<0.86631	133.5707	<0.05102	0.212306	0.22042	<0.24899		12.83987	0.498806
190057_Pyrrh_4-1_sr.csv	121.9173	6576.994	0.462034	1.7238	0.007484	0.32063	76.97377	<0.01931	<0.03766	0.072084	0.092987	2.4777	0.085058	0.057575
190057_Pyrr_1-1_sr.csv	205.5875	12189.52	<0.36707	<6.7141	<0.066139	<0.83542	139.1085	0.084163	0.109515	0.181491	<0.33195	<5.4283	0.616595	0.253569
190057_Pyrr_1-2_sr.csv	175.541	12614.37	<0.2829	<5.6978	<0.054017	<0.86601	153.5846	0.194171	0.173654	0.310634	<0.26324	<5.6771	0.287927	0.183657
190057_Pyrr_5-1_sr.csv	235.9614	11100.04	<0.33809	<4.8859	<0.095666	<0.93245	170.4637	<0.19659	0.205715	2.490203	<0.23078	<6.8449	0.134592	0.121647
190057_Pyrr_5-2_sr.csv	191.0013	11356.29	0.353839	<4.1125	<0.067087	<0.90632	139.4557	0.064576	0.149716	0.214082	<0.19025	<6.3824	0.161738	0.173191
190058_Pyrr_1-1_sr.csv	122.5567	18480.44	0.564419	<6.9102	<0.054576	<0.84803	231.9775	0.162726	1.201425	<0.18583	<0.26087	<5.9351	2.582744	1.221572
190058_Pyrr_1-2_sr.csv	73.67808	14007.03	27.71035	<2.1788	<0.020853	0.485489	137.2301	0.082154	0.121444	<0.07753	<0.095683	<2.277	0.247627	0.098024
190058_Pyrr_2-1_sr.csv	80.74785	11133.65	1.728279	<1.5642	<0.022044	<0.23354	144.6429	0.512064	1.450223	0.068883	<0.063119	<1.8938	0.674423	0.20248
190058_Pyrr_3-1_sr.csv	98.34961	13107.56	0.464261	1.401284	<0.025713	<0.27034	122.5374	0.238337	0.031356	<0.059088	<0.063293	<1.8831	1.050216	0.018796
190058_Pyrr_3-2_sr.csv	41.57087	12157.51	1.299906	1.420836	<0.027368	<0.23868	112.2165	1.134175	0.070003	<0.073984	<0.076696	<1.955	0.263434	0.753402
190058_Pyrr_5-1_sr.csv	181.0572	14769.59	0.582197	2.123683	<0.022203	<0.22764	170.3354	0.861906	0.950848	0.061581	0.055984	1.8647	2.133204	0.908264
190058_Pyrr_5-2_sr.csv	5.108874	1464.258	2.481486	1.808353	0.009588	<0.26648	<20.3177	0.09192	<0.047894	<0.072105	0.068032	<2.2617	0.194618	0.087121
190061_Pyrrh_4-1_sr.csv	67.52554	7456.083	<0.64479	4.3758	0.022136	0.96082	124.3579	<0.14671	0.317928	0.267719	<0.23246	<5.603	0.246641	<0.043829
190061_Pyrrh_4-2_sr.csv	89.281	8660.651	41.06393	<4.5058	<0.074162	<0.95135	81.39942	<0.055869	0.253235	<0.15768	0.22628	5.4222	0.873586	0.035682
190061_Pyrr_1-2_sr.csv	174.0606	7516.159	<0.36765	<5.0572	<0.08628	<1.0155	81.05801	0.080382	<0.1148	0.140924	<0.27064	<5.3072	0.214813	0.050639
190061_Pyrr_2-1_sr.csv	172.0957	7209.924	<0.33439	<5.0738	<0.12015	<1.0227	108.1213	<0.058572	<0.10799	<0.17273	<0.28725	<5.9634	0.311999	0.096887
190061_Pyrr_5-2_sr.csv	81.08457	8111.001	38.20726	<6.8285	<0.044322	<1.3032	<86.4655	0.171891	0.532187	<0.25998	<0.43502	<8.7165	0.774345	<0.072159

File	Cr52	**Mn55**	**Co59**	**Ni60**	**Cu65**	**Zn66**	Ga71	**As75**	**Se82**	Mo95	**Ag107**	**Sn118**	**Sb121**	**Te128**	Pb208	**Bi209**
	µg/g	µg/g	µg/g	µg/g	µg/g	µg/g	µg/g	µg/g	µg/g	µg/g	µg/g	µg/g	µg/g	µg/g	µg/g	µg/g
19047_Pen_3_sr.csv	5.7539	2.1563	10097.53	363553.8	<2.0867	6.851	<0.098969	<1.0166	143.8579	0.191458	0.386521	0.19562	0.2949	7.1116	0.797283	0.283587
19047_Pen_6_sr.csv	<6.4369	<2.4636	9209.365	359713	1.5047	<7.1942	0.054485	1.340792	91.69568	<0.14305	0.167217	<0.27053	<0.38158	<8.1092	0.460294	0.744476
190048_Pen_5-2_sr.csv	<5.1883	<2.569	9734.165	376065.1	1.084769	<6.0573	0.065618	57.77825	176.4887	<0.31378	<0.15563	<0.36954	<0.33362	<8.5845	<0.064348	<0.063362
190048_Pen_7-1_sr.csv	<9.3174	<4.5808	9376.004	359164	1.32448	<10.6668	<0.17986	73.30227	202.4375	<0.17847	0.238683	<0.53701	<0.49649	<15.8472	<0.096727	<0.08957
190048_Pen_8-1_sr.csv	<5.4559	<2.7458	9293.731	363338	<0.76714	<6.4133	<0.1014	49.50454	<93.0762	<0.38658	<0.24758	<0.34891	<0.29203	44.72584	0.232498	0.090004
190048_Pen_8-2_sr.csv	<5.2925	<2.6559	9522.962	359585.7	<0.65258	<6.2788	0.050934	41.58036	<90.4365	<0.090712	<0.17737	0.310225	<0.37243	<9.0783	0.06047	<0.050606
190048_Pen_11-1_sr.csv	<4.43	<2.2454	7515.387	351247.6	1.807723	<4.975	<0.037749	26.88319	104.7207	0.099255	0.323577	<0.24512	0.389769	10.77964	0.466085	0.704438
190048_Pen_11-2_sr.csv	4.1602	2.1163	7980.13	375707.8	3.451314	4.7775	<0.089977	29.58369	127.432	<0.10139	<0.14	<0.27149	0.300443	<6.9958	0.168866	0.095658
190049_Pen_6-1_sr.csv	<11.7374	<4.2603	24501.87	597460.7	<1.198	<14.7781	<0.05888	<3.4219	257.597	<0.15493	0.741382	<0.42116	<0.63285	<14.0739	0.744263	0.32411
190061_Pen_3-1_sr.csv	<7.7761	<2.8752	11972.83	381653.4	100.8038	<7.7032	<0.096466	<1.5261	119.0336	<0.091195	0.319255	<0.20426	<0.44283	<9.0653	1.218567	0.078215

APPENDIX 3: Whole-rock geochemical data from the Siivikkovaara mineralized body.

Sample ID	Sample Description	SiO2	TiO2	Al2O3	FeO	MnO	MgO	CaO	Na2O	K2O	Cr2O3	P2O5
M52441183R303 15.00-15.50	Komatiitic basalt	53.153	0.703	15.2005	9.327	0.2097	6.4648	9.518	5.0089	0.18471	0.152	0.06519
M52441183R303 52.05-52.30	Komatiitic basalt	51.067	0.7458	14.7229	11.05	0.20556	12.065	6.32826	3.59462	0.08395	0.06869	0.0635
M52441183R303 97.90-98.20	Komatiitic basalt	48.867	0.5655	10.9722	11.386	0.24237	16.497	9.68392	1.40837	0.07096	0.23239	0.0535
M52441183R304 9.35-9.90	Komatiite (thin lava flow)	45.032	0.3589	8.84126	11.907	0.22591	21.111	11.6049	0.37842	0.02064	0.42093	0.0367
M52441183R304 18.90-19.25	Komatiite (thin lava flow)	45.728	0.3402	8.51766	11.733	0.24891	22.173	10.4701	0.28544	0.01484	0.40193	0.02969
M52441183R304 32.95-33.30	Komatiite (thin lava flow)	45.97	0.267	6.03847	11.001	0.18562	27.969	7.78012	0.05729	0.00458	0.61677	0.01948
M52441183R304 38.10-38.50	Chlorite schist	40.389	0.5478	13.5328	17.931	0.23212	18.964	7.40472	0.81243	0.0383	0.09354	0.0383
M52441183R304 39.60-39.90	Komatiitic basalt	53.265	0.7276	16.4519	9.0678	0.14552	9.0241	4.82155	6.20068	0.04561	0.17539	0.05973
M52441183R304 55.70-56.05	Mafic dyke	50.851	1.5303	15.2181	12.208	0.2247	6.5388	8.16815	4.90941	0.15548	0.03069	0.16294
M52441183R304 77.00-77.30	Komatiitic basalt	56.665	0.69	12.3576	8.4948	0.20491	8.0397	8.89704	4.20283	0.22791	0.15346	0.05959
M52441183R304 114.20-114.55	Komatiitic basalt	50.922	0.7495	14.5417	11.713	0.20565	9.8336	8.35127	3.33007	0.25263	0.03215	0.06681
M52441183R304 114.20-114.55 (2)	Komatiitic basalt	51.034	0.7437	14.4975	11.69	0.19874	9.8428	8.31566	3.32626	0.25208	0.03215	0.0659
M52441183R305 38.80-39.30	Komatiitic basalt	48.35	0.6111	11.2594	11.794	0.29624	8.8545	14.7794	3.6074	0.10166	0.266	0.05575
M52441183R305 64.20-64.40	Komatiitic basalt	53.799	0.7096	14.8406	9.6243	0.18204	7.302	8.71103	4.51492	0.1121	0.14908	0.05142
M52441183R306 34.30-34.80	Komatiitic basalt	46.953	0.6018	10.654	13.758	0.29232	15.965	10.215	1.18854	0.10815	0.19877	0.0514
M52441183R306 50.80-51.40	Komatiitic basalt	53.241	0.7505	12.8708	10.177	0.19952	9.4282	8.91133	4.03181	0.23157	0.07892	0.07753
M52441183R306 88.20-88.40	Variolitic komatiitic basalt	52.199	0.6704	13.9942	10.572	0.22774	7.311	10.7803	3.82047	0.22667	0.13154	0.05853
4411/83/R305/4.35-4.60	Deposit	44.405	0.7412	11.295	17.367	0.21593	17.939	7.18117	0.72532	0.03233	0.05788	0.03377
4411/83/R305/14.00-14.40	Deposit	46.001	0.7638	12.4268	16.165	0.21245	14.716	7.84196	1.74411	0.05025	0.04209	0.03335
4411/83/R305/20.60-21.00	Deposit	46.514	0.5318	10.1371	10.149	0.328	8.32	21.0399	2.55999	0.09509	0.25504	0.03383
4411/83/R306/7.55-8.00	Deposit	48.329	0.7154	16.4277	12.007	0.16237	12.4	6.37714	3.43392	0.08064	0.02689	0.03806
4411/83/R306/14.05-14.45	Deposit	44.723	0.6331	10.8598	17.37	0.22503	17.084	8.19597	0.74756	0.05256	0.07264	0.03004
4411/83/R306/30.05-30.45	Deposit	44.288	0.6991	11.5105	18.288	0.27559	12.716	10.5162	1.41414	0.14733	0.095	0.04089
36-JSK-94-12.30	Komatiitic basalt	46.96	0.4652	10.8073	15.251	0.2721	14.373	10.4014	1.04233	0.11082	0.252	0.0406
36-JSK-94-30.50	Komatiite (thin lava flow)	48.079	0.4561	9.97074	11.616	0.20114	19.361	9.2501	0.66687	0.05593	0.285	0.03657
37-JSK-94-4.00	Metapyroxenite	44.587	0.3397	8.599	14.862	0.19427	26.54	4.79845	0	0.01805	0.032	0.02654
28-TOH-94	Metapyroxenite	46.065	0.3601	9.69909	16.349	0.33914	22.535	4.58442	0	0.00884	0.03	0.02541
73-TOH-94	Komatiite (thin lava flow)	52.12	0.275	5.83558	11.612	0.14183	28.507	0.82283	0.02165	0	0.59675	0.01841
73-TOH-94	Komatiite (thin lava flow)	53.361	0.207	5.01152	10.855	0.12884	29.115	0.70811	0	0.00406	0.57994	0.02029
74-TOH-94	Komatiitic basalt	50.002	0.3611	8.18973	13.158	0.21685	15.474	11.053	0.88424	0.06842	0.538	0.02632
TAH$-2019-2.1	Tremolite rock	21.8	0.2	2.82	11	0.152	13.3	2.28	0.506	<0.05	0.133	<0.05
TAH$-2019-2.1 (2)	Tremolite rock	21.6	0.21	2.83	11	0.152	13.3	2.29	0.508	<0.05	0.134	<0.05
TAH$-2019-2.2	Tremolite rock	20	0.22	3.81	9.19	0.153	13.6	3.65	0.575	<0.05	0.154	<0.05
TAH$-2019-2.3	Tremolite rock	20.1	0.22	3.59	11.1	0.098	14.1	0.88	0.201	<0.05	0.133	<0.05
TAH$-2019-2.4	Tremolite rock	21.6	0.21	3.28	8.54	0.124	14.2	2.8	0.403	<0.05	0.157	<0.05

Sample ID	Sample Description	Ni	Co	Cu	Zn	S	Cr	Cl	V	Y	Zr	Au	Pd	Pt
M52441183R303 15.00-15.50	Komatiitic basalt	330		<20	110	100	1040	200	220	10	40	<1	5.5	18.7
M52441183R303 52.05-52.30	Komatiitic basalt	130		<20	150	<100	470	<100	240	20	40	<1	7.4	18.9
M52441183R303 97.90-98.20	Komatiitic basalt	490		<20	170	<100	1590	<100	180	<10	40	<1	2.2	15.4
M52441183R304 9.35-9.90	Komatiite (thin lava flow)	1030	83.4	<20	120	<100	2880	<100	140	10	20	<1	1.6	11.6
M52441183R304 18.90-19.25	Komatiite (thin lava flow)	960		<20	90	<100	2750	<100	130	<10	20	<1	1.7	11.6
M52441183R304 32.95-33.30	Komatiite (thin lava flow)	1260	84.8	<20	90	100	4220	<100	110	<10	20	<1	1.2	8.5
M52441183R304 38.10-38.50	Chlorite schist	4500		1550	210	6100	640	100	100	10	30	40.8	136	88.5
M52441183R304 39.60-39.90	Komatiitic basalt	610	47.3	100	130	400	1200	100	220	10	40	2.2	13.7	23
M52441183R304 55.70-56.05	Mafic dyke	110		40	340	400	210	200	210	20	70	1.2	<1	1.6
M52441183R304 77.00-77.30	Komatiitic basalt	390		40	110	100	1050	100	230	20	40	2.5	1.4	13.7
M52441183R304 114.20-114.55	Komatiitic basalt	100	48.6	60	140	200	220	100	250	20	50	1.6	3.8	18.6
M52441183R304 114.20-114.55 (2)	Komatiitic basalt	100		50	140	200	220	100	260	10	50			
M52441183R305 38.80-39.30	Komatiitic basalt	600		70	80	200	1820	200	210	10	40	2.3	1.9	14.8
M52441183R305 64.20-64.40	Komatiitic basalt	300		20	90	<100	1020	100	240	10	40	<1	5.7	19
M52441183R306 34.30-34.80	Komatiitic basalt	470		<20	330	<100	1360	200	200	10	30	<1	1.4	17.1
M52441183R306 50.80-51.40	Komatiitic basalt	160		40	170	<100	540	200	210	10	60	1.2	1.3	12.3
M52441183R306 88.20-88.40	Variolitic komatiitic basalt	270		110	130	800	900	100	220	10	40	<1	2.5	17.1
4411/83/R305/4.35-4.60	Deposit	6789	216	3839	135	16270	396	<60	128	14	34	57.6	220	139
4411/83/R305/14.00-14.40	Deposit	4754	132	6281	272	14860	288	90	129	12	35	102	131	112
4411/83/R305/20.60-21.00	Deposit	3570	142	198	152	3212	1745	110	166	10	28	59.7	311	99.6
4411/83/R306/7.55-8.00	Deposit	1614	69.5	535	88	1646	184	80	120	13	36	8.85	41.5	16
4411/83/R306/14.05-14.45	Deposit	5704	180	1040	222	13020	497	70	119	12	32	6.73	470	163
4411/83/R306/30.05-30.45	Deposit	7144	202	3560	572	21970	650	130	149	13	33	13.2	72.9	29.7
36-JSK-94-12.30	Komatiitic basalt	890	130	280	270	720	1724.2	100	210.73	9	14.81			
36-JSK-94-30.50	Komatiite (thin lava flow)	680	90	0	70	0	1950	80	210.73	13	14.81			
37-JSK-94-4.00	Metapyroxenite	1180	140	20	120	0	218.94	50	88.37	6	7.4			
28-TOH-94	Metapyroxenite	960	150	0	130	0	205.26	40	61.18	8	7.4			
73-TOH-94	Komatiite (thin lava flow)	1249	107	7	111	90	4083	2.1	117	5	12			
73-TOH-94	Komatiite (thin lava flow)	1370	130	10	110	0	3968	40	124	4	0			
74-TOH-94	Komatiitic basalt	1070	120	40	80	0	3681	110	183.54	6	7.4			
TAH$-2019-2.1	Tremolite rock	986	110	29	108	0	133		48.5	4.6	7.2	<1	<1	<1
TAH$-2019-2.1 (2)	Tremolite rock	989	110	30	109	0	134		47.8	4.5	7.3			
TAH$-2019-2.2	Tremolite rock	1160	117	6	110	0	154		55.9	4.5	7.1	<1	<1	<1
TAH$-2019-2.3	Tremolite rock	1120	125	48	104	0	133		61.6	3	5	<1	<1	<1
TAH$-2019-2.4	Tremolite rock	1220	120	4	99	0	157		49.2	3.9	4.1	<1	<1	<1

Sample ID	Sample Description	Ir	Os	Rh	Ru	La	Ce	Pr	Nd	Sm	Eu	Gd	Tb
M52441183R303 15.00-15.50	Komatiitic basalt												
M52441183R303 52.05-52.30	Komatiitic basalt												
M52441183R303 97.90-98.20	Komatiitic basalt					0.9	2.29	0.38	2.16	0.87	0.52	1.24	0.22
M52441183R304 9.35-9.90	Komatiite (thin lava flow)					0.87	2.23	0.38	2.17	0.83	0.5	1.24	0.23
M52441183R304 18.90-19.25	Komatiite (thin lava flow)												
M52441183R304 32.95-33.30	Komatiite (thin lava flow)					0.84	2.24	0.34	1.83	0.63	0.1	0.82	0.16
M52441183R304 38.10-38.50	Chlorite schist												
M52441183R304 39.60-39.90	Komatiitic basalt					1.88	5.5	0.91	4.75	1.62	0.88	2.21	0.41
M52441183R304 55.70-56.05	Mafic dyke												
M52441183R304 77.00-77.30	Komatiitic basalt												
M52441183R304 114.20-114.55	Komatiitic basalt					2.47	6.93	1.02	5.38	1.84	0.56	2.58	0.48
M52441183R304 114.20-114.55 (2)	Komatiitic basalt												
M52441183R305 38.80-39.30	Komatiitic basalt												
M52441183R305 64.20-64.40	Komatiitic basalt												
M52441183R306 34.30-34.80	Komatiitic basalt												
M52441183R306 50.80-51.40	Komatiitic basalt												
M52441183R306 88.20-88.40	Variolitic komatiitic basalt												
4411/83/R305/4.35-4.60	Deposit	3.32	3	9	7.5	1.34	3.95	0.59	3.54	1.22	0.63	1.98	0.36
4411/83/R305/14.00-14.40	Deposit	1.64	1.25	5.1	2.55	1.21	3.62	0.56	3.15	1.22	0.46	1.81	0.33
4411/83/R305/20.60-21.00	Deposit	0.66	<1	2.58	3.31	1.21	3.4	0.52	3.45	1.21	0.36	1.64	0.27
4411/83/R306/7.55-8.00	Deposit	0.59	<1	1.62	<2	1.78	3.94	0.71	3.27	1.34	0.58	2.22	0.33
4411/83/R306/14.05-14.45	Deposit	4.06	3.29	12.2	10.1	1.02	2.89	0.48	2.84	1.18	0.46	1.99	0.32
4411/83/R306/30.05-30.45	Deposit	2.53	1.94	4.44	4.31	1.55	4.34	0.67	3.84	1.28	0.61	2.02	0.33
36-JSK-94-12.30	Komatiitic basalt												
36-JSK-94-30.50	Komatiite (thin lava flow)												
37-JSK-94-4.00	Metapyroxenite												
28-TOH-94	Metapyroxenite												
73-TOH-94	Komatiite (thin lava flow)												
73-TOH-94	Komatiite (thin lava flow)												
74-TOH-94	Komatiitic basalt												
TAH$-2019-2.1	Tremolite rock					0.88	1.79	0.3	1.6	0.56	0.11	0.83	0.16
TAH$-2019-2.1 (2)	Tremolite rock					0.8	1.92	0.3	1.5	0.57	0.11	0.82	0.15
TAH$-2019-2.2	Tremolite rock					0.7	1.52	0.28	1.59	0.61	0.17	0.93	0.16
TAH$-2019-2.3	Tremolite rock												
TAH$-2019-2.4	Tremolite rock												

Sample ID	Sample Description	Dy	Ho	Er	Tm	Yb	Lu	Co	Hf	Nb	Rb	Sc
M52441183R303 15.00-15.50	Komatiitic basalt											
M52441183R303 52.05-52.30	Komatiitic basalt											
M52441183R303 97.90-98.20	Komatiitic basalt	1.58	0.34	1.02	0.14	1.02	0.15	83.4	0.57	<3	<0.8	27.2
M52441183R304 9.35-9.90	Komatiite (thin lava flow)	1.57	0.34	1.01	0.15	1.02	0.15	86.1	0.54	<3	<0.8	26.9
M52441183R304 18.90-19.25	Komatiite (thin lava flow)											
M52441183R304 32.95-33.30	Komatiite (thin lava flow)	1.07	0.24	0.71	0.11	0.72	0.11	84.8	0.57	<3	<0.8	19.2
M52441183R304 38.10-38.50	Chlorite schist											
M52441183R304 39.60-39.90	Komatiitic basalt	2.74	0.6	1.77	0.26	1.75	0.25	47.3	1.89	<3	<0.8	36.8
M52441183R304 55.70-56.05	Mafic dyke											
M52441183R304 77.00-77.30	Komatiitic basalt											
M52441183R304 114.20-114.55	Komatiitic basalt	3.31	0.73	2.21	0.32	2.17	0.31	48.6	1.4	<3	<0.8	44.2
M52441183R304 114.20-114.55 (2)	Komatiitic basalt											
M52441183R305 38.80-39.30	Komatiitic basalt											
M52441183R305 64.20-64.40	Komatiitic basalt											
M52441183R306 34.30-34.80	Komatiitic basalt											
M52441183R306 50.80-51.40	Komatiitic basalt											
M52441183R306 88.20-88.40	Variolitic komatiitic basalt											
4411/83/R305/4.35-4.60	Deposit	2.28	0.5	1.38	0.2	1.49	0.19	216	0.93	0.91	0.34	22.7
4411/83/R305/14.00-14.40	Deposit	2.13	0.46	1.38	0.23	1.37	0.19	132	0.98	0.9	<0.2	20.6
4411/83/R305/20.60-21.00	Deposit	1.89	0.39	1.32	0.18	1.17	0.19	142	0.89	0.97	0.45	31.7
4411/83/R306/7.55-8.00	Deposit	2.22	0.51	1.25	0.21	1.28	0.21	69.5	1.06	0.87	0.52	20.7
4411/83/R306/14.05-14.45	Deposit	1.98	0.44	1.24	0.19	1.06	0.17	180	0.9	0.82	0.36	22.2
4411/83/R306/30.05-30.45	Deposit	2.13	0.51	1.39	0.24	1.44	0.2	202	0.78	0.91	0.56	25.2
36-JSK-94-12.30	Komatiitic basalt											
36-JSK-94-30.50	Komatiite (thin lava flow)											
37-JSK-94-4.00	Metapyroxenite											
28-TOH-94	Metapyroxenite											
73-TOH-94	Komatiite (thin lava flow)											
73-TOH-94	Komatiite (thin lava flow)											
74-TOH-94	Komatiitic basalt											
TAH$-2019-2.1	Tremolite rock	1.04	0.24	0.73	0.11	0.74	0.11	104	0.57	<3	3.44	13.2
TAH$-2019-2.1 (2)	Tremolite rock	1.09	0.24	0.72	0.11	0.76	0.11	102	<0.5	<3	3.22	13.4
TAH$-2019-2.2	Tremolite rock	1.08	0.24	0.72	0.11	0.75	0.11	110	0.7	<3	1.58	12.9
TAH$-2019-2.3	Tremolite rock											
TAH$-2019-2.4	Tremolite rock											